A Prediction and Decision Framework for Energy Management in Smart Buildings

Submitted in partial fulfillment of the requirements for
the degree of

Doctor of Philosophy

in

Electrical and Computer Engineering

Chaitanya Poolla

M.S., Electrical and Computer Engineering, Carnegie Mellon University
B.Tech (Honors), Aerospace Engineering, Indian Institute of Technology (IIT), Kharagpur

CARNEGIE MELLON UNIVERSITY
Pittsburgh, PA

December, 2016

Chaitanya Poolla
ORCID: 0000-0003-2174-2110

Dedicated for the pleasure of Sri Sri Radha Madan Mohan and His Holiness Radhanath Swami for enabling me to transcend the darkness born out of ignorance with the shining lamp of knowledge

ACKNOWLEDGEMENTS

There have been several people and factors responsible for the manifestation of the work in this dissertation. Firstly, I owe a lot of gratitude to my advisor Dr. Abe Ishihara. Over these years, his indispensable advise helped me realize and channelize my true potential. His guidance helped me to not just improve and harness my research abilities, but also to pose appropriate questions and make strategic decisions in pursuit of knowledge. My interactions with him offered me wider perspectives to appreciate the balance between the breadth and depth of engineering research. I am grateful to him for the time and attention he devoted to me despite his busy schedules.

During my life as a graduate student, I was challenged by various circumstances that required me stay patient and focused to be able to transcend them. I owe my gratitude to Sri Krishna for offering me timely intuition, insights, and instilling in me, the hope to seek knowledge about the otherwise abstract. I am thankful to have found within me the signature of the ultimate reality in my search for the ultimate abstraction. In the wisdom of the Bhagavad Gita [51]:

sarvasya caham hrdi sannivisto
mattah smrtir jnanam apohanam ca |
vedais ca sarvair aham eva vedyo
vedanta-krd veda-vid eva caham ||

.

I am seated in everyone's heart, and from Me come remembrance, knowledge and forgetfulness. By all the Vedas, I am to be known. Indeed, I am the compiler of Vedanta, and I am the knower of the Vedas.

I am thankful to Dan Liddell for his indispensable work on the software development leading to both the energy dashboard and the collection of the HRRR weather forecast data. Without his timely support, the experiments could have neither started nor completed as expected.

The guidance and encouragement of my committee members Dr. Rodney Martin, Dr. Steven Rosenberg, and Dr. Marija Illic has been very fruitful. Reflecting on the feedback during the research meetings proved invaluable to assess the strengths and weaknesses of different solution methodologies while respecting the problem constraints. I am also grateful for the inputs I received from Dr. Rodolfo Milito that

helped construct the optimization framework.

This section would be incomplete without mentioning the contributions of my family and friends in supporting my life as a graduate student. The regular conversations with my mom (Radha), dad (Narayana Murthy), and brother (Teja) have been both de-stressing and inspirational. The sacrifices they undertook in their personal lives empowered my professional life as a graduate student. I received similar support from my extended family Yugal Kishore P, Lakshmi M, Ashok P, Shilpa, Usha M, and Ramana P from the nascent stages of my graduate program, and am certainly indebted to them for their indispensable services.

I have been extremely fortunate to have several good friends who positively influenced me over these years. It would have been very difficult to navigate the different phases of student life without their support. I especially thank Vijay, Dhiraj, Sandeep, Ramananda sakha, Lena, Rakesh, Harivamsa, Prashant, and several others from ISV for their support. I am thankful to the enriching life that Carnegie Mellon University (CMU) has provided me over these years. I especially value the encouragement of my friends/colleagues Abhinav, Akshay, Aniruddha, David, Rahul, Vinod, Madhu, Ajit, Kaushik, Nagarathnam, Dwarakesh among many others, and thank them for making my stay memorable. The discussions I had with them on a variety of topics ranging from engineering, physical and biological sciences, philosophy, and spirituality were both encouraging and enlightening. Apart from those mentioned above, I owe my gratitude the others who contributed either directly or indirectly to my life as a graduate student.

Finally, I am thankful to CMU and the NASA Ames Research Center for their support without which this research would not have materialized. This research effort has been supported under the NASA cooperative agreement NNX13AD49A.

ABSTRACT

By 2040, global CO_2 emissions and energy consumption are expected to increase by 40%. In the US, buildings account for 40% of national CO2 emissions and energy consumption, of which 75% is met by fossil fuels. Reducing this impact on the environment requires both improved building energy efficiency and increased renewable utilization. To this end, this dissertation presents a demand-supply-storage-based decision framework to enable strategic energy management in smart buildings. This framework includes important but largely unaddressed aspects pertaining to building demand and supply such as occupant plugloads and the integration of weather forecast-based solar prediction, respectively. We devote the first part of our work to study occupant plugloads, which account for up to 50% of demand in high performance buildings. We investigate the impact of plugload control mechanisms based on the analysis of real-world data from experiments we conducted at NASA Ames sustainability base and Carnegie Mellon University (SV campus). Our main contribution is in extending existing demand response approaches to an occupant-in-the-loop paradigm.

In the second part of this work, we describe methods to develop weather forecast-based solar prediction models using both local sensor measurements and global weather forecast data from the National Ocean and Atmospheric Administration (NOAA). We contribute to the state-of-the-art solar prediction models by proposing the incorporation of both local and global weather characteristics into their predictions. This weather forecast-based solar model plus the plugload-integrated demand model, along with an energy storage model constitutes the weather-driven plugload-integrated decision-making framework for energy management. To demonstrate the utility of this framework, we apply it to solve an optimal decision problem with the objective of minimizing the energy-related operating costs associated with a smart building. The findings indicate that the optimal decisions can result in savings of up to 74% in the expected operational costs. This framework enables inclusive energy management in smart buildings by accounting for occupants-in-the-loop. Results are presented and discussed in the context of commercial office buildings.

TABLE OF CONTENTS

LIST OF ILLUSTRATIONS

LIST OF TABLES

SELECTIVE LIST OF SYMBOLS USED

$\mathbb{C}$	The plugload experiment at CMU SV
$\mathbb{N}$	The plugload experiment at NASA
$\mathbf{H}_0^{\mathbb{N}}$	Null hypothesis for testing the NASA experiment
$\mathbf{H}_0^{2\mathbb{C}}$	Null hypothesis for testing the CMU incentive experiment
$\mathbf{H}_0^{3\mathbb{C}}$	Null hypothesis for testing the CMU feedback experiment
$\mathbf{H}_0^{4\mathbb{C}}$	Null hypothesis for testing the CMU incentive and feedback experiment
$\mathbf{H}_A^{\mathbb{N}}$	Alternate hypothesis for testing power reduction in the NASA experiment
$\mathbf{H}_A^{2\mathbb{C}}$	Alternate hypothesis for testing power reduction in the CMU incentive experiment
$\mathbf{H}_A^{3\mathbb{C}}$	Alternate hypothesis for testing power reduction in the CMU feedback experiment
$\mathbf{H}_A^{4\mathbb{C}}$	Alternate hypothesis for testing power reduction in the CMU incentive and feedback experiment
$\mathcal{P}1^{\mathbb{C}}$	Baseline phase of the CMU experiment
$\mathcal{P}1^{\mathbb{N}}$	Baseline phase of the NASA experiment
$\mathcal{P}2^{\mathbb{C}}$	Incentive only phase of the CMU experiment
$\mathcal{P}3^{\mathbb{C}}$	Feedback only phase of the CMU experiment
$\mathcal{P}3^{\mathbb{N}}$	Feedback phase of the NASA experiment
$\mathcal{P}4^{\mathbb{C}}$	Incentive+Feedback phase of the CMU experiment
$x^a_{\mathcal{P}2^{\mathbb{C}}_i}(t_0, t_f)$	Random variable representing the screentime spent by the ith participant on the scoreboard during the time interval $[t_0, t_f)$ in the CMU incentive experiment
$x^a_{\mathcal{P}2^{\mathbb{C}}_i}(t_0, t_f)$	screentime spent by the ith participant on the scoreboard during the time interval $[t_0, t_f)$ in the CMU incentive experiment
$x^a_{\mathcal{P}3^{\mathbb{C}}_i}(t_0, t_f)$	Random variable representing the screentime spent by the ith participant on the dashboard during the time interval $[t_0, t_f)$ in the CMU dashboard feedback experiment

$x^a_{\mathcal{P}3^{\mathbb{C}}_i}(t_0, t_f)$ screentime spent by the ith participant on the dashboard during the time interval $[t_0, t_f)$ in the CMU feedback experiment

$X^a_{\mathcal{P}3^{\mathbb{N}}_i}(t_0, t_f)$ Random variable representing the screentime spent by the ith participant on the dashboard during the time interval $[t_0, t_f)$ in the NASA feedback experiment

$x^a_{\mathcal{P}3^{\mathbb{N}}_i}(t_0, t_f)$ screentime input of the ith participant during the time interval $[t_0, t_f)$ in the NASA experiment

$x^a_{\mathcal{P}4^{\mathbb{C}}_i}(t_0, t_f)$ Random variable representing the screentime spent by the ith participant on the dashboard during the time interval $[t_0, t_f)$ in the CMU *both incentive and dashboard* experiment

$x^a_{\mathcal{P}4^{\mathbb{C}}_i}(t_0, t_f)$ screentime spent by the ith participant on the dashboard during the time interval $[t_0, t_f)$ in the CMU *both feedback and incentive* experiment

$x^i_{\mathcal{P}2^{\mathbb{C}}_i}(t_0, t_f)$ Incentive input to the ith participant during the time interval $[t_0, t_f)$ in the CMU incentive experiment

$x^i_{\mathcal{P}2^{\mathbb{C}}_i}(t_0, t_f)$ Random variable representing the incentive input of the ith participant during the time interval $[t_0, t_f)$ in the CMU incentive experiment

$x^i_{\mathcal{P}4^{\mathbb{C}}_i}(t_0, t_f)$ Incentive input to the ith participant during the time interval $[t_0, t_f)$ in the CMU *both feedback and incentive* experiment

$x^i_{\mathcal{P}4^{\mathbb{C}}_i}(t_0, t_f)$ Random variable representing the incentive input of the ith participant during the time interval $[t_0, t_f)$ in the CMU *both feedback and incentive* experiment

$Y_{\mathcal{P}1^{\mathbb{C}}_i}(t_0, t_f)$ Random variable representing the baseline response of the ith participant during the time interval $[t_0, t_f)$ in the CMU experiment

$y_{\mathcal{P}1^{\mathbb{C}}_i}(t_0, t_f)$ Baseline response of the ith participant during the time interval $[t_0, t_f)$ in the CMU experiment

$Y_{\mathcal{P}1^{\mathbb{N}}_i}(t_0, t_f)$ Random variable representing the baseline response of the ith participant during the time interval $[t_0, t_f)$ in the NASA experiment

$y_{\mathcal{P}1^{\mathbb{N}}_i}(t_0, t_f)$ Baseline response of the ith participant during the time interval $[t_0, t_f)$ in the NASA experiment

$Y_{\mathcal{P}2^{\mathbb{C}}_i}(t_0, t_f)$ Random variable representing the response of the ith participant during the time interval $[t_0, t_f)$ in the CMU incentive experiment

$y_{\mathcal{P}2_i^{\mathbb{C}}}(t_0, t_f)$	Response of the ith participant during the time interval $[t_0, t_f)$ in the CMU incentive experiment
$Y_{\mathcal{P}3_i^{\mathbb{C}}}(t_0, t_f)$	Random variable representing the response of the ith participant during the time interval $[t_0, t_f)$ in the CMU dashboard feedback experiment
$y_{\mathcal{P}3_i^{\mathbb{C}}}(t_0, t_f)$	Response of the ith participant during the time interval $[t_0, t_f)$ in the CMU feedback experiment
$Y_{\mathcal{P}3_i^{\mathbb{N}}}(t_0, t_f)$	Random variable representing the feedback phase response of the ith participant during the time interval $[t_0, t_f)$ in the NASA experiment
$y_{\mathcal{P}3_i^{\mathbb{N}}}(t_0, t_f)$	Response of the ith participant during the time interval $[t_0, t_f)$ in the NASA experiment
$Y_{\mathcal{P}4_i^{\mathbb{C}}}(t_0, t_f)$	Random variable representing the response of the ith participant during the time interval $[t_0, t_f)$ in the CMU *both feedback and incentive* experiment
$y_{\mathcal{P}4_i^{\mathbb{C}}}(t_0, t_f)$	Response of the ith participant during the time interval $[t_0, t_f)$ in the CMU *both feedback and incentive* experiment

Chapter 1

INTRODUCTION AND LITERATURE REVIEW

Significant advances in technology and infrastructure have enabled informed decision-making in building operations. Prior to integrating sustainability-related objectives into the decision-making process, decisions pertaining to building operations were predominantly driven by occupant safety and comfort. However, with the growth in sustainability-related concerns over the years, energy efficiency and environmental factors have become increasingly important considerations in the operation and maintenance of buildings [59] [36].

The Federal Executive Order 13693 [21] outlines several sustainability-related goals and guidelines on how to achieve them. The policy (Sec 1 in [21]) states that the priority should first be placed on reducing energy use and cost, and then on finding renewable energy solutions. In order to realize this vision, emphasis must be laid on improving demand management and renewable generation techniques, especially in the context of commercial buildings, which account for approximately 20% of the total annual energy consumption in the US [47]. In this dissertation, we improve the state-of-the-art methodologies to address the challenges in demand management and renewable generation, and leverage these toward the construction of an energy management framework in smart buildings. We first focus on constructing occupant plugload models, which offer the ability to regulate occupant plugloads using incentives and feedback-related inputs. Second, we focus on improving upon the current solar power prediction mechanisms by integrating weather forecasts into the prediction models. Thereafter, we construct a weather-driven plugload-integrated framework for energy management in smart buildings. We demonstrate the utility of this framework by applying it to formulate and solve an optimal decision problem with the objective of minimizing energy-related costs within a smart building.

1.1 Occupant plugload management

Power demand in commercial buildings can be broadly categorized into HVAC, lighting and plugload-related categories [23]. Over the recent years, advancement in building automation techniques have enabled the optimization of HVAC and lighting systems for minimal energy consumption [54] [24] [62] [63]. However, the

problem of reducing plugload consumption has received significantly less attention compared to its counterparts (HVAC and lighting) [35].

It is important to acknowledge the importance of plugload regulation as it accounts for a significant one-third of the demand in commercial buildings [41]. Furthermore, in high performance buildings, where HVAC and lighting demands are highly regulated, unregulated plugloads account for a significant 40% of the overall building demand [35]. Despite the importance of regulating plugload consumption, this problem has remained largely unsolved and has challenged the field of demand management [18] [14]. This is because plugload consumption is primarily driven by human occupants within the building, and hence is difficult to regulate. In order to regulate plugload consumption, it is important to identify what motivates the occupants to conserve plugload energy. Previous studies such as [30] [48] [66] have shown that feedback mechanisms and/or incentives could result in reducing occupant energy consumption. In particular, works such as [30] [33] study the factors that constitute effective feedback for motivating behavioral changes. They conclude that the most effective factors affecting energy behavior are historical comparisons and appropriate incentives. Yun et al. [66] outlines nine intervention techniques that can motivate change of behavior in the workplace. They also note that it is possible to obtain 12%-20% savings by modifications in behavior. A study involving feedback and incentives was conducted in [48] on dormitory residents, wherein it was found that real-time feedback in conjunction with education and incentives resulted in a significant 32% energy conservation by students in dormitories. However, to the best of our knowledge, there exist no reported models that quantitatively explain the mechanisms behind such savings.

In this work, we design a controlled experiment to study mechanisms that explain the roles that incentives and awareness play in changing occupant plugload consumption. This experiment was conducted at the NASA Ames sustainability base [40], where we monitored the participants' plugload consumption under the action of incentives and feedback, as described in Chapter 2. The data obtained from the study was used to construct the occupant plugload models. In particular, we constructed models based on statistical assumptions to explain the observed data. The statistical analysis is presented in Chapter 3. A major contribution of our study is the inclusion of occupant plugload models for demand management in smart buildings.

1.2 Weather forecast-based solar prediction

While demand management in buildings is necessary to meet a target lower than usual demand [1], it is also important to increase reliance on renewable power supply. However, this is difficult for several reasons including rapid fluctuations, unpredictability, and lack of market regulation [45]. Since environmental fluctuations inevitably affect the renewable generation, it is useful to forecast these fluctuations. Using such forecast plus a model that maps the environmental states to the renewable output, we can forecast the renewable output. While there exist several forecast products from the National Oceanic and Atmospheric Administration (NOAA), the spatial resolution of each of these products are typically on the order of kilometers [11]. Resolution at such scales are inadequate for purposes of localized predictions over smaller spatial scales.

In this work, we are concerned with the problem of solar power forecasting. Methods proposed in the literature to forecast solar power are either based on time-series power data, global weather forecast data, or local weather measurement data. In models such as those in Pedro et al. [46], time-series power data with no exogenous inputs are used for short-term forecasting with a horizon of up to two hours into the future. However, using only past power data for forecasting does not directly account for weather-related changes in the forecasting model. In [6] [65], both time-series power data and global weather forecasts based on mesoscale models were used for forecasting. Bacher et al. [6] conclude that incorporating weather data into the forecast model results in a 35% better performance compared to using only time-series power inputs. However, using only global weather forecast data does not incorporate local characteristics such as shadows, bird movements, and other natural occurrences into the weather forecast model. Therefore, incorporating information about the local characteristics into the forecast model results is expected to refine the forecasts for localized predictions. Typically, the information about local characteristics are encoded in the on-site sensor data, and hence such data can help refine the forecast models. There have also been forecasting approaches that use local weather data measurements, such as the models in Chen et al. [12]. However, using only local weather data does not allow the model to be sensitive to global weather changes.

In order to overcome these limitations, we attempt to construct a model that leverages the advantages of previously mentioned approaches. In particular, we tailor the global weather forecasts to incorporate local weather characteristics based on sensor

measurements. This allows for localizing solar forecasts at the level of rooftops while simultaneously leveraging the contributions of global weather changes. We then use a data-based approach to map these local weather forecast inputs into corresponding solar power outputs at a given plant. The details of the approach are presented in Chapter 5. Our main contribution to the field of solar power forecasting is to provide localize solar forecasting by integrating localized weather prediction models with data-based power prediction models.

1.3 Energy management in smart buildings

Given the weather-driven solar generation models and plugload demand models discussed in Sections 1.1 and 1.2 respectively, we turn our attention to energy management in commercial buildings. Along with demand-supply, we also consider the presence of energy storage, which is integral to a sustainable smart building design [38] [13] [57]. We also assume that the building is connected to the grid, which acts as both an infinite source, and an infinite sink from the perspective of the building. The grid is also assumed to pre-specify cost and selling prices associated with grid transactions. The energy management problem then seeks decisions that determine the power flows between various components in the building, thereby incurring grid transaction-related costs. As an example, a decision might direct the renewable output to charge the energy storage component instead of exporting it to the grid. Such a decision could be based on forecasts about poor weather conditions and high electricity prices in the immediate future. Such decisions might incur less electricity bills compared to those decisions which always result in exporting renewable output to the grid.

We employ the above framework consisting of demand[1], supply, storage, grid, and pricing to solve a decision problem to minimize a pre-specified cost. This problem is known as the optimal decision problem, and the corresponding solutions are known as optimal decisions. Although related formulations have been studied in recent literature [61] [55] [34] with several simplifications, this problem has not been solved in its present form to the best of the author's knowledge. The novelty in this formulation is two-fold: (i) we incorporate weather-related uncertainties into the solar predictions, and (ii) we incorporate controllable plugloads into the demand model, thereby making it partially controllable. In Wang et al. [61], controllable solar generation and load models were employed within a deterministic

[1] We use the terms demand and load interchangeably to refer to the instantaneous power usage within the building

prediction framework to obtain power flows based on model predictive control (MPC) techniques. In Kanchev et al. [34], non-controllable deterministic demand-supply models were considered, but without the notion of optimality. However, in this case, the renewable supply is treated as a non-controllable weather-driven first order Markov chain under the assumption that the solar power output operates at its maximum power point. Furthermore, the demand is assumed to be partially controllable due to the presence of controllable plugloads, which is modeled as a controllable markov chain. In Ono [43], a distributed robust control method was proposed for a smart grid using a chance-constrained programming framework that accommodates risky solutions with bounds on the constraint-failure probabilities. In comparison, our work involves developing non-risky solutions for optimal energy management in smart buildings wherein the solutions are guaranteed to satisfy the constraints. Furthermore, Ono describes a chance-constrained model predictive control framework to solve the optimization problem while this work focuses on using stochastic dynamic programming to determine the optimal control within a Markov decision process framework. Also, unlike in [55] and [34], where the dynamics of the energy storage were not explicitly considered, we regard the energy storage as a dynamical system along with its charging and efficiency constraints. Unlike the conventional Markov chain models [4][39] which employ stationary Markov chains, we incorporate time-dependent transitions in the solar and the load Markov processes by representing them as cyclo-stationary stochastic processes. Given the representations of these individual components which constitute a Markov decision process in the storage state, we solve for the optimal decisions using a stochastic dynamic programming (SDP) approach as detailed in Chapter 6.

1.4 Main Contributions

The main contributions of this dissertation are as follows:

1. This dissertation provides a novel experimental design for studying occupant plugload consumption in the presence of feedback and incentives. Unlike most related studies which monitor aggregate consumption, we adopt an individual device level real-time monitoring of each participant using smart powerstrips, and provide a detailed statistical analysis on the data from the experiment consistent with the design assumptions.

2. This dissertation addresses the challenging problem of occupant plugload modeling based on feedback and incentive interventions. To the best of

our knowledge, there do not exist studies that quantify the mechanisms by which these interventions influence the observed changes in the occupant plugload consumption. We employ autoregressive models with exogenous interventions as the tool to explain these mechanisms.

3. This dissertation proposes a novel local weather forecasting model via integration of global weather forecasts with local sensor-based data. Several methods have been proposed in literature based exclusively on local data or global data, and we suggest that the performance of a conventional autoregression-based local prediction model can be augmented using global weather forecasts as exogenous inputs.

4. This dissertation introduces a novel plugload-integrated energy management framework by integrating controllable plugload models and weather-driven solar generation models in the presence of energy storage and pricing models. This contribution extends energy management in buildings into a new paradigm by including occupants-in-the-loop.

1.5 Dissertation Outline

This dissertation is organized as follows: Chapter 2 describes the experimental setup. It is followed by statistical analysis of the experimental data in chapter 3. The plugload-integrated controllable demand model is described in Chapter 4. Solar forecasting based on weather forecasts is presented in Chapter 5. The entire energy management framework and its application to address the optimal decision problem is described in Chapter 6, followed by concluding remarks in Chapter 7.

Chapter 2

EXPERIMENTAL DESIGN

We are interested in understanding and quantifying the influence of incentives and/or feedback on the plugload consumption of building occupants. We employ the scientific method [27] to gather this knowledge. Our research hypothesis is:

Providing incentives and/or feedback to building occupants results in the reduction of their plugload consumption.

A logical consequence of this hypothesis is that *the average plugload consumption of the occupants in the presence of an incentive and/or feedback is less than their average plugload consumption of the occupants in the absence of incentive or feedback*. Given that the prediction is testable, we designed and conducted a carefully controlled plugload experiment within the constraints imposed by the available facilities, participants, and the institutional review board (IRB). This experiment enabled us to record observations that could be used to test these predictions, and hence the validity of the research hypothesis. We discuss various aspects of the experimental setup in the following sections.

2.1 Location of the experiment

The two plugload experiments were conducted in three buildings at the NASA research park in Mountain View, California. One experiment was conducted at the NASA sustainability base, a test-bed for a typical work environment in a medium office building. The other experiment was conducted at the CMU SV campus in buildings 19 and 23, a test-bed for an academic environment. Let $\mathbb{N}$ and $\mathbb{C}$ denote the plugload experiments at NASA and CMU respectively.

2.2 Experiment design

The experiment was designed to monitor the power usage of occupant plugloads in the presence of the treatment factors such as incentives and/or feedback. Therefore, the response variable was the time-averaged power usage of a participant, and the input variables were the incentives and/or feedback provided to the participant. The input factors are also known as treatment factors or simply, treatments. The incentives were provided in the form of monetary rewards to promote energy conser-

vation among the participants. The feedback was provided by a web browser-based self-monitoring dashboard to raise awareness about the participant's own power use. In designing the experiment, we took note of the difference between providing feedback and receiving it because different participants receive different amounts of feedback based on the attention paid to their dashboard. We intended to quantify the attention paid by each participant based on the time spent by the participants on their respective dashboards.

2.2.1 Design principles and implementation

The objective of the experiment is to determine the impact of feedback and/or incentives on building occupants. The objective of the experimental design is then to strengthen the causal connection between the treatment/input and the response variables. The objective of the design is realized by eliminating or minimizing the effect of nuisance factors using the core principles of experimental design [37], namely, randomization, replication, and blocking. These principles have a direct impact on the validity of the statistical assumptions used to analyze the experiment's results. The principles and their implementation are described below.

2.2.1.1 Randomization

We recruited subjects based only on the willingness to participate without attempting to introduce systematic bias. This ensures that any effect that might be observed due to the treatment on the sample is not due to the random factors such as work schedules or work loads. Furthermore, this principle helps us to make the assumption of random sampling from the underlying occupant population for purposes of statistical analysis.

2.2.1.2 Replication

While each subject is sampled randomly from the occupant population, this alone does not guarantee that any effects observed due to a treatment/input are generalizable to the entire population. A treatment can be considered truly effective if it is repeatable over the population. Therefore, the principle of replication is important. We implement this principle by assigning several subjects to each treatment factor (feedback and/or incentive). This allows us to draw more general inferences under the assumption of a replicated design. The number of replicates in an experiment is commonly known as the sample size.

2.2.1.3 Blocking

While randomization and replication allow for averaging out the effects of random factors, there is a danger of introducing systematic bias due to practical constraints. For example, in this investigation, factors related to the work environment, such as industry vs academic, may affect the results from the experiment as found in the literature [67]. For this reason, we intend to block the influence of this nuisance factor by conducting separate experiments, one in a university environment, and the other in an industry environment. Though blocking limits the inferences drawn to a university or an industry setting, it helps in homogenizing the experimental conditions. This homogenization helps in minimizing the effects of the nuisance factor across the individual samples within an experiment.

Despite the efforts to randomize and block away the effect of nuisance factors, certain nuisance factors may still manage to confound any observed experimental effects. This arises due to incomplete randomization. For example, the randomization might not have occurred across all levels of all nuisance factors. This is especially true in the case of subjects with intrinsic variability, such as humans. Therefore, we adopt a special case of the randomized block design called the matched pairs design to further strengthen the causal connection between the treatments provided and any observed effects. This is done by exposing the same set of subjects to both the baseline and the treatment conditions. In this manner, the effect of treatment across subjects is deduced by comparing each subject's response under treatment to his/her baseline response.

2.2.2 Dashboard design

The dashboard was designed to provide relevant information to the participants to help reduce their energy consumption. The elements of the feedback consisted of appropriate information and analytics that were previously found effective in motivating energy conservation among building occupants in the workplace [66] [67] [29]. The various power analytics on the dashboard were represented by easily comprehensible elements with minimal cognitive and visual load [9]. The designed dashboard was implemented in PHP (back end), HTML CSS and JavaScript (front end) by the software developers who worked on this project. An image of the dashboard consisting of these analytics is shown in Figure 2.1. The different graphical features of the dashboard are explained below in section 2.2.2.1.

2.2.2.1 Graphical elements

1. Radio buttons (upper left): The radio buttons represent the comfort reporting feature of the dashboard. It consists of seven levels, in line with the ASHRAE 7-point scale for reporting thermal comfort [17] [64]. This element served two purposes, namely, (i) engaging the attention of the participants, and (ii) building comfort models using the reported comfort values in light of the building conditions.

2. Dial (center): The central dial provides a comparison of the participant's instantaneous power use to that of his/her historical baseline power use. The dial's needle was set to saturate beyond the maximum power consumption represented by the dial. Similar analytics were found to motivate households to reduce energy consumption [49]. In this study, the dial was calibrated using the baseline data as follows. The average baseline power use computed after eliminating the power data below a threshold of 5 W was chosen to represent the zenith of the dial. The threshold was chosen to prevent the low consumption during either non-business hours or absence from pulling down the mean value on the dashboard dial. This ensured that the needle wouldn't stay pegged (saturated) during hours of normal operations. The participants were asked to interpret the dial as representing their current performance in light of their typical performance.

3. Scoreboard/Leaderboard (upper right): The scoreboard helps participants to realize their position in the competition to remain ahead of the other participants. In cases where an incentive is provided, the participant with the highest score (rank 1) by the end of the day (11:59:59 PM local time) is declared the winner. The score of a participant is a measure of the improvement of the participant over his/her baseline. Section 2.2.2.2 below describes the scoring mechanism in further detail.

4. Line charts (lower left): The line chart provides a comparison between the participant's total instantaneous usage and the average participant's total instantaneous usage. Such social comparisons have shown success in motivating participants to reduce energy consumption [3] [5].

5. Bar charts (lower right): The bar charts provide channel-specific feedback to the participant. While the other power analytics represent the participant's aggregate consumption across all channels/sockets, the bar chart represents

the consumption split across these channels. Therefore, the bar chart provides actionable feedback to the participant by indicating the power consumption across all devices connected to the channels.

6. Message box (top right): An additional feature to send messages to the participant's dashboard was provided in the dashboard. This was used to notify the winners during the study by sending a link to the dashboard from an email reminder.

2.2.2.2 Score computation

The scoreboard described above represents the participant's score in comparison to the other participants. In case of the experiments involving incentives, the participant with the highest score at the end of the day (11:59:59 PM local time) was declared the winner and was provided the incentive. The steps involved in the scoring mechanism are described as follows:

1. The time-averaged power across each channel was computed for the average baseline day by excluding data points below a threshold (5 W). The threshold served as a measure of power consumption during absence or inactivity.

2. The channel-specific averages computed above were aggregated over all the channels assigned to a participant to obtain the average active baseline consumption of a participant.

3. The above steps were repeated for all the participants to obtain their individual baseline usage. This information was incorporated into the score computation.

4. During each day of the incentive experiment, average power consumption of the participant averaged across the time-of-activity was determined similar to the baseline case. The only difference between the average power computation during the experiment day and during the baseline days was that the average power during the experiment day was computed from local midnight till the time the score computation occurred.

5. The score was then computed as the percentage improvement during the experiment in comparison to the baseline, and can be written as $score = 900 + 100 \times \frac{baseline\_average - expt\_average}{baseline\_average}$. The variable $baseline\_average$ represents the baseline average power computed for a given participant in step 2 above,

and the variable $expt\_average$ represents the experiment day average power computed for a given participant in step 4 above.

The 5 W threshold, which was unknown to the participants, ensured that participants could not win due to absence or inactivity. The participants were informed that the scoring mechanism only rewards reducing power consumption via active changes as opposed to reducing the consumption via passive changes such as turning off devices, or by being inactive or absent. Despite all the inactivity measures, it was also possible that a participant could win due to constant activity such as leaving a computer monitor on. In such cases, a moving average of time metric was used to eliminate such participants from winning. In this manner, a participant could not win an incentive without active changes in power consumption.

2.3 Recruitment

As stated in section 2.1 above, the study locations consisted of participants from three buildings. The recruitment for the experiments began after the approval from both the CMU and NASA Institutional review boards. The reader is referred to chapter A in the Appendix for more information regarding the IRB approvals.

The recruitment for the experiment at NASA was conducted by holding one-on-one meetings with the occupants in the building who were potentially interested in participating in the study. The interested candidates signed the consent forms (ARC 475), and were briefed about the study in further detail.

The recruitment for the experiment at CMU was conducted by approaching the potential participants in buildings 19 and 23, which constitute the CMU campus in Silicon Valley. The pool of interested candidates comprised of students, faculty, and staff. The interested candidates were briefed about the study in further detail.

The recruitment process was followed by the installation of the smart powerstrips [20] for each participant at NASA and CMU, thereby enabling us to monitor the power consumption of the participants.

2.4 Data collection

The response variable (power consumption) was monitored by sensors from Enmetric systems [20], which were placed between the power source and the load. The inputs provided to the participants were incentives and/or feedback. These incentives were provided as equivalents of monetary rewards, whose values ranged from $5 to $50 in multiples of $5. The feedback was provided in the form of a web

application, that contained a personalized energy dashboard displaying power consumption analytics of the participants in relation to their respective baseline usages. The amount of feedback received by the participants was quantified based on the time spent by the participants on their dashboards. Therefore, the feedback-related input variable was monitored by monitoring the amount of screen time associated with the dashboard of every participant.

2.5 Execution of the experiment

The two experiments were conducted based on the same principles but with different objectives. For example, in the NASA experiment, there were no incentives provided to the participants. These differences in objectives led to the differences in execution of both experiments. The execution procedures of both experiments are summarized below:

2.5.1 Experiment 1 at NASA sustainability base

The experiment at the sustainability base was conducted in two phases. The first phase was the baseline phase, wherein the power consumption data of each participant was recorded in the absence of any treatment variable. This data constituted the baseline dataset, which was assumed to represent the typical usage patterns of the participants. Let the baseline phase be denoted by $\mathcal{P}1^{\mathbb{N}}$. The second phase was the phase of the experiment, wherein all the participants were provided with the dashboard feedback with all the five elements indicating their power analytics and the scoreboard/leaderboard. Let this phase be represented by $\mathcal{P}3^{\mathbb{N}}$. An explanation of each feature of the dashboard was provided as shown in Figure 2.3. Furthermore, the time spent by each participant on the web-based dashboard screen was recorded. The screen time variable served as an indication of how much attention was paid by each participant to his/her respective dashboard. In the NASA experiment, the baseline phase was conducted for a period of 5 weeks from 12 Sep 2016 to 17 Oct 2016, and the phase of the experiment was conducted for a period of 4 weeks from 18 Oct 2016 to 11 Nov 2016 as shown in figure 2.2.

2.5.2 Experiment 2 at CMU buildings 19 and 23

The experiment at the CMU campus (buildings 19 and 23) was conducted in four phases, and its schedule is shown in Figure 2.6. The first phase was the baseline phase was conducted for five weeks from 12 Sep 2016 to 17 Oct 2016, wherein the power consumption data of each participant was recorded in the absence of any

treatment variable. This data constituted the baseline dataset, which was assumed to represent the typical usage patterns of the participants. We represent this phase of the experiment by $\mathcal{P}1^{\mathbb{C}}$.

The second phase of the experiment was the *incentive only phase* phase was conducted for two weeks from 18 Oct 2016 to 30 Oct 2016, wherein all the participants were asked to compete for the incentive by reducing their power consumption with respect to their own baseline consumption. Let this phase of the experiment be denoted by $\mathcal{P}2^{\mathbb{C}}$. In order to help participants realize their position in the competition and help them be aware of the competition itself, scores and rankings of the participants were displayed to them. The participants were asked to compete for incentives, which were provided during each weekday. The values of the incentives provided each day varied in their value between \$5 and \$50 in a random order. Therefore, there was no systematic bias introduced due to the order of the incentive treatments. The were awarded to the individual with the highest score at the end of the day (11:59:59 PM local time). The score was displayed to the participants on their respective dashboards on a near real-time basis (updating once a minute), along with the scores of the other participants. However, there was no other feedback provided on the participants' dashboards regarding their power consumption. In other words, only elements 1 and 3 were displayed on the dashboard during the *incentive phase*. The near real-time score was quantified the improvement of a participant over his/her average baseline consumption, based on their average power usage from midnight (00:00:00 AM local time) until the time the score was computed. An explanation of the relevant elements was provided to the participants as shown in Figure 2.4.

The third phase was the *dashboard feedback only* phase was conducted for two weeks from 31 Oct 2016 to 13 Nov 2016, wherein all the participants were provided with the dashboard feedback containing power analytics relating to the comparison of individual power consumption against individual historical usage as well as to that of the participant pool. We represent this phase of the experiment by $\mathcal{P}3^{\mathbb{C}}$. Specifically, all the elements of the dashboard except for the scoreboard/leaderboard were made visible to the participants. Furthermore, the time spent by each participant on the web-based dashboard screen was recorded. The screen time variable was assumed to serve as an indicator of how much attention was paid by each participant to his/her respective dashboard. An explanation of the relevant elements were provided to the participants as shown in Figure 2.5.

Device name	*Number of devices*
Monitor	21
Laptop	11
Docking station	9
Desktop	2
Headset	7
Phone	9

Table 2.1: Device list of participants in the NASA experiment

Device name	*Number of devices*
Monitor	23
Laptop	13
Desktop	8
Phone	6

Table 2.2: Device list of participants in the CMU experiment

The final phase of the experiment was the *both incentive and dashboard feedback* phase of the experiment was conducted for two weeks from 14 Nov 2016 to Nov 25 2016, wherein all the participants were provided with both incentives and the dashboard feedback. The proximity to winning the incentive was indicated by the scoreboard component of the dashboard as provided in the second phase. All the other elements of the dashboard representing power analytics of the participant with respect to their historical usage and the participant pool were also made available during the *both incentive and dashboard phase* of the experiment. Let the *both incentive and dashboard feedback* phase of the experiment be denoted by $\mathcal{P}4^{\mathbb{C}}$. The explanations provided are similar to the complete dashboard study at NASA and are shown in Figure 2.3.

2.5.3 Device list

A list of devices associated with each participant were also listed for personalizing the feedback, both for the CMU and the experiment. A list of devices for the NASA and CMU experiments are provided in the tables 2.1 and 2.2 respectively.

Prior to the experiment, the participants were provided with an information sheet which provided them information on how to reduce energy consumption, should they wish to. In other words, this information was intended as a tool to help them realize the change in their energy-related behavior, if any. In that manner, we hoped to have any behavioral change reflect in the individual's energy consumption.

The sheet contained a graphical representation of possible energy conservation practices associated with the majority of devices present in both the experimental environments, as shown in Figure 2.7.

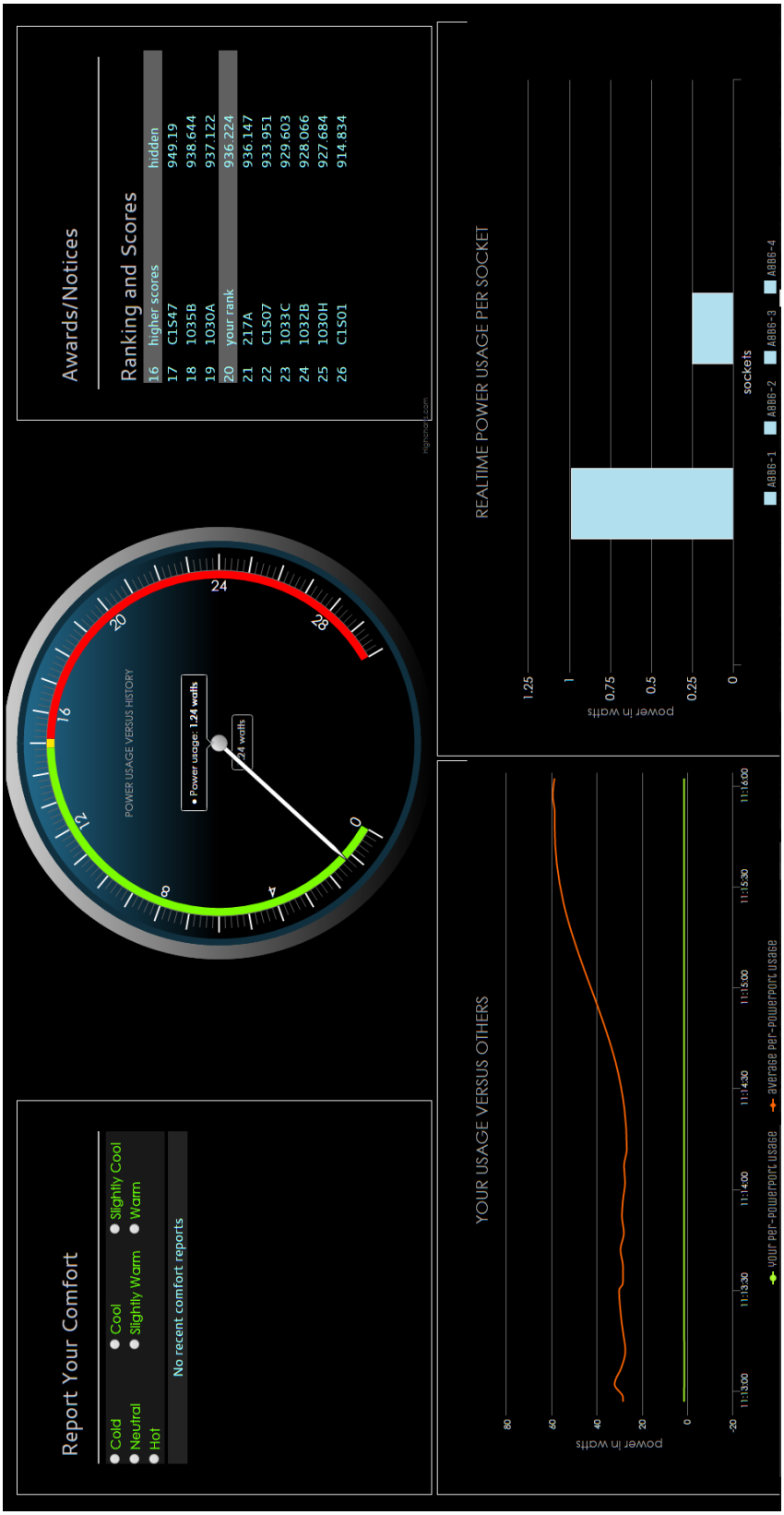

Figure 2.1: A screenshot depicting all the elements of the dashboard

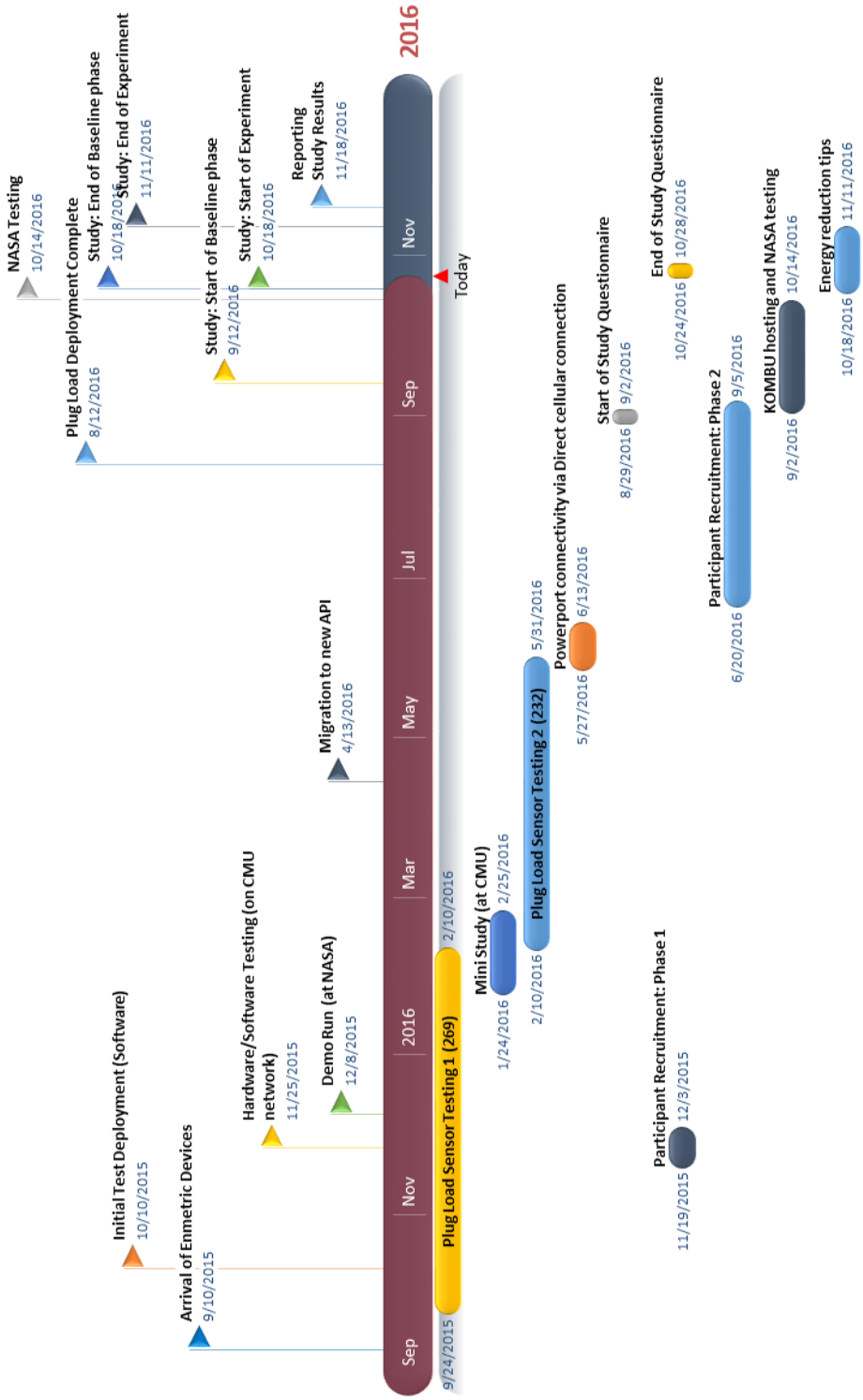

Figure 2.2: NASA experiment schedule

Power dial (top center)

The **central dial** represents your instantaneous power use in the light of your baseline use

- green zone indicates less than baseline use,
- yellow zone indicates around baseline use, and
- red zone indicates higher than baseline use

Bar chart (right bottom)

The **bar chart** represents your socket/channel-specific usage across all the channels in your powerstrip(s). The labels are based on the last 4 digits of the MAC address of your powerstrip, *found on the back side of your powerstrip*, and the socket/channel number, *illuminated in green on the top of every socket*.

Line chart (left bottom)

The green line in the **line chart** represents your instantaneous power usage aggregated across all of your powerstrips. The orange line represents the instantaneous aggregated consumption of an average user. In other words, it represents the average of aggregated usages represented by the green line charts in every dashboard.

- If green is below (above) the orange, then your instantaneous aggregate consumption is less (more) than that of the "average" user's instantaneous aggregated power consumption

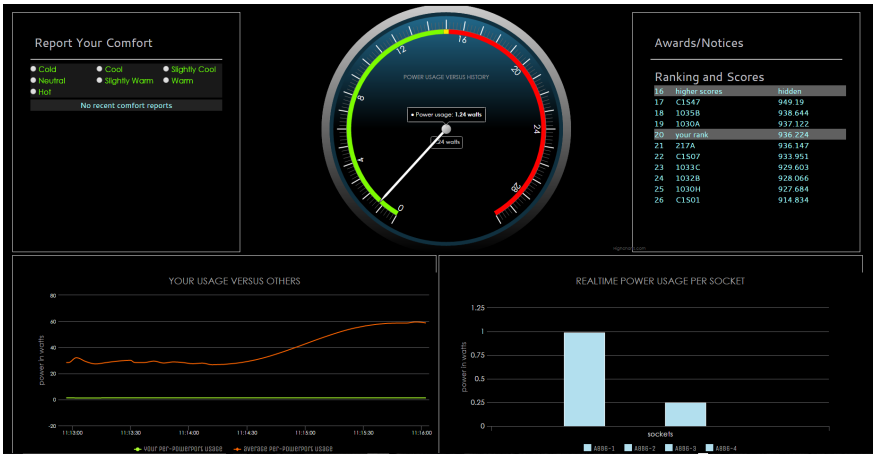

Comfort report (left top)

The comfort reporting feature allows you to report your comfort levels at the click of a button.

- Hit the radio buttons to report your comfort levels
- You are strongly encouraged to report the comfort levels multiple times at different times of the day

Scoreboard/Leaderboard (right top)

The **scoreboard** ranks your usage in the participant pool anonymously. The less your rank, the better your performance.

- Your score is determined by how your power since midnight today (00:00:00 till NOW) fares in comparison to your average baseline use.
- Please note that the scoring mechanism accounts for inactivity/absence.
    - In other words, credit (or discredit) is not awarded for reducing consumption of energy due to passive means such as by absence (or) by remaining inactive. Credit is awarded only for reducing energy usage during hours of active operation.
- Ranks are assigned based on scores. In other words, ranks are based on how your improvement over your baseline consumption compares to the others' improvement over their baseline consumption.

Figure 2.3: Information provided to the participants during the complete dashboard experiment

Comfort report (left)

The comfort reporting feature allows you to report your comfort levels at the click of a button.

- Hit the radio buttons to report your comfort levels.

- You are strongly encouraged to report the comfort levels multiple times at different times of the day.

Scoreboard/Leaderboard (right)

The **scoreboard/leaderboard** ranks your usage in the participant pool anonymously. The lower the rank, the better your performance.

- Your score is determined by how your power since midnight today (00:00:00 till NOW) fares in comparison to your average baseline use.
-
- Please note that the scoring mechanism accounts for inactivity/absence.

    - In other words, credit (or discredit) is not awarded for reducing consumption of energy due to passive means such as by absence (or) by remaining inactive. Credit is awarded only for reducing energy usage during hours of active operation.

- Ranks are assigned based on scores. In other words, ranks are based on how your improvement over your baseline consumption compares to the others' improvement over their baseline consumption.

Figure 2.4: Information provided to the participants during the *incentive only* experiment

Power dial (top center)

The **central dial** represents your instantaneous power use in the light of your own baseline use

- green zone indicates less than baseline use,
- yellow zone indicates around baseline use, and
- red zone indicates higher than baseline use

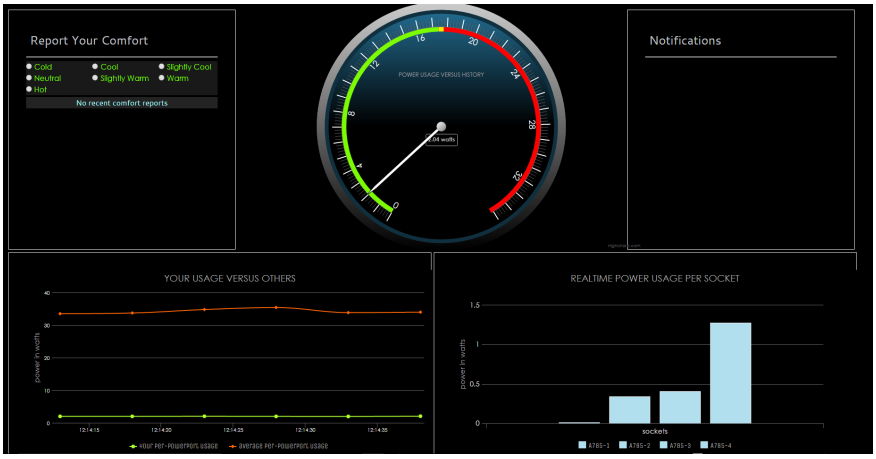

Bar chart (right bottom)

The **bar chart** represents your socket/channel-specific usage across all the channels in your powerstrip(s). The labels are based on the last 4 digits of the MAC address of your powerstrip, *found on the back side of your powerstrip*, and the socket/channel number, *illuminated in green on the top of every socket*.

- Use the knowledge about the high power devices to shape your power conservation strategies, should you wish to

Line chart (left bottom)

The green line in the **line chart** represents your instantaneous power usage aggregated across all of your powerstrips. The orange line represents the instantaneous aggregated consumption of an average user. In other words, it represents the average of aggregated usages represented by the green line charts in every dashboard.

- If green is below (above) the orange, then your instantaneous aggregate consumption is less (more) than that of the "average" user's instantaneous aggregated power consumption

Figure 2.5: Information provided to the participants during the *feedback only* phase of the experiment

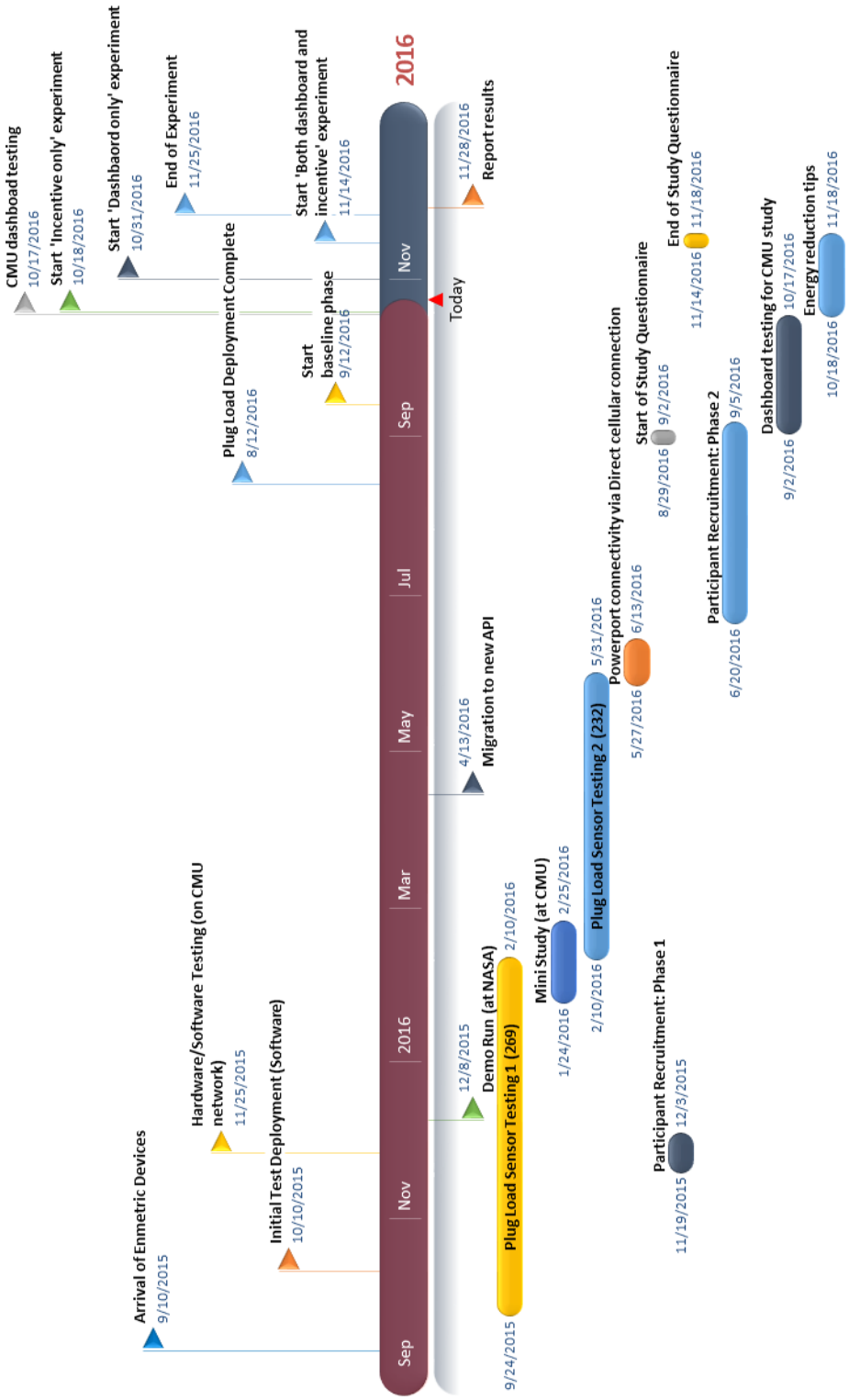

Figure 2.6: CMU experiment schedule

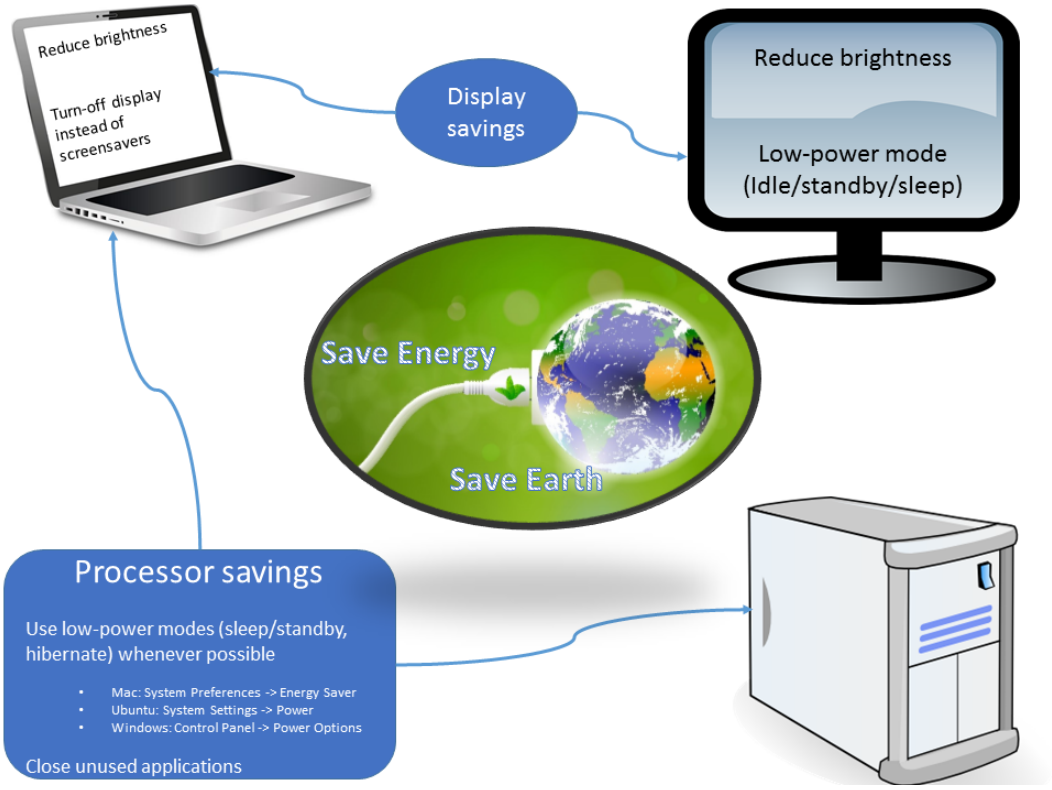

Figure 2.7: Possible energy conservation practices associated with workspace devices

Chapter 3

STATISTICAL INFERENCE

The results from the experiments at NASA and CMU were analyzed in the light of the assumptions made during the experiment design. The analysis involved hypothesis testing and confidence interval estimation based on a set of statistical assumptions. For developing regression-based models from the experimental data, the classical linear regression model are employed. In what follows, we describe the statistical analysis of the data from the NASA experiment followed by that of the CMU experiment. For the purpose of analysis, we consider the time window to be situated within the time frame of a day. Let the time window within a day be represented by $[t_0, tf)$, where $(t_f - t_0)$ denotes the number of seconds elapsed since the begin of the time window $t_0 >= 0$ until the end of the window $t_f < 86400$.

3.1 Analysis of the NASA experiment

The objective of the NASA feedback experiment was to quantify the impact of feedback on energy consumption. We start our analysis by introducing the relevant notation. For the baseline phase of the experiment, let the response variable (average power consumption) of the ith participant during the time interval $[t_0, t_f)$ be denoted by $y_{\mathcal{P}1_i^{\mathbb{N}}}(t_0, t_f)$. For the experiment phase, let the response and the input variables of the ith participant during the time interval $[t_0, t_f)$ be denoted by $y_{\mathcal{P}3_i^{\mathbb{N}}}(t_0, t_f)$ and $x^a_{\mathcal{P}3_i^{\mathbb{N}}}(t_0, t_f)$ respectively. The input variable refers to the screentime spent by the participant on the dashboard-based feedback provided to him/her. In order to perform statistical inference, we assume that the observed data points are the realizations of a random sample from the occupant population. This assumption is supported by the randomized design of the experiment. Let the random sample corresponding to the baseline response observation of the ith participant during the time interval $[t_0, t_f)$ be denoted by $Y_{\mathcal{P}1_i^{\mathbb{N}}}(t_0, t_f)$. Similarly let the corresponding random samples associated with the response and input observations of the experiment be represented by $Y_{\mathcal{P}3_i^{\mathbb{N}}}(t_0, t_f)$ and $X^a_{\mathcal{P}3_i^{\mathbb{N}}}(t_0, t_f)$ respectively. The realizations of these random samples from the current experiment are represented by the lower case names $y_{\mathcal{P}3_i^{\mathbb{N}}}(t_0, t_f)$ and $x^a_{\mathcal{P}3_i^{\mathbb{N}}}(t_0, t_f)$ respectively. Also, we represent the statistical summaries of random samples graphically using box plots. For purposes of interpretation, the legend associated with the box plot format used in this dissertation is shown in Figure 3.1.

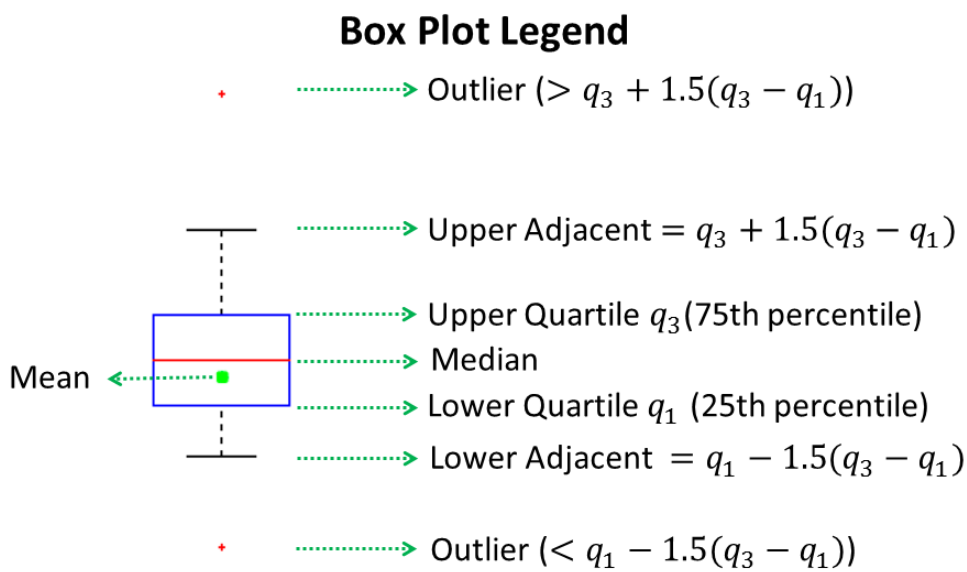

Figure 3.1: Legend associated with the box plot legend for representing statistical sample characteristics

3.1.1 Statistical assumptions

Given the random samples, we are interested in drawing inferences about the population behind the sample. To enable statistical inferences, we assume that the response samples $Y_{\mathcal{P}1_i^{\mathbb{N}}}(t_0, t_f)$ and $Y_{\mathcal{P}3_i^{\mathbb{N}}}(t_0, t_f)$ have a mean, variance and we represent them by $\left(\mu_{\mathcal{P}1_i^{\mathbb{N}}}(t_0, t_f), [\sigma_{\mathcal{P}1_i^{\mathbb{N}}}(t_0, t_f)]^2\right)$ and $\left(\mu_{\mathcal{P}3_i^{\mathbb{N}}}(t_0, t_f), [\sigma_{\mathcal{P}3_i^{\mathbb{N}}}(t_0, t_f)]^2\right)$ respectively for the different phases of the experiment. Furthermore, for purposes of regression analysis, we are almost always not concerned with the statistics of the input sample $X^a_{\mathcal{P}3_i^{\mathbb{N}}}(t_0, t_f)$ since we deal only with the conditional expectation of the response random variable conditioned upon the input variable. We refer the readers to [10] for further discussion on the requirement of specifying distributions of the input random variables in the context of regression analysis.

Given the knowledge about the statistics of the response variables, we draw our attention to the population constituted by differences between the random variables pertaining to the baseline and experiment responses. Let this difference

$Y_{\mathcal{P}1_i^{\mathbb{N}}}(t_0, t_f) - Y_{\mathcal{P}3_i^{\mathbb{N}}}(t_0, t_f)$ be represented by $\mathbb{Y}_i^{\mathbb{N}}(t_0, t_f)$. Given a matched pairs design in our case, this difference captures the improvement of an experiment response sample over its corresponding baseline response sample, both drawn from the population of occupants. Furthermore, any significant difference between the response variables during the experiment and baseline conditions can be attributed to a change in experiment conditions instead of attributing the difference to idiosyncratic factors in a participants behavior. In other words, the matched pairs design reduces the effects of confounding factors and strengthens the causal relationship, if any, between the differential response and the experimental conditions.

3.1.2 Hypothesis testing and confidence interval estimation

The statistical significance of the difference in means between the baseline and the experimental response samples was tested via a paired t-test. We note that the t-test can be used even for departures from the normality assumption in the population, more so if differences in populations are compared or if the sample sizes are large [7] [8], which happens to be case in our matched pairs t-test. The t-test requires that the means of the samples from the experiment be normally distributed and in our case, this assumption can be strengthened by using larger number of samples and appealing to the central limit theorem. For this t-test, let t_0 refer to midnight and t_f denote the subsequent midnight so that $t_0 = 0$ and $t_f = 24 \times 3600 = 86400$ sec. This allows the sample observations to correspond to average power data, averaged across the day for each day during both the baseline phase $\mathcal{P}1^{\mathbb{N}}$ and the experiment phase $\mathcal{P}3^{\mathbb{N}}$. The null and the alternative hypotheses are presented below:

1. $\mathbf{H}_0^{\mathbb{N}}$: $\mu_{\mathcal{P}1_i^{\mathbb{N}}}(0, 86400) - \mu_{\mathcal{P}3_i^{\mathbb{N}}}(0, 86400) = 0$
2. $\mathbf{H}_A^{\mathbb{N}}$: $\mu_{\mathcal{P}1_i^{\mathbb{N}}}(0, 86400) - \mu_{\mathcal{P}3_i^{\mathbb{N}}}(0, 86400) \neq 0$

Under the above assumptions, we conducted a paired sample two tailed t-test. The mean pre-treatment score was found to be 55.16 W and the mean post-treatment score was found to be 51.93 W. A matched-pairs t-test was performed to determine if the difference was significant. The t-statistic was significant at the .05 critical alpha level, t(219)=4.6512, p=5.7063×10^{-6}. Therefore, the evidence against the null hypothesis is statistically significant ($\alpha = 0.05$) and we conclude that the power usage during the experiment phase was (statistically) significantly different than the power usage during the baseline phase. The corresponding 95% confidence

interval of the mean parameter $\mu_{\mathcal{P}1_i^{\mathbb{N}}}(0, 86400) - \mu_{\mathcal{P}3_i^{\mathbb{N}}}(0, 86400)$ was found to be [3.74,9.26] W, or equivalently, a reduction of [6.79,16.78]% with a confidence of 95%. Since the difference is difference in means is positive, the conclusion is that the experimental usage $\mu_{\mathcal{P}3_i^{\mathbb{N}}}(0, 86400)$ is (statistically) significantly less than the baseline usage $\mu_{\mathcal{P}1_i^{\mathbb{N}}}(0, 86400)$. The statistical summary of both the experiment and the baseline phase energy consumption (kWh) is shown in Figure 3.2.

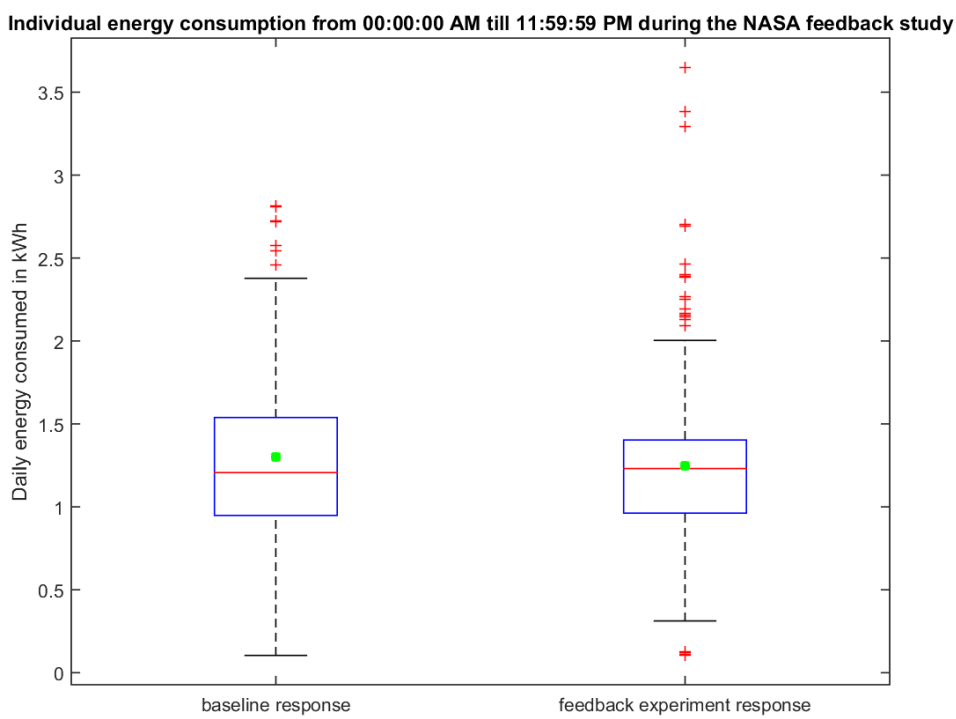

Figure 3.2: Statistical summary of the data from the NASA experiment

3.1.3 Regression-based modeling

Given the observed reduction, we seek explanations to quantify this reduction based on the knowledge of input variables. For the purposes of regression analysis, let d_e, d_b denote a day in the experiment dataset and the corresponding day in the baseline dataset respectively. We also use a single argument $h \in \{1, ..., 24\}$ to represent the hour of a day enclosed in an interval $[t_0^h, t_f^h]$. Therefore, we can write the experiment and baseline hourly consumption of the ith participant during hour h as $Y_{\mathcal{P}3_i^{\mathbb{N}}}(h)$, $Y_{\mathcal{P}1_i^{\mathbb{N}}}(h)$ respectively. Also, let ':' denote the sample mean of the participant pool when used in place of 'i', the index corresponding to the ith participant. We then hypothesize that the mean differential response $\Delta\mu_{\mathbb{N}_:}(h) := \mu_{\mathcal{P}1_:^{\mathbb{N}}}(h) - \mu_{\mathcal{P}3_:^{\mathbb{N}}}(h)$ can

$\alpha^{\mathbb{N}}$	$\beta^{\mathbb{N}}$	$\gamma^{\mathbb{N}}$	$\sigma_{\epsilon_{\cdot}}$
-0.05116	0.8253	-0.00453	4.0583

Table 3.1: Regression model parameter estimates from the NASA experiment

be modeled as a linear first-order autoregressive model AR(1) with screentime as the exogenous regressor. Written otherwise,

$$\Delta\mu_{\mathbb{N}_{\cdot}}(h) = \alpha^{\mathbb{N}} + \beta^{\mathbb{N}}\Delta\mu_{\mathbb{N}_{\cdot}}(h-1) + \gamma^{\mathbb{N}} x^{a}_{\mathcal{P}3^{\mathbb{N}}_{i}}(h-1) + \epsilon_h \tag{3.1}$$

The time-lagged dependent term $\Delta\mu_{\mathbb{N}_{\cdot}}(h-1)$ is instrumental in weakening the residual serial correlation across the various time instants. Figure 3.3 shows the impact of adding time-lagged dependent variables on the serial correlation of the errors. The consistency in the residual serial correlation after one lag indicates that most of the time-dependent information is captured by the introduction of one-lag in the model, and introducing additional lags does not contribute to significant new information as far as weakening the residual serial correlation is concerned. From the experimental standpoint, this time-lagged dependent variable captures the change in experiment conditions with respect to the baseline conditions. For example, any change in work schedules between the baseline and the experiment can be captured by the time-lagged dependent term in the model, and hence allow us to strengthen the assumption that the residuals corresponding to consecutive hours are a result of random factors between those hours and that the residuals are uncorrelated in time given the model inputs. Along with the residual autocorrelation plot, the root mean square error as a function of time-lags (shown in figure 3.4) was considered to make the decision about the number of lags that need to be introduced in the model.

We also note that the above model can be interpreted as representing $\Delta\mu_{\mathbb{N}_{\cdot}}(h)$ by a first-order discrete-time continuous-state Markov chain with screentime as the exogenous input. Consequently, we also observe that the power consumption during the current hour $Y_{\mathcal{P}3^{\mathbb{N}}_{i}}(h)$ depends on the power consumption during the previous hour $Y_{\mathcal{P}3^{\mathbb{N}}_{i}}(h-1)$. Therefore, we note that $Y_{\mathcal{P}3^{\mathbb{N}}_{i}}(h)$ also follows a Markov process with the baselines and screentime as exogenous inputs. Given this rationale behind the autoregressive model, we proceed to estimate the coefficients of the model. The parameters of the linear model are listed in table 3.1, and were estimated using ordinary least squares (OLS) by the MATLAB system identification toolbox.

The prediction performed on the test dataset is shown in the figure 3.5. The figure represents the power consumed (absolute power and not the difference with respect to

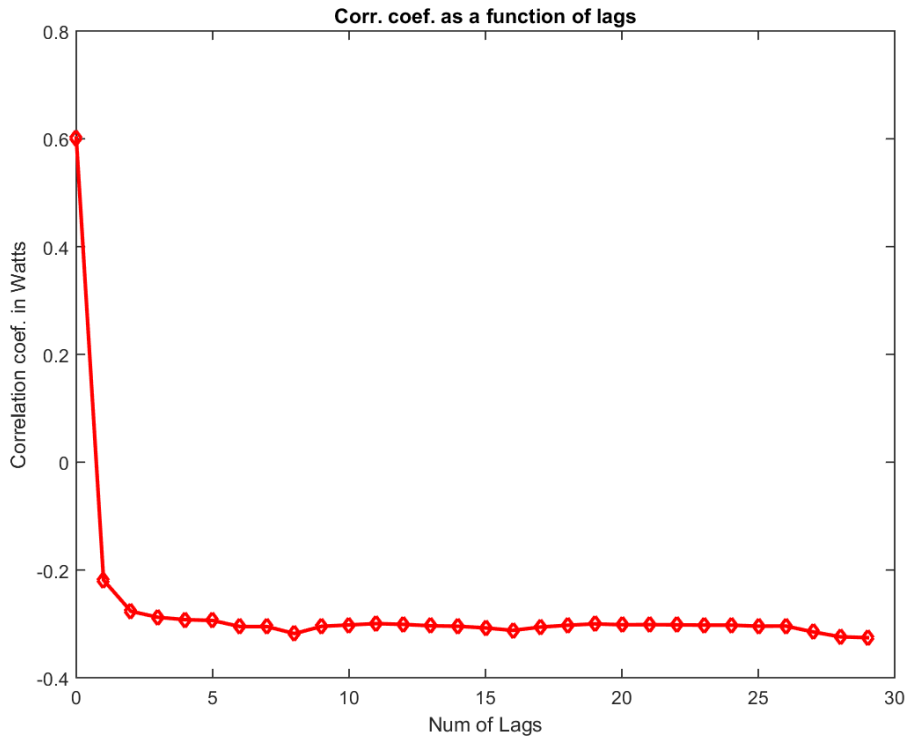

Figure 3.3: Serial correlation of residuals against the number of time-lagged dependent variable in the NASA experiment

the baseline) in the experiment against the predictions, along with their confidence intervals. The root mean square error was found to the 5.19 W, and the 95% confidence interval (averaged across all data points) was found to be [13.18, 17.18] W.

3.1.4 Discussion

Our findings indicate that the average plugload reduction between the baseline and the experiment is 11.79%, along with a 95% confidence interval corresponding to a [6.79,16.78]% reduction per occupant. Prior to the statistical analysis, the inactivity of the participants (using no power) were accounted for by applying a threshold of 2.5 W per channel on the dataset during the pre-processing stage. This ensured that any savings estimated are only due to reducing power consumption actively. However, this also means that the analysis didn't account for any change in behavior due to turning off devices when not in use, and hence our estimates may be considered conservative. The observed significant reduction could be the result of feedback-induced behavioral changes captured by the screentime variable or due

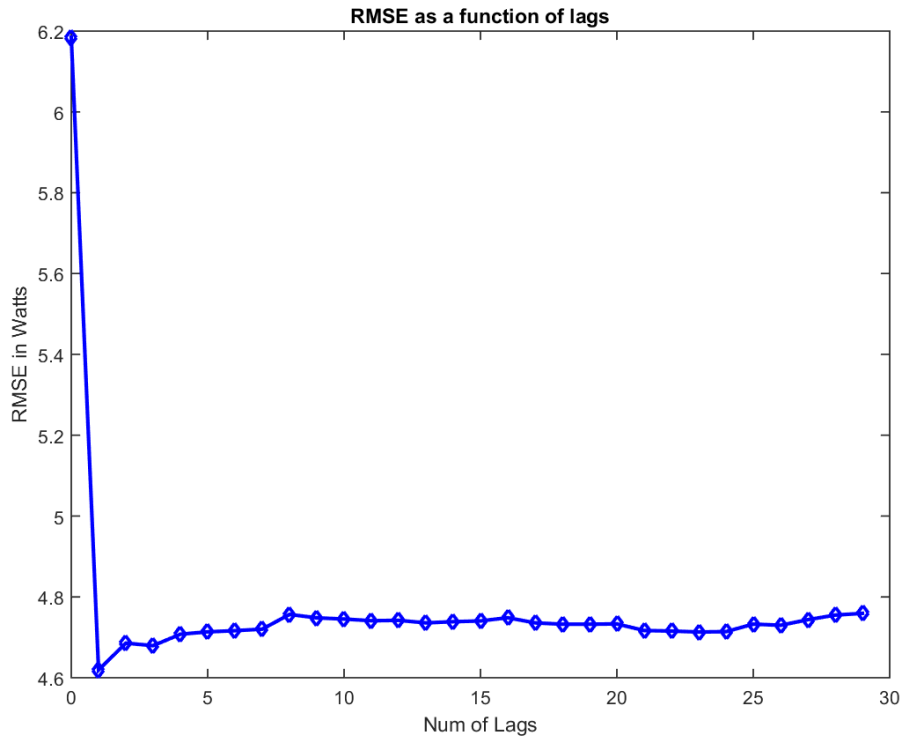

Figure 3.4: Residual RMS against the number of time-lagged dependent variable in the NASA experiment

to changes induced by factors such the hawthorne effect indicated by the bias term [56]. In the auto-regressive model, we note that by increasing the number of lags the root mean squared error does not vary much as shown in Figure 3.4. This suggests that the relationship between the inputs and the output in the auto-regressive model is non-linear, which can only be approximated by a linear model. Furthermore, since the residuals have zero-mean, and are uncorrelated, we note that the extent to which the random factors dictating the residual processes result in a constant variance in the residuals determines the validity of the conditions for the application of the Gauss-Markov theorem. Given the validity of these conditions, the linear least squares estimator can be considered the best linear unbiased estimator.

3.2 Analysis of the CMU experiment

The objective of the experiments conducted at CMU was to quantify the impact of feedback and incentives on occupant plugload consumption. This objective is realized by comparing the power usage from the three phases of the experiment $\mathcal{P}2^{\mathbb{C}}$,$\mathcal{P}3^{\mathbb{C}}$, and $\mathcal{P}4^{\mathbb{C}}$ against the baseline usage to draw inferences about the impact

of *incentives alone*, *feedback alone*, and *both incentives and feedback* respectively. We introduce the relevant notation prior to the analysis. Let the response variable (average power consumption) of the ith participant during the time interval $[t_0, t_f)$ within the baseline phase $\mathcal{P}1^{\mathbb{C}}$ be denoted by $y_{\mathcal{P}1_i^{\mathbb{C}}}(t_0, t_f)$. For the incentive experiment phase $\mathcal{P}2^{\mathbb{C}}$, let the response and the input variables of the ith participant during the time interval $[t_0, t_f)$ be denoted by $y_{\mathcal{P}2_i^{\mathbb{C}}}(t_0, t_f)$ and $\left(x^a_{\mathcal{P}2_i^{\mathbb{C}}}(t_0, t_f), x^i_{\mathcal{P}2_i^{\mathbb{C}}}(t_0, t_f)\right)$ respectively. The input variables in the ordered pair represent the screentime spent on the scoreboard and the incentive quantity respectively. In this experiment, the incentive was held fixed during each day. Written otherwise, $x^i_{\mathcal{P}2_i^{\mathbb{C}}}(t_0, t_f)$ is constant between $t_0 = 0$ and $t_f = 86400$ sec for a given observation. Similarly, for the dashboard feedback experiment phase $\mathcal{P}3^{\mathbb{C}}$, let the response and the input variables (screentime) of the ith participant during the time interval $[t_0, t_f)$ be denoted by $y_{\mathcal{P}3_i^{\mathbb{C}}}(t_0, t_f)$ and $x^a_{\mathcal{P}2_i^{\mathbb{C}}}(t_0, t_f)$ respectively. During the last phase of the experiment $\mathcal{P}4^{\mathbb{C}}$ consisting of both the feedback and incentives, let the response and the input variables of the ith participant during the time interval $[t_0, t_f)$ be denoted by $y_{\mathcal{P}4_i^{\mathbb{C}}}(t_0, t_f)$ and $\left(x^a_{\mathcal{P}4_i^{\mathbb{C}}}(t_0, t_f), x^i_{\mathcal{P}4_i^{\mathbb{C}}}(t_0, t_f)\right)$ respectively. In this case, the input ordered pair represents the time spent on the dashboard and the incentive amount respectively. In order to perform statistical inference, we assume that the observed data points are the realizations of a random sample from the occupant population. Let the random sample corresponding to the response observations of the ith participant during the time interval $[t_0, t_f)$ for each of the phases $\mathcal{P}1^{\mathbb{C}}$, $\mathcal{P}2^{\mathbb{C}}$, $\mathcal{P}3^{\mathbb{C}}$, and $\mathcal{P}4^{\mathbb{C}}$ be denoted by $Y_{\mathcal{P}1_i^{\mathbb{C}}}(t_0, t_f)$, $Y_{\mathcal{P}2_i^{\mathbb{C}}}(t_0, t_f)$, $Y_{\mathcal{P}3_i^{\mathbb{C}}}(t_0, t_f)$, and $Y_{\mathcal{P}4_i^{\mathbb{C}}}(t_0, t_f)$ respectively. Similarly, let the corresponding random samples associated with the input observations during each of the three experiment phases $\mathcal{P}2^{\mathbb{C}}$, $\mathcal{P}3^{\mathbb{C}}$, and $\mathcal{P}4^{\mathbb{C}}$ be represented by $\left(X^a_{\mathcal{P}2_i^{\mathbb{N}}}(t_0, t_f), X^i_{\mathcal{P}2_i^{\mathbb{N}}}(t_0, t_f)\right)$, $\left(X^a_{\mathcal{P}3_i^{\mathbb{N}}}(t_0, t_f)\right)$, and $\left(X^a_{\mathcal{P}4_i^{\mathbb{N}}}(t_0, t_f), X^i_{\mathcal{P}4_i^{\mathbb{N}}}(t_0, t_f)\right)$ respectively.

3.2.1 Statistical assumptions

Given the random samples above, we make assumptions about the distributions of their respective populations to infer statistical properties of the observed sample. Specifically, we assume that the first and second moments of the distribution of the response samples exist for all the phases of the experiment. Written otherwise, $Y_{\mathcal{P}1_i^{\mathbb{C}}}(t_0, t_f)$, $Y_{\mathcal{P}2_i^{\mathbb{C}}}(t_0, t_f)$, $Y_{\mathcal{P}3_i^{\mathbb{C}}}(t_0, t_f)$ are assumed to have a mean, variance represented by $\left(\mu_{\mathcal{P}1_i^{\mathbb{C}}}(t_0, t_f), [\sigma_{\mathcal{P}1_i^{\mathbb{C}}}(t_0, t_f)]^2\right)$, $\left(\mu_{\mathcal{P}2_i^{\mathbb{C}}}(t_0, t_f), [\sigma_{\mathcal{P}2_i^{\mathbb{C}}}(t_0, t_f)]^2\right)$, $\left(\mu_{\mathcal{P}3_i^{\mathbb{C}}}(t_0, t_f), [\sigma_{\mathcal{P}3_i^{\mathbb{C}}}(t_0, t_f)]^2\right)$, and $\left(\mu_{\mathcal{P}4_i^{\mathbb{C}}}(t_0, t_f), [\sigma_{\mathcal{P}4_i^{\mathbb{C}}}(t_0, t_f)]^2\right)$ respectively. Similar to the regression analysis from the NASA experiment, we are not concerned with

either the normality of the response data or with the statistics of the input samples since we deal only with the conditional expectation of the response random variable conditioned upon the realizations of the input random variable(s) [10]. To infer the difference between populations exposed to the experimental conditions vs the baseline populations, we draw our attention to the population constituted by differences between the random variables pertaining to the baseline and experiment responses. Let the difference in the ith random variables during $\mathcal{P}1^{\mathbb{C}}$ and $\mathcal{P}j^{\mathbb{C}}$, $j \in \{1, 2, 3\}$ be denoted by $Y_{\mathcal{P}1\mathcal{P}j_i^{\mathbb{N}}}(t_0, t_f) := Y_{\mathcal{P}1_i^{\mathbb{C}}}(t_0, t_f) - Y_{\mathcal{P}j_i^{\mathbb{C}}}(t_0, t_f)$. Given a matched pairs experimental design similar to that of the NASA experimental design, any inferences from the difference population $Y_{\mathcal{P}1\mathcal{P}j_i^{\mathbb{N}}}(t_0, t_f)$ can be attributed to change in the conditions during $\mathcal{P}j^{\mathbb{N}}$, and not to the idiosyncratic factors in individual participant's behavior. Therefore, this strengthened causal connection enables a more focused experimental analysis.

3.2.2 Hypothesis testing and confidence interval estimation

Given the assumptions about the population consisting of the difference in baseline and experiment responses $Y_{\mathcal{P}1\mathcal{P}j_i^{\mathbb{N}}}(t_0, t_f)$, $j \in 2, 3, 4$, we seek to answer if there exists any underlying difference in the population responses that indicate a statistically significant power reduction over the baseline conditions. We perform hypothesis tests and also obtain the 95% confidence interval estimates on the differential mean parameter $\mu_{\mathcal{P}1_i^{\mathbb{C}}}(t_0, t_f) - \mu_{\mathcal{P}j_i^{\mathbb{C}}}(t_0, t_f)$, $j \in 2, 3, 4$.

3.2.2.1 CMU incentive experiment phase $\mathcal{P}2^{\mathbb{C}}$

Since we are concerned in the population consisting of the difference in means, we can formulate our null and alternate hypothesis for the incentive experiment analysis as follows:

1. $\mathbf{H}_0^{2\mathbb{C}}$: $\mu_{\mathcal{P}1_i^{\mathbb{C}}}(0, 86400) - \mu_{\mathcal{P}2_i^{\mathbb{C}}}(0, 86400) = 0$
2. $\mathbf{H}_A^{2\mathbb{C}}$: $\mu_{\mathcal{P}1_i^{\mathbb{C}}}(0, 86400) - \mu_{\mathcal{P}2_i^{\mathbb{C}}}(0, 86400) \neq 0$

By performing a paired difference two tailed t-test, we found the following. The pre-treatment and the post-treatment scores were found to be 68.83 W and 53.66 W. The t-statistic was significant (t(117)=2.8597, $\alpha = 0.05$) with a p-value of 0.005. Therefore, the evidence against the null hypothesis is statistically significant ($\alpha = 0.05$) and we conclude that the power usage during the incentive experiment phase

was (statistically) significantly different than the power usage during the baseline phase. The corresponding 95% confidence interval of the mean parameter was found to be [4.22,23.23] W, or equivalently a reduction [6.13,33.76]% with a confidence of 95% compared to the baseline power use. Since the difference is difference in means is positive, the conclusion is that the incentive experimental usage $\mu_{\mathcal{P}2_i^{\mathbb{C}}}(0, 86400)$ is (statistically) significantly less than the baseline usage $\mu_{\mathcal{P}1_i^{\mathbb{C}}}(0, 86400)$. The statistical summary of both the incentive experiment and the baseline phase energy consumption (kWh) is shown in the Figure 3.6.

3.2.2.2 CMU feedback experiment phase $\mathcal{P}3^{\mathbb{C}}$

Similar to the incentive experiment analysis, we formulate the null and alternate hypothesis for the feedback experiment analysis as follows:

1. $\mathbf{H}_0^{3\mathbb{C}}$: $\mu_{\mathcal{P}1_i^{\mathbb{C}}}(0, 86400) - \mu_{\mathcal{P}3_i^{\mathbb{C}}}(0, 86400) = 0$
2. $\mathbf{H}_A^{3\mathbb{C}}$: $\mu_{\mathcal{P}1_i^{\mathbb{C}}}(0, 86400) - \mu_{\mathcal{P}3_i^{\mathbb{C}}}(0, 86400) \neq 0$

For the matched pairs two tailed t-test, the pre-treatment and the post-treatment scores were found to be 65.53 W and 50.26 W. The t-statistic was significant (t(94)=2.9567, $\alpha = 0.05$) with a p-value of 0.0039. Therefore, the evidence against the null hypothesis is statistically significant ($\alpha = 0.05$) and we conclude that the power usage during the feedback experiment phase was (statistically) significantly different than the power usage during the baseline phase. The corresponding 95% confidence interval of the mean parameter was found to be [5.21,26.53] W, or equivalently a reduction of [7.95,40.48]% with a confidence of 95% compared to the baseline. Since the difference in means is positive, the conclusion is that the incentive experimental usage $\mu_{\mathcal{P}3_i^{\mathbb{C}}}(0, 86400)$ is (statistically) significantly less than the baseline usage $\mu_{\mathcal{P}1_i^{\mathbb{C}}}(0, 86400)$. The statistical summary of both the incentive experiment and the baseline phase energy consumption (kWh) is shown in the Figure 3.7.

3.2.2.3 CMU incentive and feedback experiment phase $\mathcal{P}4^{\mathbb{C}}$

Similar to the analysis with either interventions (feedback or incentives), we formulate the null and alternate hypothesis for the incentive and feedback experiment analysis as follows:

1. $\mathbf{H}_0^{4\mathbb{C}}$: $\mu_{\mathcal{P}1_i^{\mathbb{C}}}(0, 86400) - \mu_{\mathcal{P}4_i^{\mathbb{C}}}(0, 86400) = 0$

2. $\mathbf{H}_A^{4\mathbb{C}}$: $\mu_{\mathcal{P}1_i^{\mathbb{C}}}(0, 86400) - \mu_{\mathcal{P}4_i^{\mathbb{C}}}(0, 86400) \neq 0$

A matched pairs t-test confirmed that the t-statistic was significant (t(75)=2.83, α = 0.05) with a p-value of 0.006. Therefore, the evidence against the null hypothesis is statistically significant (α = 0.05) and we conclude that the power usage during the incentive and feedback experiment phase was (statistically) significantly different than the power usage during the baseline phase. The corresponding 95% confidence interval of the mean parameter was found to be [4.92,28.30] W, or equivalently a relative change of [7.75,44.61]% with a confidence of 95% compared to the baseline. Since the difference in means is positive, the conclusion is that the usage in the presence of both incentive and feedback interventions $\mu_{\mathcal{P}4_i^{\mathbb{C}}}(0, 86400)$ is (statistically) significantly less than the baseline usage $\mu_{\mathcal{P}1_i^{\mathbb{C}}}(0, 86400)$. The statistical summary of both the incentive experiment and the baseline phase energy consumption (kWh) is shown in the Figure 3.8.

3.2.3 Regression-based modeling

Given the knowledge about the significant mean difference in the responses of the underlying occupant population, it is of interest to construct a model that can explain the observed changes. We attempt to construct a linear model based on data from all the experiment phases. For the purposes of regression analysis, let d_e, d_b denote a day in the experiment dataset (from any phase of the experiment) and the corresponding day in the baseline dataset respectively. We also use a single argument $h \in \{1, ..., 24\}$ to represent the hour of a day enclosed in an interval $[t_0^h, t_f^h]$. Therefore, we can write the feedback experiment and baseline hourly consumption of the ith participant during hour h as $Y_{\mathcal{P}3_i^{\mathbb{N}}}(h)$ and $Y_{\mathcal{P}1_i^{\mathbb{N}}}(h)$ respectively. Furthermore, since the regression model includes the data from all the phases of the experiment, we denote all the experiment phases (*incentive only*,*feedback only*, and *both incentive and feedback*) by $\mathcal{P}e^{\mathbb{C}}$, and that the notation influences the downstream such as the experimental response, observed, mean variables as $y_{\mathcal{P}e_i^{\mathbb{C}}}(h)$, $\left(xa_{\mathcal{P}e_i^{\mathbb{C}}}(h), xi_{\mathcal{P}e_i^{\mathbb{C}}}(h)\right)$, $\mu_{\mathcal{P}e_i^{\mathbb{C}}}(h)$ respectively. Also, let ':' denote the sample mean of the participant pool when used in place of 'i', the index corresponding to the ith participant. We then hypothesize that the mean differential response, denoted by $\Delta\mu_{\mathbb{C}_:}(h) := \mu_{\mathcal{P}1_:^{\mathbb{C}}}(h) - \mu_{\mathcal{P}e_:^{\mathbb{C}}}(h)$ can be modeled as a linear first-order autoregressive model AR(1) with screentime as the exogenous regressor. Written otherwise,

$$\Delta\mu_{\mathbb{C}_:}(h) = \alpha^{\mathbb{C}} + \beta^{\mathbb{C}}\Delta\mu_{\mathbb{C}_:}(h-1) + \gamma^{\mathbb{C}}x^a_{\mathcal{P}e_i^{\mathbb{C}}}(h-1) + \delta^{\mathbb{C}}x^i_{\mathcal{P}e_i^{\mathbb{C}}}(h-1) + \epsilon_h \tag{3.2}$$

$\alpha^{\mathbb{C}}$	$\beta^{\mathbb{C}}$	$\gamma^{\mathbb{C}}$	$\delta^{\mathbb{C}}$	$\sigma_{\epsilon_{\cdot}}$
-1.744	0.7898	-0.05778	-0.4293	6.6873

Table 3.2: Regression model parameter estimates from the CMU experiment

The time-lagged dependent term $\Delta\mu_{\mathbb{C}_{\cdot}}(h-1)$ is instrumental in weakening the residual serial correlation across the various time instants. Figure 3.9 shows the impact of adding time-lagged dependent variables on the serial correlation of the errors. The consistency in the residual serial correlation after a couple of lag indicates that most of the time-dependent information is captured by the introduction of two lags in the model, and introducing additional lags does not contribute to significant new information as far as weakening the residual serial correlation is concerned. From the experimental standpoint, this time-lagged dependent variable captures the change in experiment conditions with respect to the baseline conditions. For example, any change in work schedules between the baseline and the experiment can be captured by the time-lagged dependent terms in the model, and hence allow us to strengthen the assumption that the residuals corresponding to consecutive hours are a result of random factors between those hours and that the residuals are uncorrelated in time given the model inputs. Along with the residual autocorrelation plot, the root mean square error as a function of time-lags (shown in figure 3.10) was considered to make the decision about the number of lags that need to be introduced in the model. We also note that the above model can be interpreted as representing $\Delta\mu_{\mathbb{C}_{\cdot}}(h)$ by a first-order discrete-time continuous-state controllable Markov chain with incentive as the control input and screentime as the exogenous input. Consequently, we also observe that the power consumption during the hour 'h' $Y_{\mathcal{P}e_i^{\mathbb{C}}}(h)$ depends on the power consumption during hour 'h-1' $Y_{\mathcal{P}e_i^{\mathbb{C}}}(h-1)$. Therefore, we note that $Y_{\mathcal{P}e_i^{\mathbb{C}}}(h)$ also follows a controllable Markov process with the incentive as the control input, and the baselines, screentime as exogenous inputs. Given this rationale behind the autoregressive model, we proceed to estimate the coefficients of the model. The parameters of the linear model are listed in table 3.2, and were estimated using ordinary least squares (OLS) by the MATLAB system identification toolbox. The prediction performed on the test dataset is shown in the figure 3.11. The figure represents the power consumed (absolute power and not the difference with respect to the baseline) in the experiment against the predictions, along with their confidence intervals. The root mean square error was found to the 2.1543 W, and the 95% confidence interval (averaged across all data points) was found to be

[16.28, 23.58] W.

3.2.4 Discussion

The data from three experiment subjects from the CMU study was not considered for analysis due to the following reasons: plugging in new loads (space heaters), extreme increase in workloads due to very different work schedule, or for taking a vacation during the experiment phases. Furthermore, similar to the NASA experiment, we accounted for inactivity by only considering some samples for hypothesis testing whose power data was larger than a threshold (2.5 W per channel/device). Therefore the results of the hypothesis test in terms of the percentage reduction in experiment phase may be considered conservative as in the case of the NASA experiment.

We also note that the 95% confidence intervals indicate that the power reduction over the feedback phase [7.95,40.48]% is, on an average, greater than the power reduction over the incentive phase [6.13,33.76]%. This can be explained as follows based on our interactions with the participants after the experiment. During the incentive phase $\mathcal{P}2^{\mathbb{C}}$, some participants were reported to have cultivated energy conservation practices, which possibly manifested in the observed power reduction during the dashboard feedback phase. In other words, after the incentive phase was complete, there were only a couple of days prior to the begin of the experiment phase due to design constraints. This did not provide a sufficient washout period for the participants to revert back to their baseline behavior, which supposedly represents their stable equilibrium. These findings from the CMU experiment can be leveraged by the building manager to prepare an efficient power reduction strategy by an incentive intervention phase followed by feedback phase. This strategy seeks to achieve power reduction over a greater period of time by investing in the incentives of a relatively lesser period of time [1]. In case of both the incentive and the feedback phase $\mathcal{P}4^{\mathbb{C}}$, the mean reduction was found to be only slightly higher than the feedback phase $\mathcal{P}3^{\mathbb{C}}$. This could be due to the limited scope to reduce the consumption without significantly affecting the productivity of the participants. In other words, the scope for reduction could have been realized to a large extent during the incentive-only or feedback-only phases of the experiment thereby reducing the further scope available for reduction during the incentive and baseline phase of the experiment.

In the auto-regressive model, the observed significant reduction can be explained as a collective result of feedback, incentives, and/or bias factors such as the hawthorne

[1] The duration of these time periods would depend on the ability of the participant pool to imbibe and retain energy conservation practices

effect [56]. We also note that the addition of lags to the auto-regressive model does not vary the root mean squared error significantly as shown in Figure 3.10. This suggests that the linear model has fundamental limitations in attempting to approximate the possible non-linear relationships between the output and the inputs. Furthermore, since the residuals have a zero-mean, and are uncorrelated, we note that the extent to which the random factors determining the residual processes have closer to a constant variance the validity the assumptions pertaining to the Gauss-Markov theorem are strengthened, and in such cases the OLS estimates would be closer to the best linear unbiased estimate.

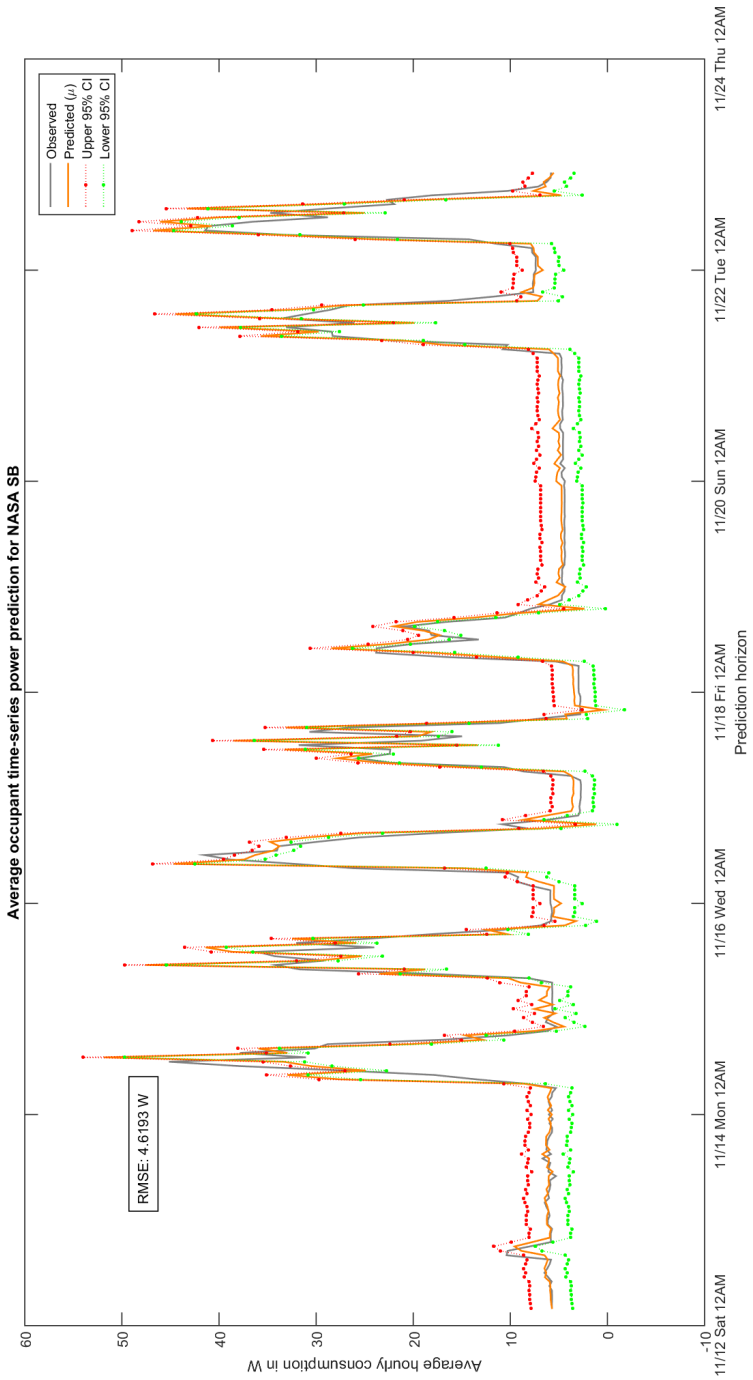

Figure 3.5: Power prediction in light of the observed data from the NASA experiment

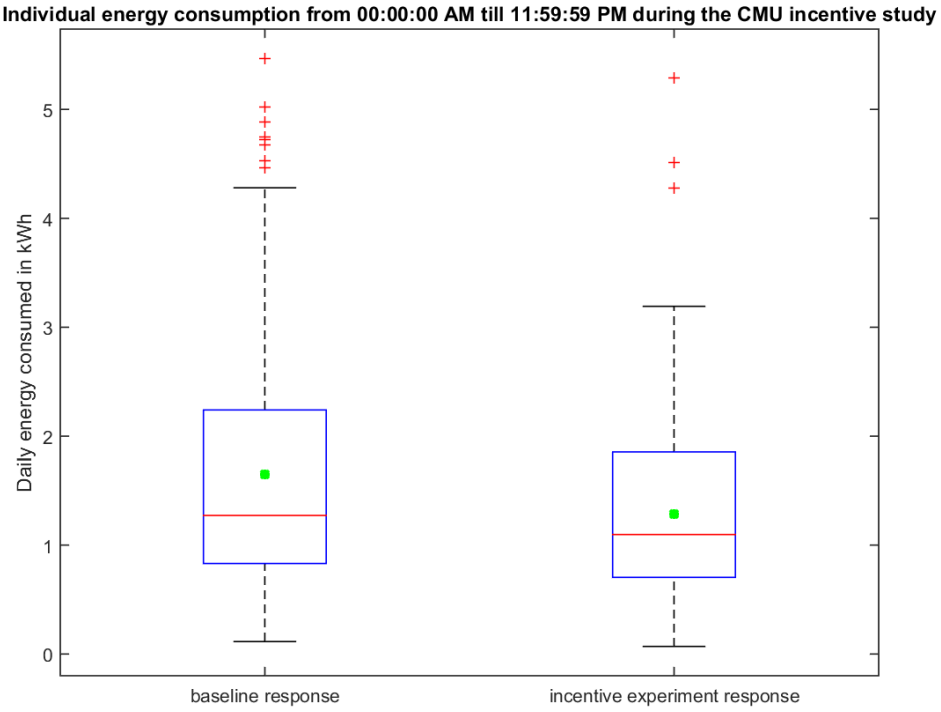

Figure 3.6: Statistical summary of the data from the CMU incentive experiment

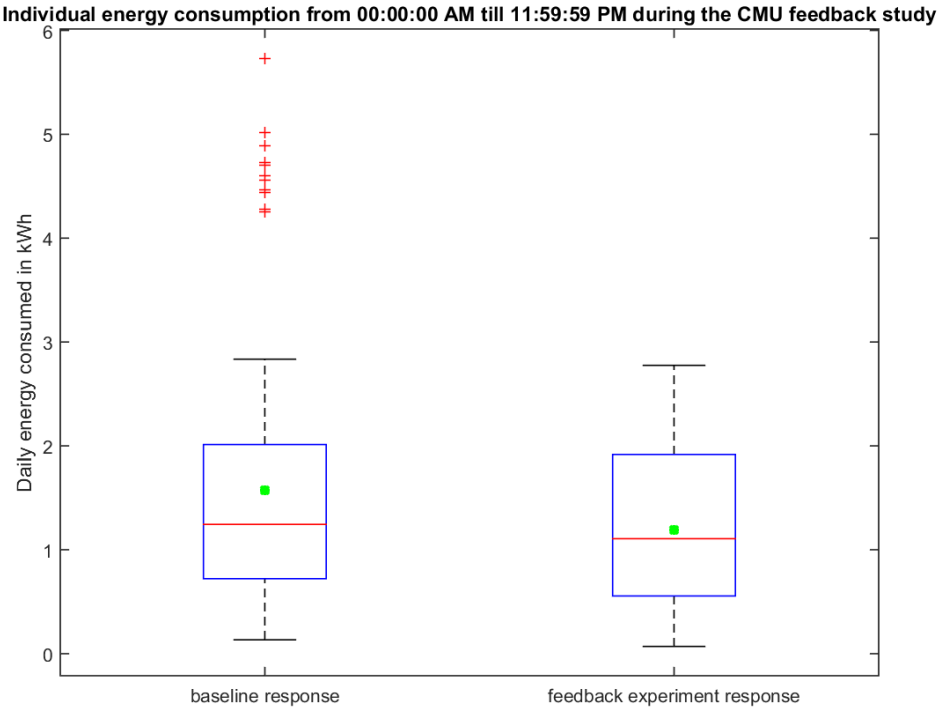

Figure 3.7: Statistical summary of the data from the CMU feedback experiment

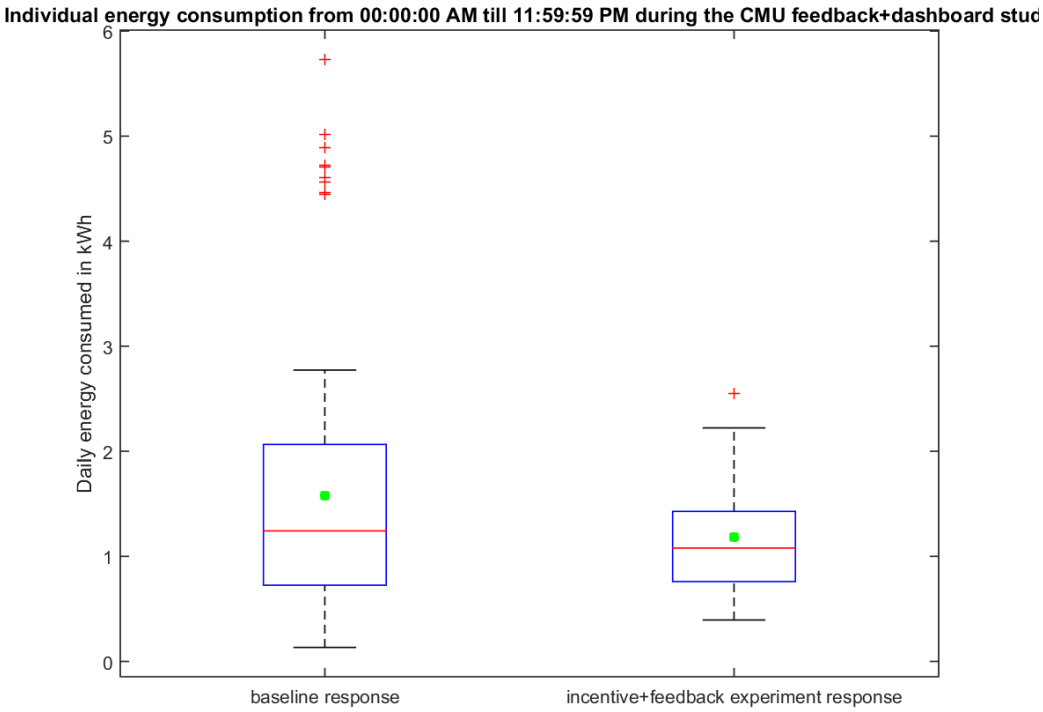

Figure 3.8: Statistical summary of the data from the CMU incentive and feedback experiment

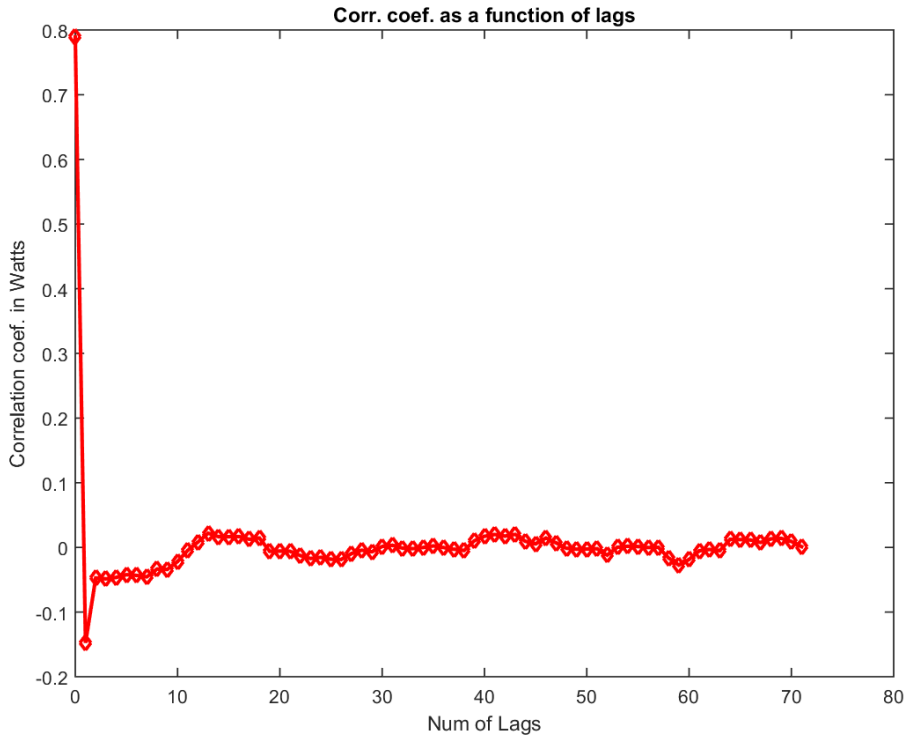

Figure 3.9: Serial correlation of residuals against the number of time-lagged dependent variable in the NASA experiment

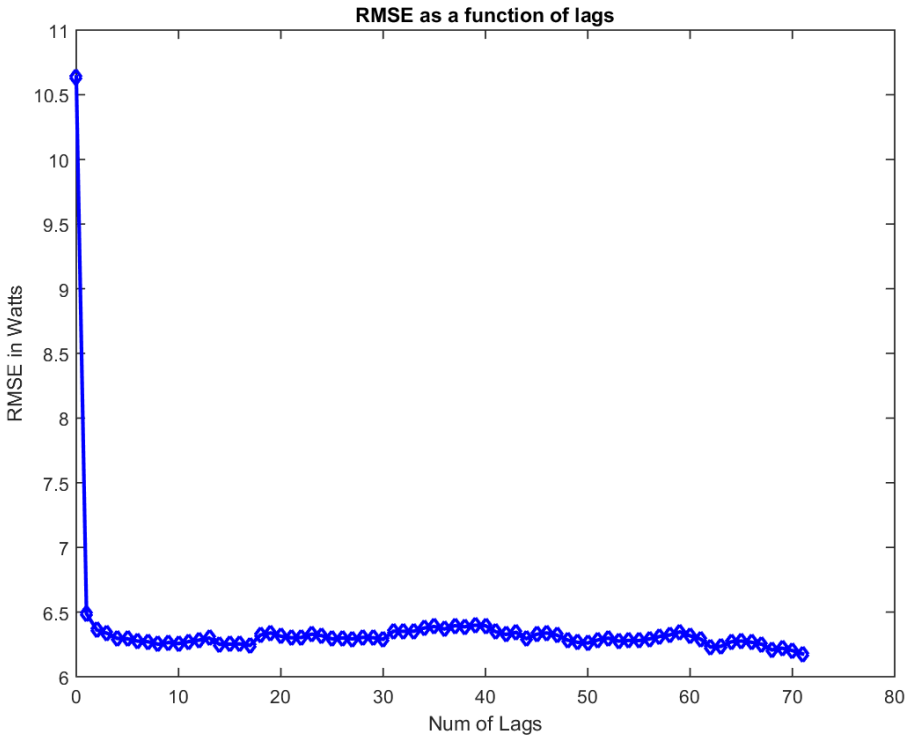

Figure 3.10: Residual RMS against the number of time-lagged dependent variable in the CMU experiment

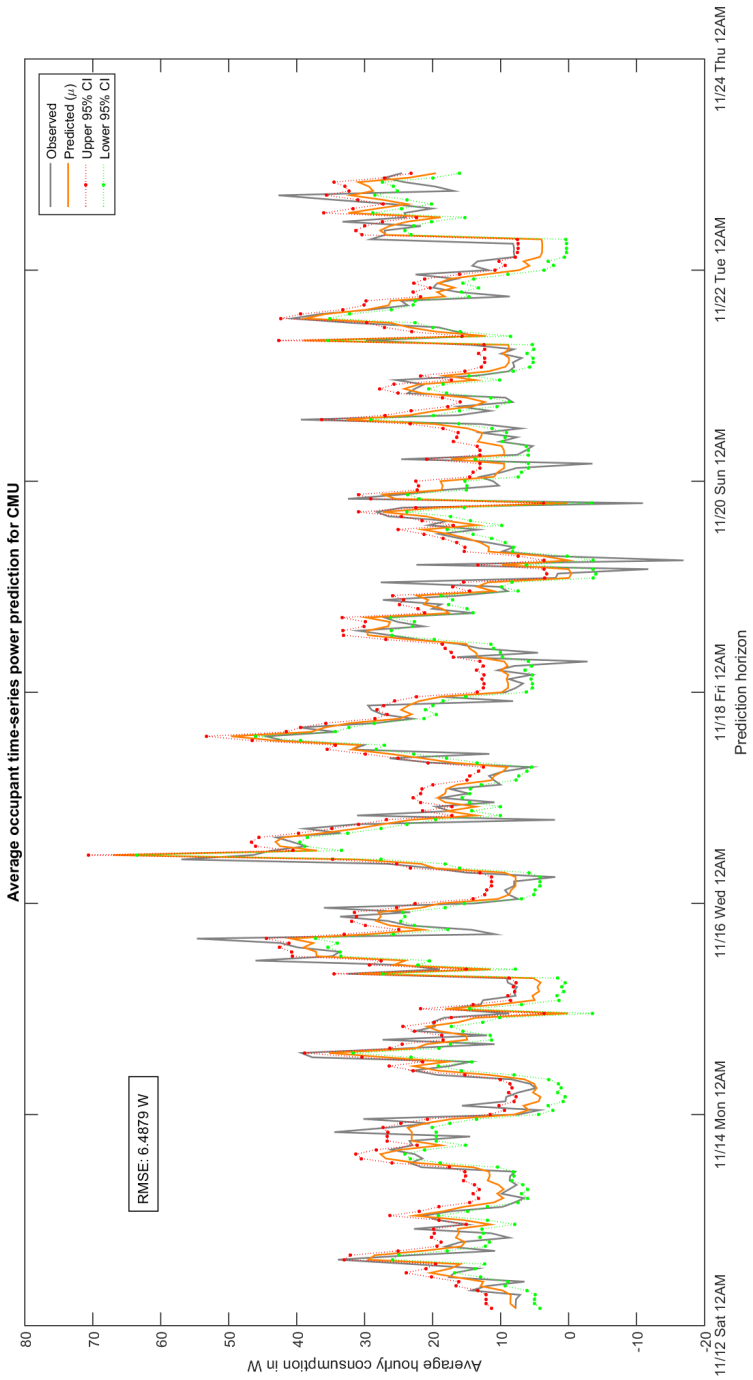

Figure 3.11: Power prediction in light of the observed data from the CMU experiment

Chapter 4

PLUGLOAD-INTEGRATED CONTROLLABLE DEMAND MODEL

Given the ability of feedback and incentives in lowering plug load consumption within commercial buildings, we attempt to integrate the plugload model into larger building demand models. In this chapter, we illustrate the proof-of-concept integration of the plugload models into the building model. First, we formulate a data-based demand model by excluding plugload consumption, and then include the incentive and screentime-driven plugload consumption model to obtain a plugload-integrated controllable demand model in Section 4.2.

4.1 Discrete time notation

We develop the temporal notation in this section that will be referred to in this chapter (demand model) and the subsequent ones that describe the weather forecast-driven solar model, and the integrated decision framework.

Let the time interval of interest be denoted by $\mathcal{I} := [t_{st}, t_{end}]$, where t_{st} and t_{end} denote the start and end times respectively. Also, let a collection of subsets $\{[t_{k-1}, t_k)\}_{k=1}^{N}$ denote a partition $\mathbf{T}$ of the interval $\mathcal{I}$ such that the following properties hold:

$$\begin{aligned} t_0 &= t_{st} \\ t_N &= t_{end} \\ t_k &= t_1 + (k-1)\Delta t \end{aligned} \tag{4.1}$$

where Δt represents the difference between consecutive instants in time. We also construct a sequence of points $\mathcal{T} = \{t_k\}_{k=0}^{N}$ that represents a discrete time instants in the interval $\mathcal{I}$ at which we make predictions and decisions. For this reason, we refer to the elements in the set $\mathcal{T}$ as decision-epochs. In addition to the interval $\mathcal{I}$, we also consider a time interval $\mathcal{I}_p$ representing time in the past to be able to integrate weather data from the past. Similar to the above description, we also construct the partition $\mathbf{T}_p := \{[T_{i-1}, T_i)\}_{i=1}^{N_p}$ corresponding to $\mathcal{I}_p$, wherein N_p represents the number of elements of the partition. Furthermore, we also construct the sequence of points $\mathcal{T}_p := \{T_i\}_{i=0}^{N_p}$ that represents the discrete time instants in $\mathcal{I}_p$, such that $T_i - T_{i-1} = \Delta T \ \forall i = \{1, \cdots, N_p\}$. In this work, we use $\Delta T = \Delta t = 3600$ seconds so that the time instants in $\mathcal{T}_p$ and $\mathcal{T}$ are one hour apart in time for purposes of modeling

both the building load in this chapter and the solar generation in the subsequent ones. In the next section, we rely on this temporal notation to build a data-driven building demand model.

4.2 Building demand model

The load in a building is primarily due to Heating Ventilation and Air Conditioning (HVAC), lighting, and plug loads. The previous chapter developed regression models to predict the plugload statistics of an average occupant in time. In this section, we attempt to integrate the plug load model into building load model in order to develop a plugload-integrated controllable demand model in section 4.3. Let the building load be represented as a discrete time stochastic process denoted by L_k with corresponding realizations $l_k, \forall\ k \in \{0, \cdots, N\}$ with N_{lo}-states so that $lo_k \in \{l^{min}, \cdots, l^{max}\}$. We classify the load process into two, namely, the plugload stochastic process L_k^p, and the non-plugload stochastic process L_k^{np}. We make two assumptions regarding the nature of these loads, namely, the markovian nature of the plugload process L_k^p (similar to the assumption in 3.2.3) and cyclo-stationarity of the non-plugload process L_k^{np}. The rationale behind cyclo-stationarity in the non-plugload building demand (HVAC, lighting) is that this demand is driven by periodically varying factors such as occupancy schedules, temperatures, lighting whose variation within a day is repeated across days[1]. The Markovian assumption of the plugload stems from the consideration that the variation in the plugload process at k is explained significantly by the variation at $k-1$. Therefore, the building demand model can be written as:

$$P(L_k^p = l_k^p | l_{k-1}^p, l_{k-2}^p, ..., l_0^p) = P(L_k^p = l_k^p | l_{k-1}^p) \tag{4.2}$$

$$P(L_k^{np} = l_k^{np} | l_{k-p_l}^{np}) = P(L_{k-p_l}^{np} = l_k^{np}) \tag{4.3}$$

where, $P(\cdot)$ denotes the probability mass function of the corresponding random variable $\cdot$ and p_l denotes the time period of the cyclostationary non-plugload process. In this work, we use a value of 24×3600 seconds for p_l, thereby assuming that the cyclostationary load has a period of 24 hours. The commercial medium office building data from openEI [44] was used to compute the model characteristics such as the hourly load statistics. Figure 4.1 shows the statistics of the building demand over a 24 hour period assuming cyclo-stationarity for the overall building demand process.

[1]This assumption is invalidated by the effect of seasonal factors, which can be integrated with the models developed in this work

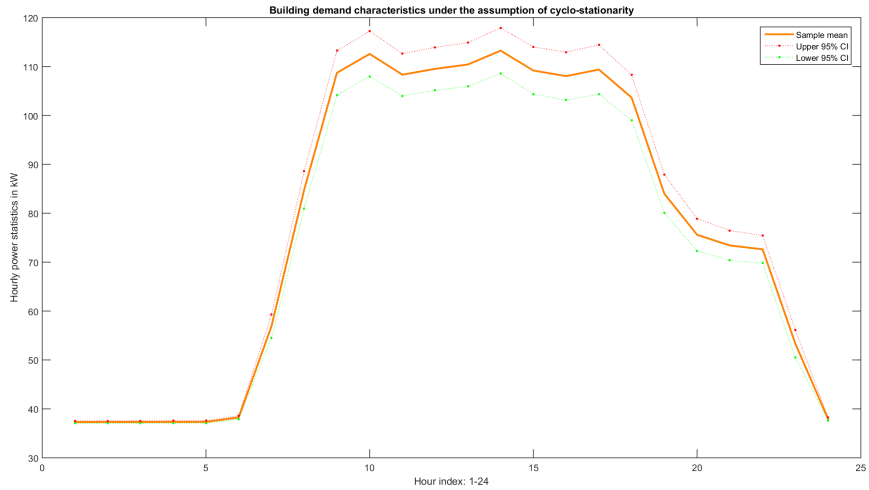

Figure 4.1: Demand characteristics of a commercial medium office building

4.3 Plugload-integrated controllable demand model

Given the overall building demand, it is estimated that almost one-third of commercial building load is due to plug and process loads [41]. In case of high efficiency buildings, plugloads can contribute to as high as 50% of the overall load [28]. This is due to significant reduction in the HVAC and lighting loads as a result of tight integration of automated HVAC and lighting systems into the building operations. Given the additive nature of the loads from various categories, the plugload model can be additively integrated into the non-plugload demand model. Let the fraction of plugload be denoted by $f_p, 0 < f_p < 1$, then the overall plugload-integrated demand model can be written as:

$$L_k = L^{np}_{k-p_l} + L^p_k \tag{4.4}$$

Let η_k denote the factor by which the baseline plugload is reduced into l^p_k due to use of feedback and/or incentives. Then, we can write $l^p_k = (1 - \eta_k) l^{p_b}_k$. Given the fraction of plugload consumption in the building f_p, we note that $l^{p_b}_k = f_p l_k$ and $l^{np}_{k-p_l} = (1 - f_p) l_{k-p_l}$ by definitions. Let the reduction process corresponding to η_k be denoted by R_k. We develop a model for R_k similar to the autoregressive model detailed in 3.2.3. The corresponding autoregression model for predicting fractional changes with respect to the baseline can be written as follows:

$$R_k = \alpha_l + \beta_l R_{k-1} + \gamma_l x a_{k-1} + \delta_l x i_k + \xi_k \tag{4.5}$$

The regression coefficients found are listed in table 4.1. Based on equations 4.5 and

α_l	β_l	γ_l	δ_l	$\sigma_{\xi.}$
-0.06534	0.8078	0.005597	0.07303	1.2779

Table 4.1: Regression model parameter estimates from the CMU experiment

4.4, we can constitute the plugload-integrated demand model as follows

$$L_k = L^{np}_{k-p_l} + l^{p_b}_k(1 - \alpha_l - \beta_l R_{k-1} - \gamma_l x^a_{k-1} - \delta_l x^i_k - \xi_k) \tag{4.6}$$

where, x^a_{k-1} and x^i_k represent the screentime variable (exogenous input) and the incentive variable (control input) respectively. In the optimization problem to be discussed in chapter 6, we will use $f_p = 0.5$ to demonstrate potential impact of plugload regulation on the overall building costs.

Chapter 5

WEATHER-DRIVEN SOLAR FORECAST MODEL

With the recent interest in net-zero sustainability in commercial buildings, integration of photovoltaic (PV) assets becomes even more important. While PV technology has made significant progress, its long-term efficiency and reliability remains a challenge. Furthermore, it is a highly variable source and its integration into existing building energy management systems remains an open question. Specifically, there is a need to optimally integrate PV assets with other building technologies to improve overall energy efficiency. The power output from a PV is known to depend on environmental variable such as irradiance, temperature (ambient and cell), wind velocity, relative humidity, air pressure, and sky conditions in various forms. Previous works have shown that the lack of accurate information about these variables can affect the prediction error significantly [32]. Ultimately, the most important factor for solar power forecasting is irradiance [60] and hence the need for accurate prediction.

5.1 Weather forecast-based irradiance prediction

Several methods have been proposed in literature for irradiance forecasting which are based on cloud cover satellite imagery, numerical weather prediction models, autoregressive models based on past data. A review of these methods can be found in [19]. We note that these methods are either based on global weather forecast models or local sensor data-driven models. In this work, we seek to integrate global weather forecast data into the local sensor data. The motivation behind this integration stems from two considerations, namely, (i) the global weather forecast data contains information about the global characteristics such as cloud covers that influence the local irradiance, and is provided at a spatial resolution in the order of kilometers [2] and (ii) the local sensor data contains exclusive information about the local characteristics such as shadows induced by obstacles such as buildings or trees. We propose an autoregressive model with global irradiance forecast as the exogenous input (ARMAX) to forecast the local irradiance. We use the High Resolution Rapid Refresh (HRRR) [2] data in the forecast model below. NOAA also provides the 0-hour forecast based on data from several sensors, and the 0-hour forecast was regarded as the measured sensor in the HRRR results below.

Let $\mathcal{M}_i$ denote the irradiance data obtained from sensor measurement at a time instant in the past $T_i \in \mathcal{T}_p$ and let $\mathcal{F}_i$ denote the forecast value available at t_i (based on the archived data from an 15-hour ahead forecast). Then the ARMAX model can be written as:

$$\mathcal{M}_i^H = \alpha_s \mathcal{M}_{i-86400}^H + \beta_s \mathcal{F}_i^H + \xi_s^H \tag{5.1}$$

where, $\mathcal{M}_{i-86400}$ represents the irradiance 24 hours prior to the time t_i (seconds). The model was trained over seven days of data, and the resulting predictions were tested over two days of data. Figure 5.1 illustrates the comparison between the observed and the predicted data over the test dataset. The RMSE of the ARMAX was found to be $\approx 62.4\ W/m^2$. This corresponds to a RMSE of 21%, which was found to be 3% lower compared to the baseline prediction accuracy with an autoregressive model using only the sensor data from 24 hours in the past. It was also found that the using the forecasts alone as the input resulted in an error of $\approx$ 30%. Similar ARMAX-based predictions were made for temperature and windspeed and the illustrations are shown in Figures 5.2 and 5.3.

5.2 Weather-based power prediction

Given the knowledge of local weather states, we proceed to construct a data-based power prediction model that can be incorporated into the energy management model described in Chapter 6. Let the power output generated by a given solar array be represented by a discrete time stochastic process $e_k, \forall\ k \in \{0, \cdots, N\}$ with discrete states $pv_k \in \{0, \cdots, N_{pv}\}$.

5.2.1 Integrating NOAA Forecasts

NOAA provides a wide variety of weather forecast products varying in spatio-temporal resolution, prediction horizon and update frequency [42]. In this illustration, forecast data from the NOAA North American Mesoscale Model (NAM) archives are used to infer the probability distributions of the measured solar irradiance. Using the historical sensor data $\mathcal{M}_i$ and the forecast archives $\mathcal{F}_i$, the error can be computed as shown in 5.2.

$$\mathcal{E}_i = \mathcal{M}_i - \mathcal{F}_i \tag{5.2}$$

For this part of the work, sensor data from Carnegie Mellon University (CMU) in Moffett Field, California was used. The sensor data was available at a sub-hourly granularity. However, the data from the NAM model was available only at a granularity of 6 hours since the NAM model runs 4 times per day at $\mathcal{T}_f \in \{00, 06, 12, 18\}$ hr UTC (i.e. $\{5, 11, 17, 23\}$ hr PST) forecasting up to 84 hours

ahead. We note that $\mathcal{E}_i$ obtained from equation 5.2 is available only when $(\frac{T_i}{3600} \mod 23) \in \mathcal{T}_f$ since the temporal resolution of NAM data is one data point 6 hours. In order to mitigate the coarse temporal resolution, we assumed that the data for $\mathcal{E}_i$ is available at all instants in the past $i \in \{0, \cdots, N_p\}$ by applying a first-order hold over the data $\mathcal{E}_i \; \forall \; i \in N_p \mid (\frac{T_i}{3600} \mod 23) \in \mathcal{T}_f$. Thereafter, the error measurements $\mathcal{E}_i$ were well defined for every $T_i \in \mathcal{T}_p$.

Given the error population $\mathcal{E}_i \; \forall \; i \in \{0, \cdots, N_p\}$, let $\mathbf{E}_j$ denote the dataset available at the time instant $T_j \in \mathcal{T}_p$ containing the error data $\mathcal{E}_i$, where $i = \left\{m \in \{0, \cdots, N_p\} \mid (T_m \mod T^{(P_p)}) = (T_j \mod T^{(P_p)})\right\}$. Here $T^{(P_p)}$ denotes the periodicity factor, which determines the grouping of the elements $\mathcal{E}_i \; \forall \; i \in \{0, \cdots, N_p\}$ into $\mathbf{E}_j$ for each j in $\{0, \cdots, N_p\}$. The reader is referred to section 4.1 for the discrete time notation employed here. We note that the dataset $\mathbf{E}_j$ is constituted by the set of errors $\mathcal{E}_i$ such that the corresponding time instants t_j and t_i leave the same remainder when divided by $T^{(P_p)}$. Let the error generating process be represented by a stochastic process $\hat{\mathcal{E}}_k \; \forall \; k \in \{0, \cdots, N\}$ with its corresponding distribution denoted by $\mathbb{F}_k$. Based on the error datasets $\mathbf{E}_j$ constructed above, the empirical distribution was obtained at each time instant T_j. In what follows, we assume that the time instants T_j in the past and t_k in the future correspond to various hours of the day $h \in \{1, ..., 24\}$. Furthermore, we assume that the error process $\hat{\mathcal{E}}_k$ is cyclostationary with a time period of 24-hours. Given the description of the error process $\hat{\mathcal{E}}_k, \forall \; k \in \{0, \cdots, N\}$, we employ a linear signal-noise regression model to predict the measured value $\hat{\mathcal{M}}_k$ as shown in the Equation 5.3.

$$\hat{\mathcal{M}}_k = \mathcal{F}_k + \hat{\mathcal{E}}_k \tag{5.3}$$

In this manner, the distribution of the estimated irradiance measurements $\hat{\mathcal{M}}_k$ is computed based on the error distribution of the stochastic process $\hat{\mathcal{E}}_k$ and the deterministic forecast $\mathcal{F}_k$. Similar to the irradiance estimation, other weather-related variables such as temperature, cloudiness can be estimated. With the knowledge of distributions corresponding to these weather processes, models that map the weather-related variables to the solar power output can be employed to obtain the solar power distribution. Although any sophisticated model can be used [58] [50], we resort to a linear scaling for a proof-of-concept illustration on how the solar power prediction can be integrated into the larger framework for energy management described in chapter 6. The resulting solar power distributions are denoted by $P^e(k, pv_k)$, where k represents the time instant $t_k \in \mathcal{T}$ and $pv_k \in \{e^{min}, \cdots, e^{max}\}$ represents the N_{pv}-states of the photovoltaic generation.

5.2.2 NAM-based prediction results

We analyzed the weather forecast data from the NAM model in light of both the sensor measurements as well as the true data as provided by NAM (0-hr ahead forecast). Results from the error distribution were used to determine the probability distributions of the solar generation process. Firstly, to analyze the similarity between the true data provided by NAM (0-hr ahead forecast) and the sensor measurements, we compared both these datasets over a period of two months (Aug - Oct 2014). The comparisons at different hours of the day - 11 AM PST and 5 PM PST are shown in Figures 5.4 and 5.5 respectively. It can be observed that the NOAA NAM model describes trends similar to those of the sensor measurements. To obtain a better understanding of the accuracy, the Root Mean Square (RMS) errors were computed based on percentage errors between NOAA and sensor measured data. The mean error was found to be 17.9% along with a standard deviation of 33.4%. Assuming the integrity of the sensor measurements, the mismatch arising from both these datasets can be attributed to several factors including coarse spatial granularity, modeling error, and low update frequency of the NAM model (4 per day). Since the NAM model forecasts up to 84 hours ahead, we compared the accuracy of the forecasts against several prediction window lengths assuming that the 0-hr ahead forecasts represented the truth. The comparison depicting the absolute RMS errors between the NAM truth (0-hr ahead) and the NAM forecasts up to 84 hours ahead is shown in Figure 5.6. To better illustrate the error magnitudes, this figure also depicts the percentage accuracies relative to the NAM truth data (shown in green). The overall accuracy across various prediction window lengths was found consistent with a mean of 81.9% and a standard deviation of 1.5%. Thus the use of 84 hour ahead NAM forecast provides predictions comparable to that of a 6 hour ahead NAM forecast. Based on the error distributions obtained from the irradiance archives, we estimated the distributions of the measured irradiance state with the knowledge of the forecasts (equation 5.3).

5.2.3 Solar forecast distributions

Based on the distribution of the measured irradiance estimates described above, the expected values of the irradiance process were obtained. Assuming an installation capacity of $84kW$ based on the usable roof area for solar panels for a commercial medium office building in the US [16] under standard conditions, the expected solar power was computed based on the above computed distribution and is shown in Figure 5.7. As aforementioned, the NAM model provides data at a temporal

granularity of 6 hours (4 per day). However, the forecast $\mathcal{F}_k \forall k \in \{0, \cdots, N\}$ as well as the error datasets $\mathbf{E}_i \forall i \in \{0, \cdots, N_p\}$ were reconstructed at an hourly granularity based on a first-order hold. In this manner, we obtained the hourly resolution depicted in the Figure 5.7.

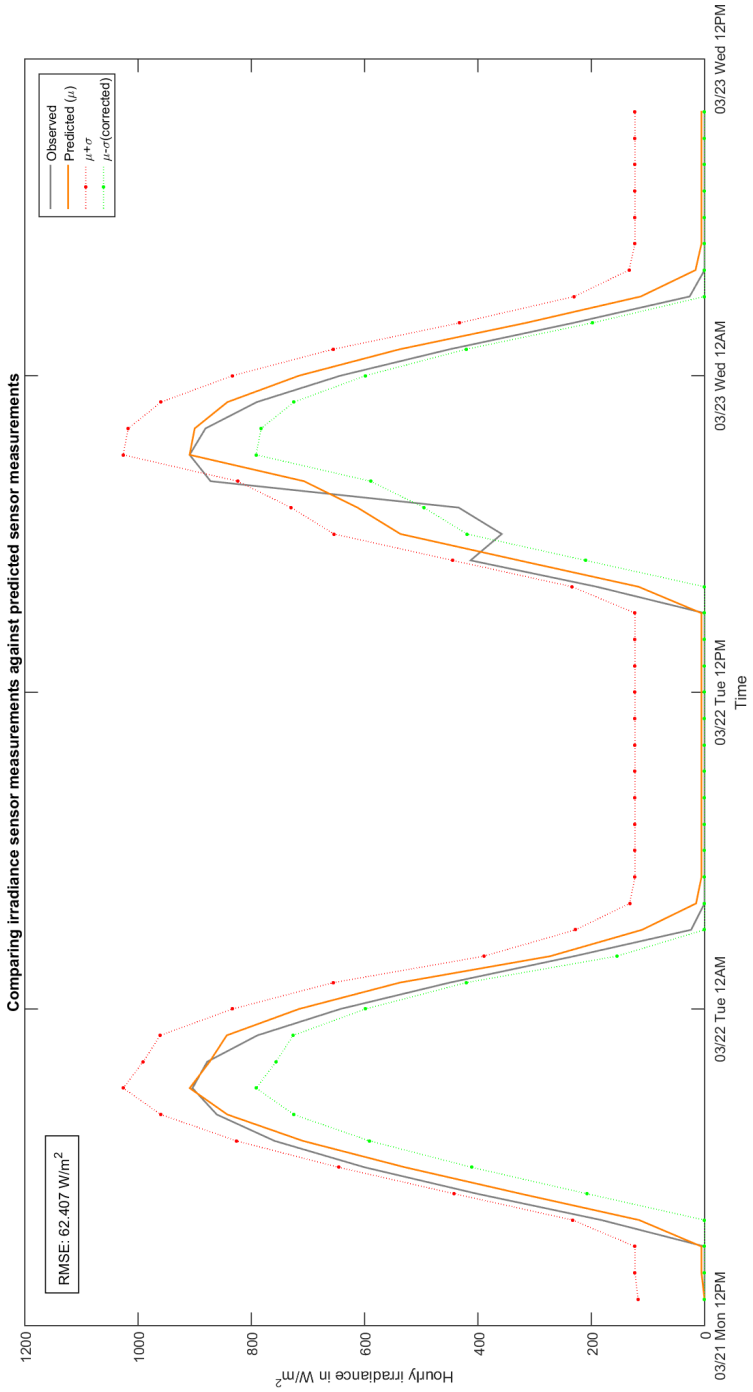

Figure 5.1: Solar irradiance prediction using the ARMAX model

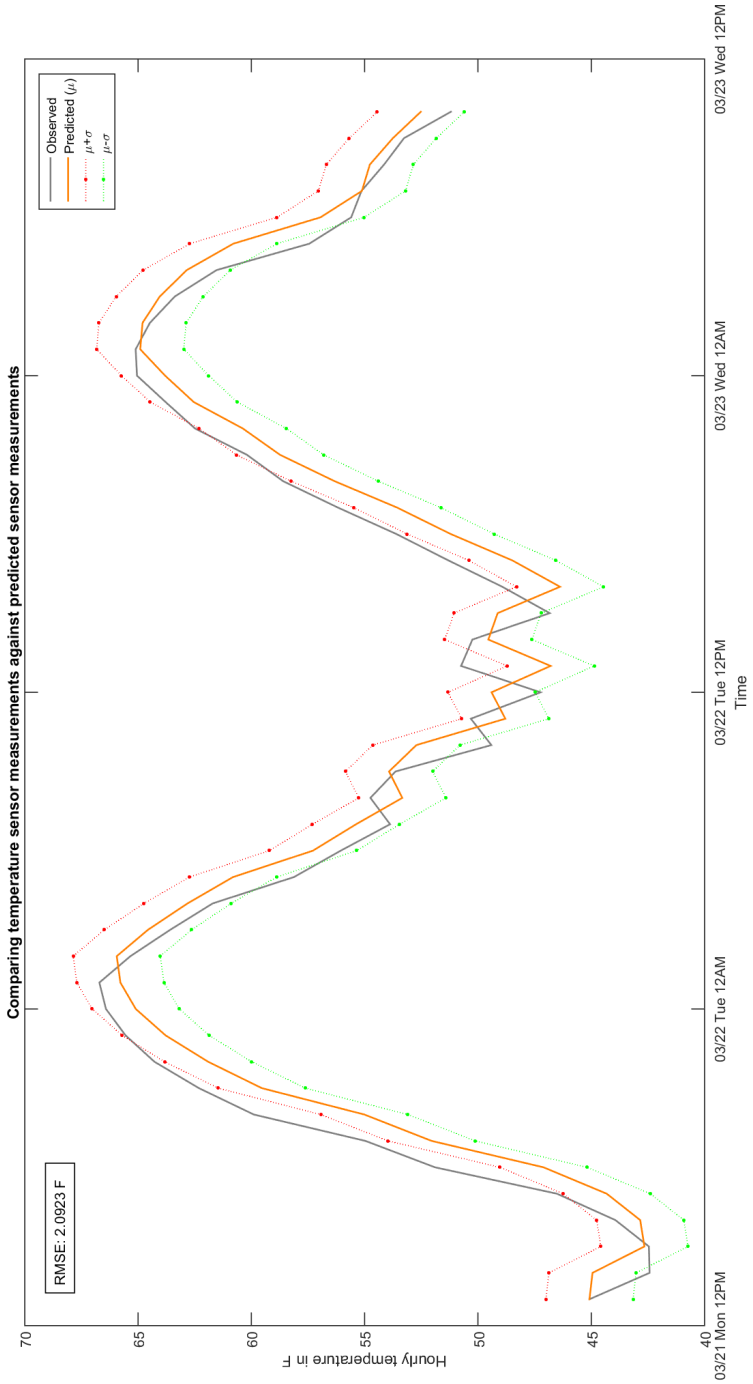

Figure 5.2: Temperature prediction using the ARMAX model

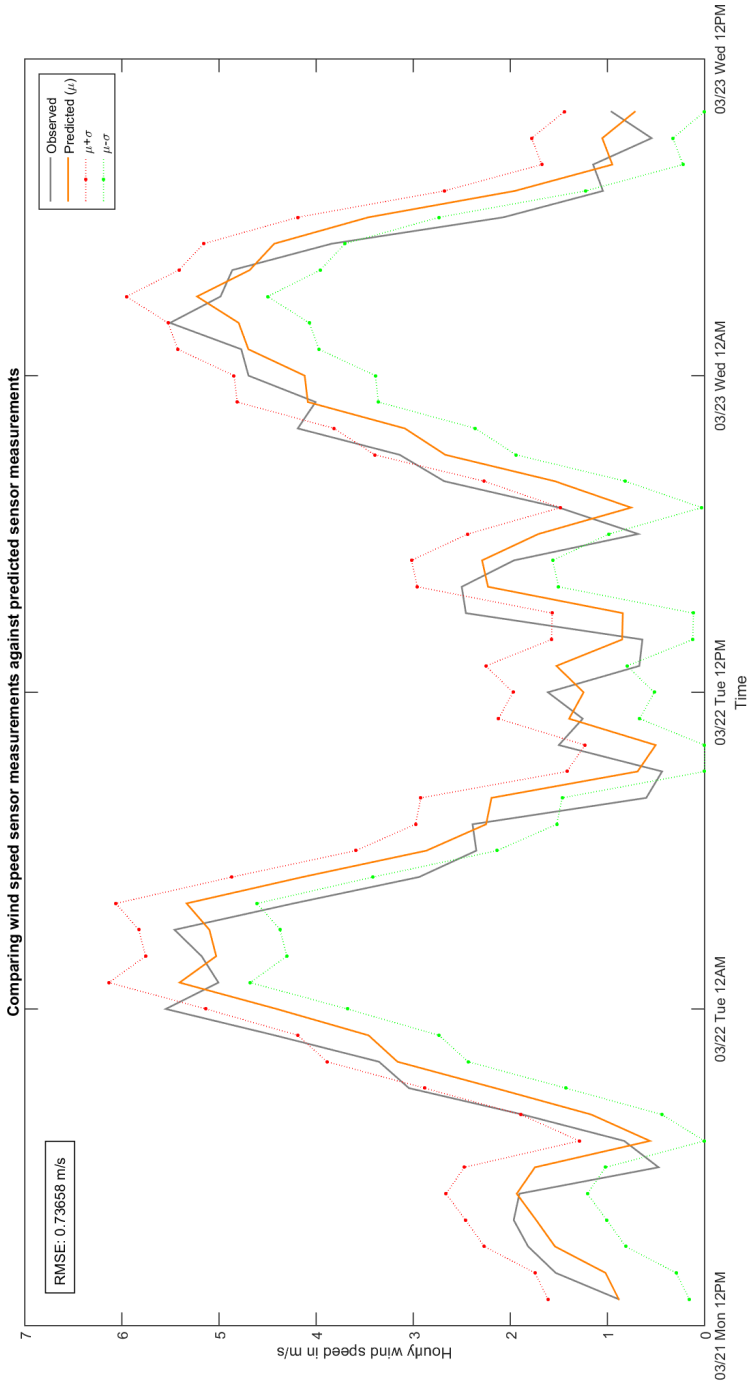

Figure 5.3: Windspeed prediction using the ARMAX model

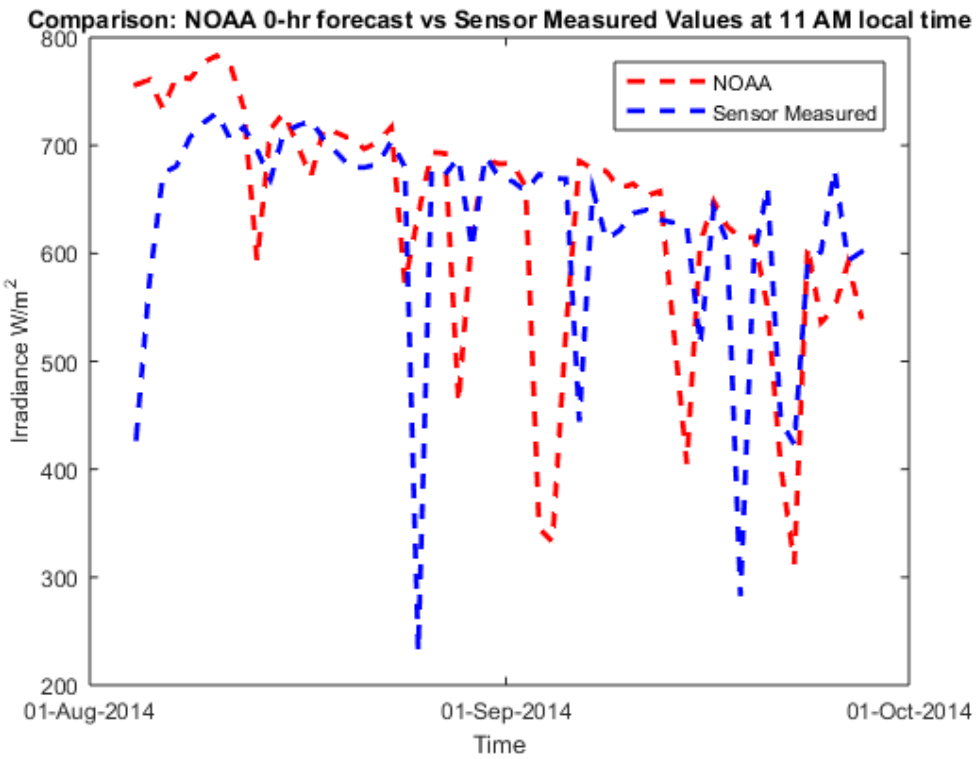

Figure 5.4: Comparison between NOAA and Sensor irradiance data at 11 AM, $\mu_{accuracy_{RMS}}$ = 82.2%

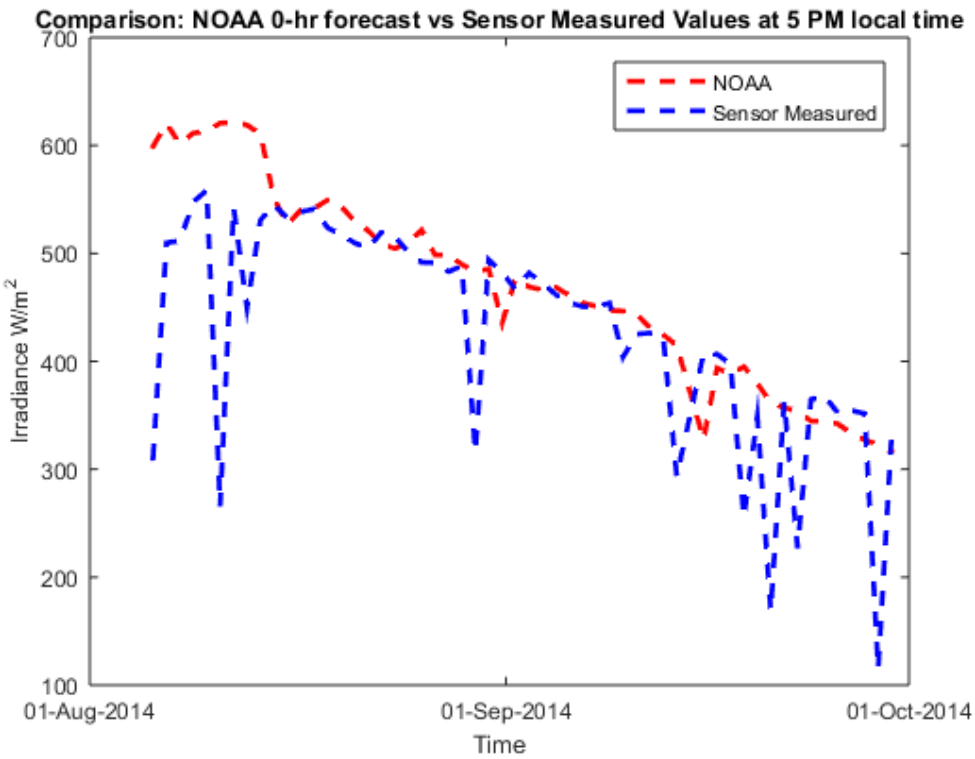

Figure 5.5: Comparison between NOAA and Sensor irradiance data at 5 PM, $\mu_{accuracy_{RMS}}$ = 81.8%

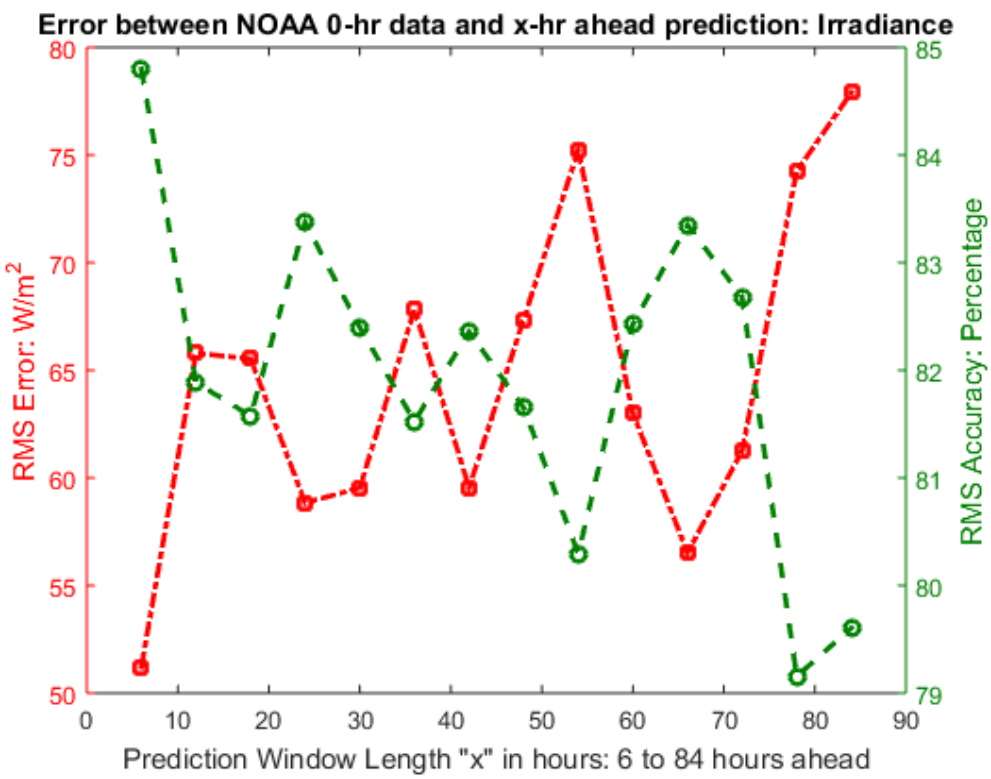

Figure 5.6: Comparison between NAM truth and x-hour ahead forecasts: $x \in \{6, 12, \cdots, 84\}$

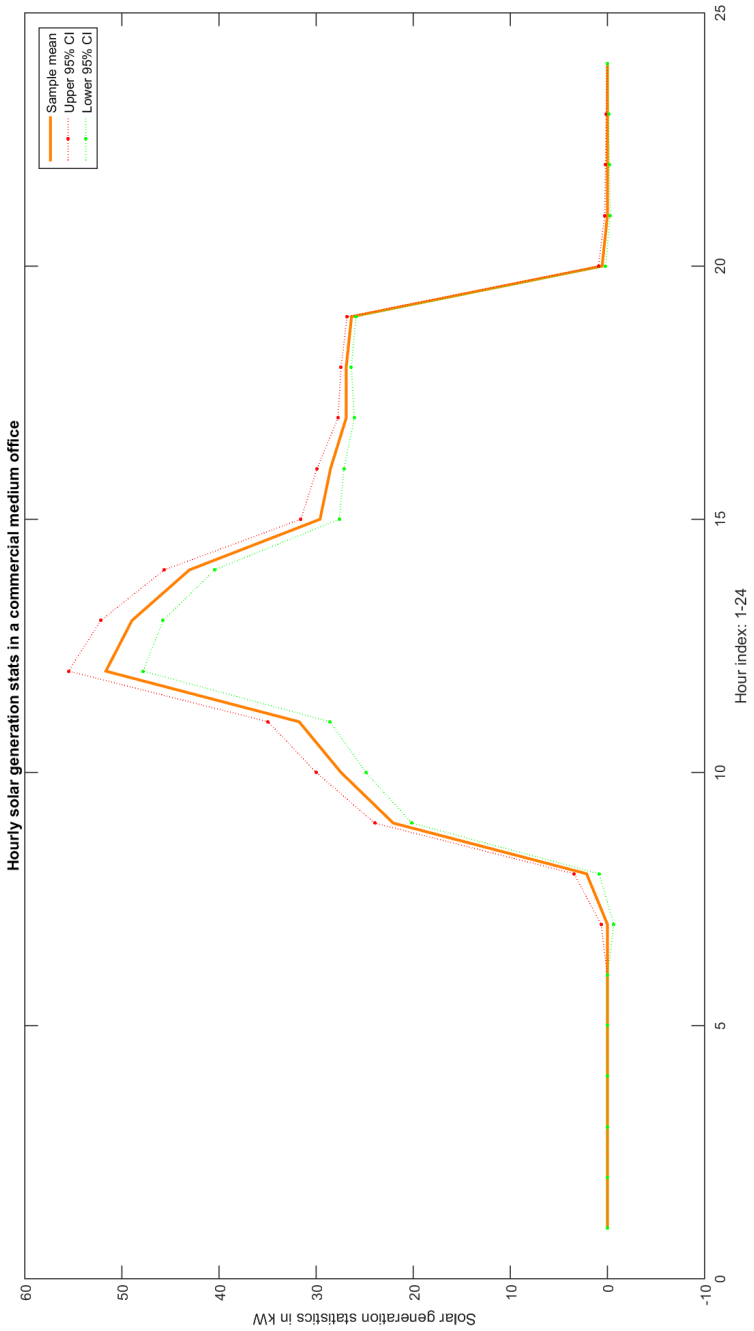

Figure 5.7: Expected Solar Generation data based on NOAA NAM irradiance estimates

Chapter 6

A DECISION FRAMEWORK FOR ENERGY MANAGEMENT IN SMART BUILDINGS

Given the cyclo-stationary solar generation and load processes described in chapters 5 and 4 respectively, we proceed to integrate these into the framework for energy management in smart buildings as shown in Figure 6.1. The energy management framework in smart buildings comprises of load, renewable solar generation, energy storage, decision-making unit (DMU), and their interconnections. A model of this system allows us to (1) study the evolution of the overall building energy in time and (2) provide a framework to design and evaluate power-flow decisions within the building. The schematic of a grid-connected smart building is depicted in Figure 6.2. In what follows, we describe the various elements required to constitute the framework.

6.0.1 Energy Storage

The objective of furthering renewable penetration and simultaneously maintaining grid stability can be practically realized by incorporating energy storage systems [52]. In a more localized environment like a building, storage systems help achieve self-reliance independent of the main grid and enable reduced electricity costs. In this work, the building storage system is represented by a dynamical system with capacity $\mathcal{S}$. There are several approaches to modeling the storage dynamics with varying levels of complexity [31]. To illustrate the concept of energy management in the context of a single building, we resort to a linear dynamic representation of the storage system similar to [61]:

$$s_{k+1} = \eta_s s_k - \xi_p v_k \Delta t \tag{6.1}$$

where, $s_k \in [0, \mathcal{S}]$ represents the energy content (state) of the energy storage at $t_k \in \mathcal{T}$ and v_k represents the net power output from the storage system from the current time instant t_k until the next instant t_{k+1}.The power flow constraints associated with the storage system are represented by $v_k \in [P_{min}, P_{max}]$. Furthermore, the self-discharge losses [53] are represented by the storage efficiency factor η_s and the closed-circuit losses by the factor ξ_p[1] [22].

[1]Note that $\xi_p < 1.0$ during charging and $\xi_p > 1.0$ during the discharge phase. In other words, more power is discharged from the storage system compared to the storage output and less power is

6.0.2 Grid Transactions

The electric grid facilitates the transfer of power from the suppliers to the consumers over transmission and distribution networks. In this work, we assume that the grid is is an infinite resource. As depicted in Figure 6.2, we assume that the transactions between the grid and the building are enabled by the Decision-Making Unit (DMU). Let the power flow from the grid to the building DMU at any $t_k \in \mathcal{T}$ be denoted by u_k[2]. These grid transactions incur a monetary cost for the building depending on the quantity of power exchanged and the pricing scheme offered by local utility company or the energy market [15]. We consider a deterministic pricing model, where the purchase prices $(c_p(k), k \in \{0, \cdots, N\})$ are based on the $PG\&E$ schedule A10 [25] and selling prices $(c_s(k), k \in 0, \cdots, N)$ are based on the $PG\&E$ E-SRG PPA [26]. Thus, the monetary cost incurred due to the grid transactions over the horizon $\mathcal{T}$ becomes:

$$\mathbf{C}(u_0, \cdots, u_{N-1}; w_0, \cdots, w_{N-1}) = \sum_{i=0}^{N-1} \{c_p(i)I(u_i > 0) + c_s(i)I(u_i <= 0)\} u_i \Delta t \quad (6.2)$$

where, positive $\mathbf{C}$ indicates the cost to be paid by the building to the grid on the account of the grid transactions $(u_0, \cdots, u_{N-1})$.

6.0.3 Nanogrid Topology

In a distributed power system consisting of several generation units, loads, storage systems and the main grid, the interconnecting topologies play a critical role in routing power effectively. From a decision-making perspective, there exist interconnected designs with varying levels of decentralization, each differing in autonomy and complexity. In the building under consideration, we employ a centrally interconnected design wherein all the components are connected via the DMU as depicted in Figure 6.2.

6.0.4 Smart building DMU

The smart building consists of two interdependent networks: (1) a communication network for routing information and (2) a power network for routing power. The 'smart' aspect is in leveraging the information available to make informed decisions. In our work, we assume that the information about the various components of the building is available to the DMU. Depending on the states of the storage system, the generation, the load, and the electricity pricing, the DMU computes the power flow

used to charge the storage system compared to the storage input due to losses incurred

[2] According to our convention, power flowing into the DMU is considered positive

decisions. Specifically, the decisions involve determining the power flows from/to the battery v_k and from/to the grid u_k. We describe the decision-making process below.

Let the generation output and the load at an instant $t_k \in \mathcal{T}$ be denoted by $e_k^{(r_e)}$ and load $l_k^{(r_l)}$ respectively. Here $e_k^{(r_e)}$ and $l_k^{(r_l)}$ represent the real-world realizations of the non-controllable stochastic processes e_k and l_k at the time t_k. Given the power flows $e_k^{(r_e)}$ and $l_k^{(r_l)}$, the decisions computed at the DMU (u_k, v_k) must result in the power balance at every time instant $t_k \in \mathcal{T}$ as shown:

$$e_k^{(r_e)} + u_k + v_k + l_k^{(r_l)} = 0 \tag{6.3}$$

6.0.5 System Parameters

Decision-making within the building requires information about the system parameters. Let the system parameters at $t_k \in \mathcal{T}$ be denoted by $\mathcal{W}_k$. Also, let $\mathcal{W}_k$ be classified into the deterministic parameters of the system (denoted by z_k) and the distribution of the random parameters the system (denoted by w_k). The deterministic parameters consist of $z_k = [c_p(t_k), c_s(t_k), \mathcal{S}, P_{min}, P_{max}, \eta_s, \xi_p, N, \Delta t]$ and the distribution parameters of the stochastic processes (e_k, l_k) consist of $w_k = [P^e(k, \cdot), P^l(k, \cdot)]$. Thus, the system parameters can be written as $\mathcal{W}_k = (z_k, w_k)$.

6.1 Policy Formulation

The framework described above enables structured power-flow decision-making. Specifically, the information about the state s_k is useful in determining the "decision pair" (u_k, v_k). The mapping between the state space and the decision space of the system is provided by a policy, denoted by π. The building energy policy π can be viewed as a collection of two policies, namely the storage transaction policy π_B and the grid transaction policy π_G. Thus, the policy map π between the states (s_k) and the decisions (u_k, v_k) can be written as:

$$\begin{aligned} \pi &:= \{\pi_B, \pi_G\}, \text{where} \\ \pi_B &: \{0, \cdots, N-1\} \times \mathcal{S}_k \rightarrow \mathcal{V}_{s_k} \\ \pi_G &: \{0, \cdots, N-1\} \times \mathcal{S}_k \rightarrow \mathcal{U}_{s_k} \end{aligned} \tag{6.4}$$

where, the admissible decision space is represented by $(\mathcal{U}_{s_k}, \mathcal{V}_{s_k}) \subset \mathbf{R}^2$ and $\mathcal{S}_k$ denotes the storage state space. It must be noted that the admissible decision space consists of the decisions which, when implemented do not result in the violation of the system constraints (Refer to Appendix B for details). Furthermore, it can be

observed that only one of the decisions (u_k or v_k) is made explicitly, since the other decision will the be fixed to ensure system power balance 6.3. In what follows, we describe heuristics-based policies, also known here as 'naive' policies:

1. *Policy 1: Exhaustive Storage Dependence Policy* π_1: This policy seeks to utilize the storage to the fullest extent for meeting the power balance (equation 6.3). Given the non-controllable supply $e_k^{(r_e)}$ and demand $l_k^{(r_l)}$, the policy seeks to offset the supply-demand gap using the storage resource transactions v_k. When the storage resource can no longer be used to maintain power balance, the policy resorts to the grid transactions u_k to handle the excess or deficit condition faced by the building. The decision-making process for this policy (π_1) is illustrated by the flowchart in Figure 6.3.

2. *Policy 2: Look Ahead Policy* π_2: The notion behind the look-ahead policy design is to make informed decisions based on the present as well as the expected future supply-demand gap. With these considerations, four scenarios are possible: (i) excess supply in the present as well as in the expected future, (ii) excess supply in the present and deficit supply in the expected future, (iii) deficit supply in the present and excess supply in the expected future, and (iv) deficit supply in the present as well as in the expected future. When there is excess supply in the present as well as in the expected future, the storage is charged before exporting power to the grid. In the scenario with deficit supply in the present as well as in the expected future, the storage is partially discharged to meet the deficit provided the storage does not get exhausted after discharging. The rest of the deficit is met by both the solar generation and the grid. In the other scenarios, the policy relies on the generation and the grid for power balance, leaving the storage state unchanged. The policy π_2 is illustrated by the flowchart in Figure 6.4.

6.2 Optimal Power Flow Problem

Given heuristics-based policies such as the ones described above, it is important to compare the performance of these policies based on cost metrics, one of which was described in equation 6.2. This allows the policy-maker to order and choose policies based on their cost. In this work, we attempt to design policies that result in decisions minimizing the building energy costs.

We consider the scenario where the cost metric describes the expected monetary cost over a finite horizon $\mathcal{T}$. Thus, the cost metric depends on the costs associated with both the grid transactions u_k, $\forall k \in 0, \cdots, N-1$ as well as the expected storage state at the end of the horizon. It must be noted that the storage state at the end of the horizon is uncertain at all instants $k < N$ and hence regarded as a random variable $\hat{s}_N$. The probability distribution of $\hat{s}_N$ can, however, be computed with the knowledge of (i) probabilistic supply and load distributions $P^l(k, pv_i)$ and $P^l(k, pv_i)$ respectively over the instants $\{k, \cdots, N-1\}$, and (ii) the storage dynamics described in Equation 6.1. Therefore, the cost metric over the horizon[3] $\{t_k, \cdots, t_N\}$ can be written as:

$$
\begin{aligned}
&J(s_k, u_k, u_{k+1}, \cdots, u_{N-1}; \mathcal{W}_k, \cdots, \mathcal{W}_N) \\
&\qquad = E\Big\{ \sum_{i=k}^{N} L(u_i; \mathcal{W}_i) + g_1(\hat{s}_N; \mathcal{W}_k, \cdots \mathcal{W}_N) \Big\} \\
&\qquad = E\Big\{ \sum_{i=k}^{N} \big(\mathbb{1}(u_i > 0) c_p(t_i) + \mathbb{1}(u_i \leq 0) c_s(t_i) \big) u_i - \hat{s}_N c_s(t_N) \Big\} \qquad (6.5)
\end{aligned}
$$

where, $\mathbb{1}(\cdot)$ denotes the indicator function, E denotes the expectation operator with respect to the solar and load distributions, and $\mathcal{W}_k$ denotes the system parameters at the time instant $t_k \in \mathcal{T}$. Given the above cost metric J, the problem of interest is to compute the optimal policy π^* that minimizes J over the entire horizon $[t_0, t_N]$.

6.3 Optimal Policy Computation

In order to solve for the optimal policy, we first note that the states (s_k), the decisions (u_k, v_k), the Markovian state transitions (Equation 6.1), and the cost metric J (Equation 6.5) together constitute a discrete time stochastic control process, commonly known as the Markov decision process (MDP). Within the MDP framework, the policy-maker enforces a decision (u_k, v_k) on the system and the system state s_k responds by randomly transitioning into a new state s_{k+1} while incurring a transition cost L. We consider a problem of the policy-maker, where the objective is to obtain the policy (π^*), which, when enforced, results in a sequence of decisions that minimize the cost J over the optimization horizon $[t_0, t_N]$. The optimal policy can

[3] In the dynamic programming formulation of decision-making problems, the cost metric over the horizon $\{t_k, \cdots, t_N\}$ is also known as the cost-to-go from stage k to N.

be obtained by solving the following optimization problem:

$$\pi^*(s_0; (\mathcal{W}_k)_{k=0}^N) = (u_k^*, v_k^*)_{k=0}^{N-1}, \text{ such that}$$

$$(u_k^*)_{k=0}^{N-1} = \underset{\left[(u_k)_{k=0}^{N-1} \in \prod_{k=1}^{N-1} \mathcal{U}_{E\left\{\hat{s}_k | s_0\right\}}\right]}{\operatorname{argmin}} J(s_0, u_0, \cdots, u_{N-1}, \{\mathcal{W}_k\}_{k=0}^N),$$

$$\textit{and } v_k^* = -(u_k^* + E(e_k) + E(l_k)), \ \forall k \in \{0, \cdots, N-1\} \quad (6.6)$$

where, $\hat{s}_k$ denotes the random variable representing the uncertain state of the storage in the future. The corresponding optimal cost then becomes:

$$V_0(s_0; \{\mathcal{W}_k\}_{k=0}^N) = J(s_0, u_0^*, \cdots, u_{N-1}^*; \{\mathcal{W}_k\}_{k=0}^N) \quad (6.7)$$

where, $V_0(s_0; \{\mathcal{W}_k\}_{k=0}^N)$ is known as the value of the state s_0 at the time instant t_0. The function V, known as the value function maps the states and parameters $(k, s_k; \{\mathcal{W}_k\}_{k=0}^N)$ at the time instant t_k to a real value as shown:

$$V_k(s_k; \{\mathcal{W}_i\}_{i=k}^N) = J(s_k, u_k^*, \cdots, u_{N-1}^*; \{\mathcal{W}_i\}_{i=k}^N) \quad (6.8)$$

In other words, the value function at the instant k describes the optimal cost-to-go from stage k through the final stage N.

We address the above discrete time stochastic dynamic optimization problem by applying the principle of optimality and solving the resulting sub-problems using a stochastic dynamic programming (SDP) approach. The sequence of solutions to these sub-problems are obtained using the backward induction algorithm, wherein the updated values at the previous time step are obtained by solving the Bellman equation. In our work, the Bellman equation is solved approximately by interpolating the value function at the subsequent stage. In what follows, we describe the details of the SDP approach to arrive at near-optimal solutions to the problem described in Equation 6.6. By applying the principle of optimality, we can transform the decision-making problem into a sequence of sub-problems as shown:

$$J(s_0, u_0^* \cdots, u_{N-1}^*; \mathcal{W}_0, \cdots, \mathcal{W}_N) = \min_{u_0} \Bigg\{ L(u_0; \mathcal{W}_0) + \left[\sum_{k=1}^{N-1} E\left\{ J\left(\hat{s}_k, u_k^*, \cdots, u_{N-1}^*; \mathcal{W}_{k-1}, \cdots, \mathcal{W}_N\right)\right\}\right]\Bigg\} \quad (6.9)$$

Using the definition of the value function in equation 6.8, we can rewrite the equation 6.9 as:

$$V_0(s_0; \{\mathcal{W}_k\}_{k=0}^N) = \min_{u_0} \left\{ L(u_0; \mathcal{W}_0) \ + E\left\{ V_1(\hat{s}_1; \{\mathcal{W}_k\}_{k=0}^N) \right\} \right\} \tag{6.10}$$

Continuing the course of dividing the problem into sub-problems, we arrive at the following generalized equation:

$$V_k(s_k; \{\mathcal{W}_i\}_{i=k}^N) = \min_{u_k} \left\{ L(u_k; \mathcal{W}_k) \ + E\left\{ V_{k+1}(\hat{s}_{k+1}; \{\mathcal{W}_i\}_{i=k}^N) \right\} \right\} \tag{6.11}$$

which describes a recursive relationship between the values at consecutive time steps. This equation, known as the Bellman equation, offers a recursive method to compute the values at the current instant of time based on the knowledge of values at the next of time. We apply backward induction to solve for the values in the Bellman equation 6.11, starting with the end of the horizon $t_N \in \mathcal{T}$ and solving backwards in time.

To solve for the value function as well as the optimal decisions, we resort to a numerical approach. First, we observe that the domain of the value function is the continuous state space $s_k \in [0, \mathcal{S}]$. We proceed to quantize the state space only for the purposes of computing the values and the optimal decisions, thereby introducing sub-optimality into the solution. Let the discretized version of the continuous state space $[0, \mathcal{S}]$ be represented by the finite sequence $\mathbf{S} := \{\mathbf{s}_1 = 0, \mathbf{s}_2, \cdots, \mathbf{s}_{N_s} = \mathcal{S}\}$.

At the end of the horizon t_N, the values are computed for the quantized state space $s_N \in \mathbf{S}$:

$$V_N(s_N; \mathcal{W}_N) = g(s_N; \mathcal{W}_N) \tag{6.12}$$

At every previous time step $\{t_k\}_{k=N-1}^0$, the decisions resulting in the minimum expected cost-to-go are computed by solving equation 6.11 across the feasible decision space $\mathcal{U}_{s_k}$ (see Appendix B). This results in a near-optimal sequence of decisions $\{u_k^*\}_{k=0}^{N-1}$ that constitutes the non-stationary near-optimal policy π^*.

6.4 Results

We simulated the nanogrid model under the action of both the naive and the optimal policies over an optimization horizon of 30 days (720 hours). The storage capacity was chosen to be $500kWh$ with a peak power of $500kW$ such that the building could be run off the grid entirely on the storage for 6 hours. The storage parameters (η_s, ξ_p) were set to their ideal values $\eta_s = \xi_p = 1.0$ in the simulation. The remain aspects

such as the pricing scheme, load and solar processes were chosen for a commercial medium office building as described previously. Given the assumption of cyclo-stationarity, the distributions of the estimated load and solar were pre-computed over a 24-hour horizon. In what follows, we present the results and discussion pertaining to the various policies.

The expected state evolution under the action of policy π_1 is shown in Figure 6.5. We note that the policy π_1 was designed to primarily rely on the storage resource. In other words, we expect the policy to charge the storage device in the case of excess solar generation and discharge during deficit generation prior to any dependence on the grid. From the bottom subplot in Figure 6.5, we note that there exists only deficit generation throughout the horizon which directs the policy to make decisions that discharge the storage. This explains the observed behavior of battery discharge since the beginning of the horizon.

In case of the look ahead policy π_2 design, the decisions are influenced by both the current imbalance (solar minus load) as well as the expected imbalance in the future as described in the Figure 6.4. These decision-making factors are shown in the bottom subplots of Figure 6.6. As can be noticed from the bottom two subplots in the figure, both the current imbalance in the future are always negative. As per the policy, this should allow the battery to discharge until the point where supplying for further deficit doesn't discharge the battery completely. Given that the maximum imbalance (solar-load) is $-40kW$, it can be observed that the storage doesn't discharge the battery as soon as the state reaches $40kWh$ (since $Deltat = 1$ hour).

The optimal policy π^* described in Section 6.3 was computed by backward induction. By using the values computed at the forward time instant t_{k+1}, optimal decisions and current values at t_k that minimize the expected cost were computed using the Bellman equation 6.11. The optimal policy along with its impact on state evolution is shown in figure 6.7. The optimal decision depends on several factors that combine together to result in the least expected cost-to-go over the optimization horizon. These factors include the solar generation, demand, cost price, selling price, the current state of the system, and the distributions of the solar and load processes.

The behavior of the optimal policy can be better understood by observing Figure 6.8 that describes the evolution of the system over a two day horizon. We note that the optimal policy charges and discharges the battery multiple times during the time period when the selling prices are higher than the cost prices. During this time,

the policy directs withdrawal and selling transactions with the grid respectively. Therefore, it can be stated that the withdrawal from the grid charges the battery in light of the low cost prices compared to the selling prices so as to sell at a later point.

The complexity involved in computing the optimal policies pays off in terms of minimizing the expected cost. The expected costs associated with the various policies and scenarios are shown in Figure 6.9. The first scenario depicts the average monthly cost incurred by a commercial building with similar load profile in Santa Clara county ($7568.14) based on the average prices for Santa Clara from the US Energy Information Administration (EIA). The parameters used in the simulation for the demand model with the A10 pricing scheme yields comparable costs ($7549.78) as shown by the second bar, thereby indicating that the pricing scheme used in the simulation reasonably matches that of the one provided by US EIA. On using the solar panels for a commercial building (84 kW), the expected monthly costs drop to $5715.51 as shown by the yellow bar, which is expected due to the availability of in-house generation to meet partial demand. The performance of the exhaustive battery utilization policy (policy 1) and the look ahead policy (policy 2) yield costs that closely match the case with no energy storage. This means that these heuristics-based policies do not effectively capitalize on the energy storage resource. However, in case of the optimal policy, the performance results in costs that are more than 60% lower than the heuristic policies, thereby indicating that the optimal policy could capitalize on the energy storage resource much more than the heuristic policies. Furthermore, we also investigated the case of the plugload-integrated controllable demand model for energy management based on the results of the plugload experiment chapter 2 for the case of a high performance building with $f_p = 0.5$. In this case, the cost function also included the cost incurred in $ due to providing the incentives to the occupants for lowering their energy consumption. The findings indicated that the plugload-integrated optimal policy outperformed the optimal policy with non-controllable loads by 13%, thereby quantifying the impact of plugload management on the operating costs of a building. The lower costs in case of the controllable plugloads are expected due to the increase in dimensionality of the search space for the optimization problem. In other words, the optimization problem with non-controllable demand can be viewed as a problem with constrained search space in comparison to the optimization problem with controllable demand.

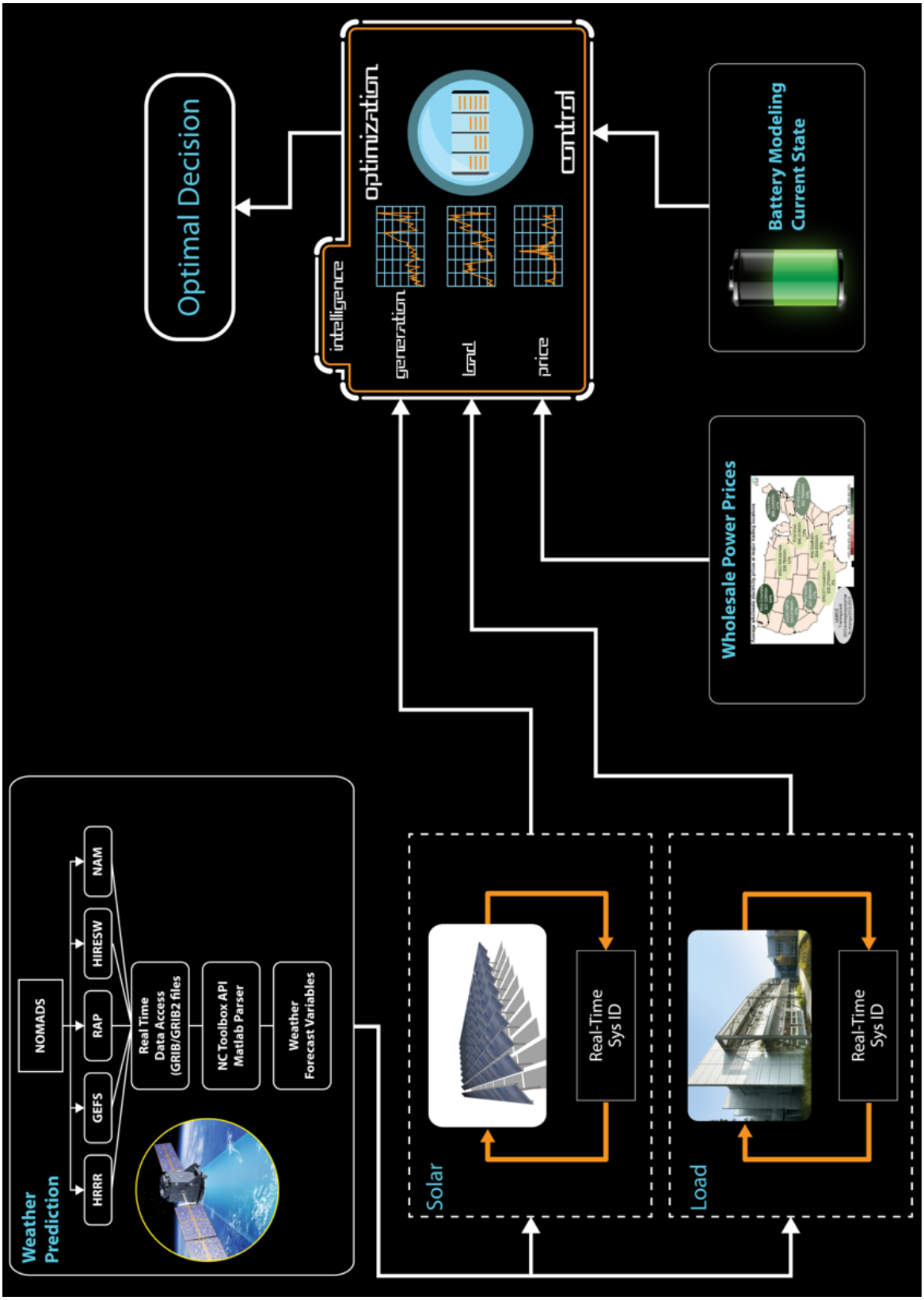

Figure 6.1: Energy management framework in a smart building

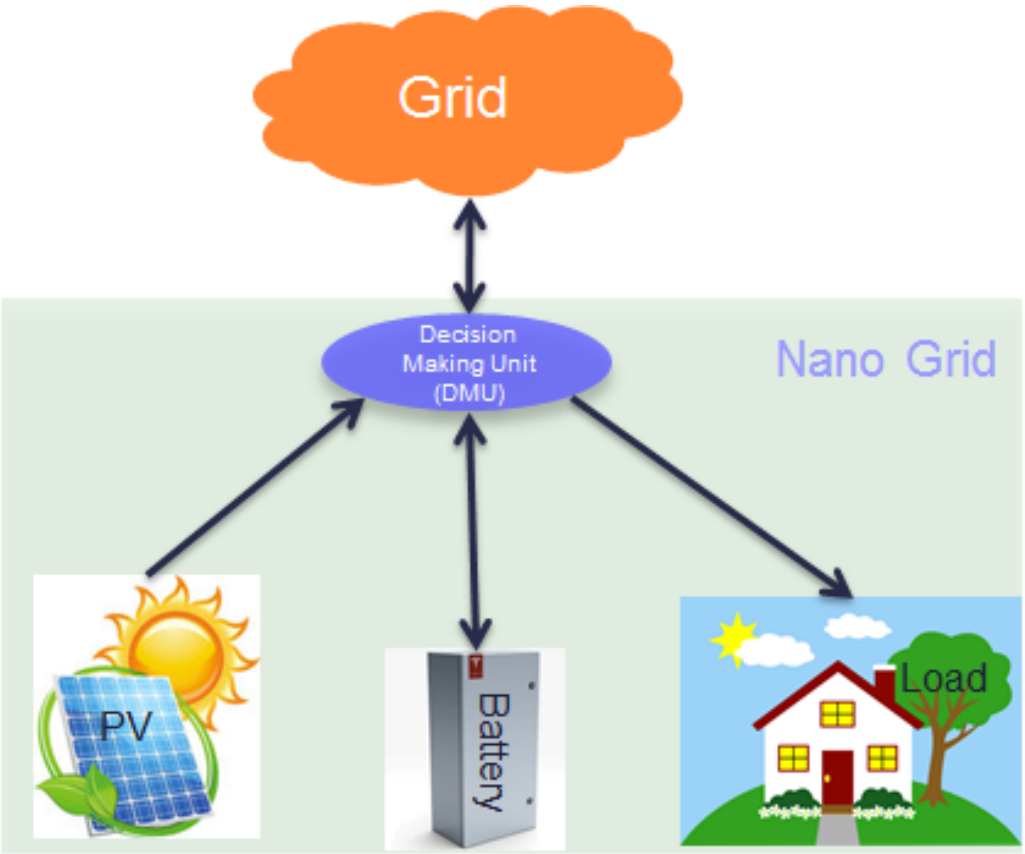

Figure 6.2: Schematic of a grid connected smart building

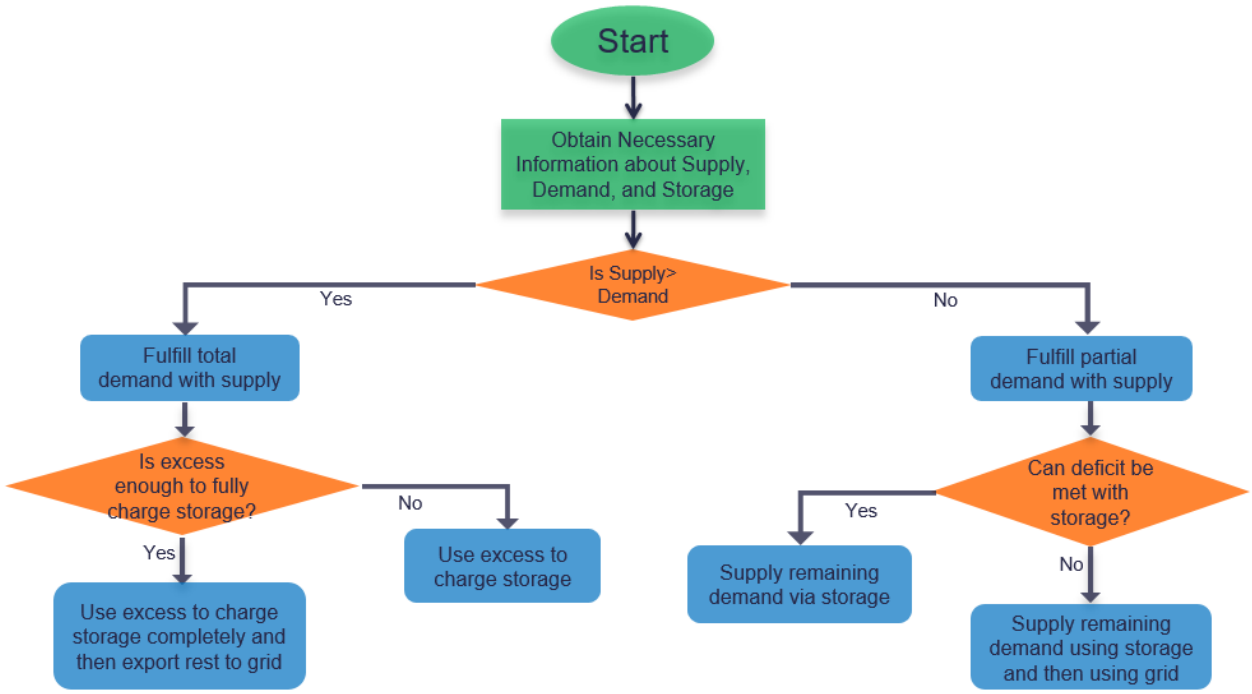

Figure 6.3: Flow Chart depicting the Exhaustive Storage Dependence Policy

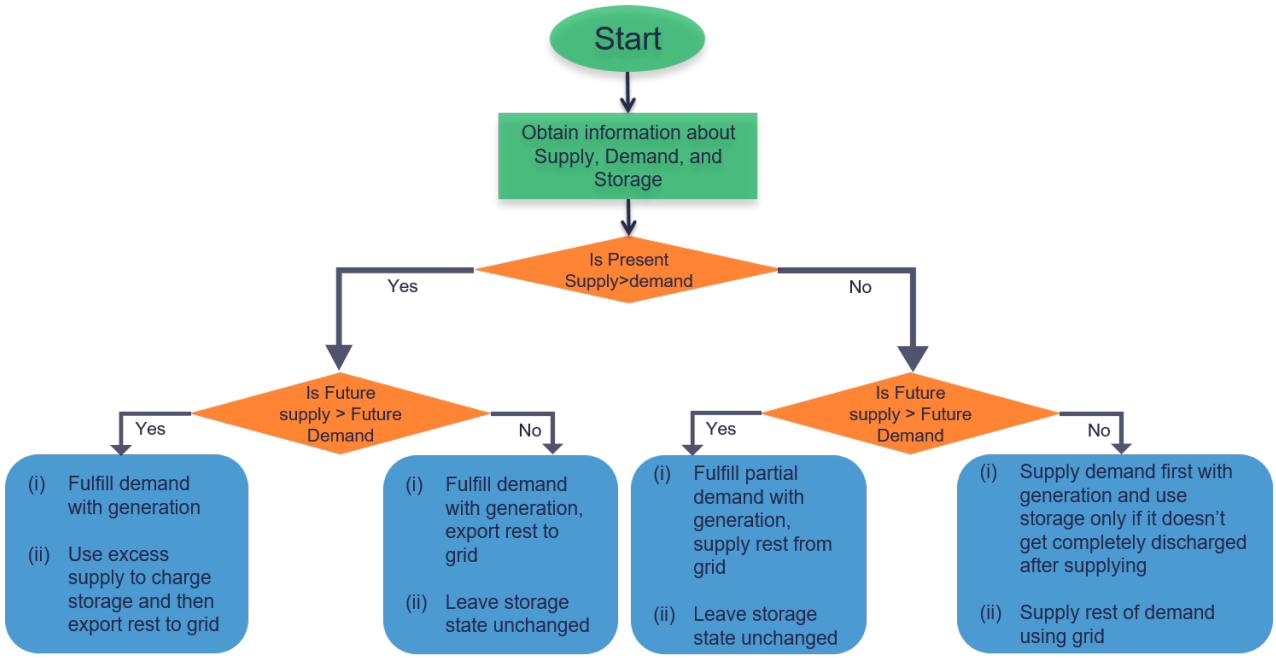

Figure 6.4: Flow Chart depicting the Look Ahead Policy

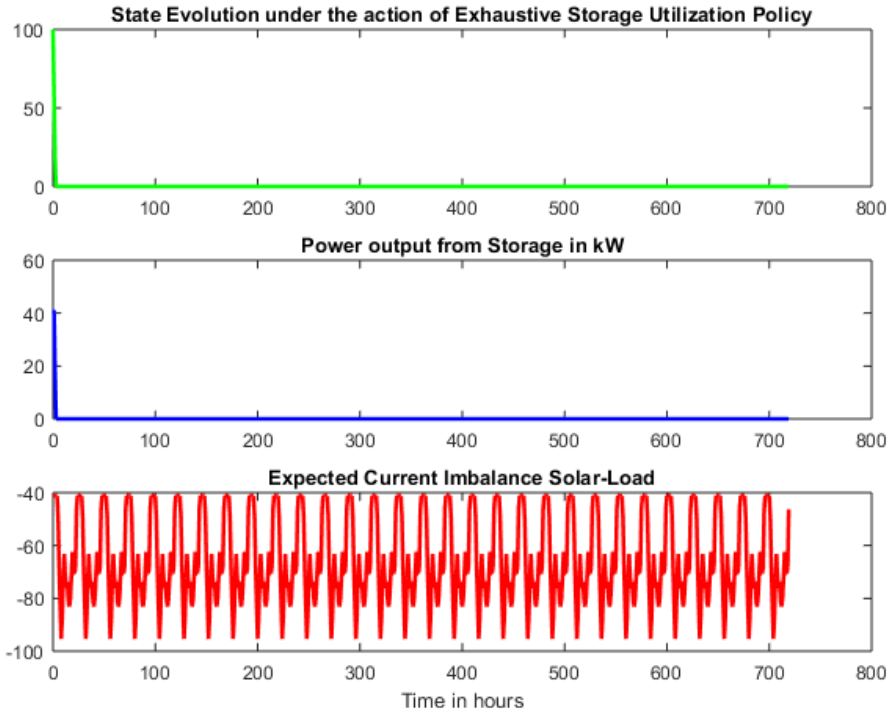

Figure 6.5: System evolution under the action of Policy 1

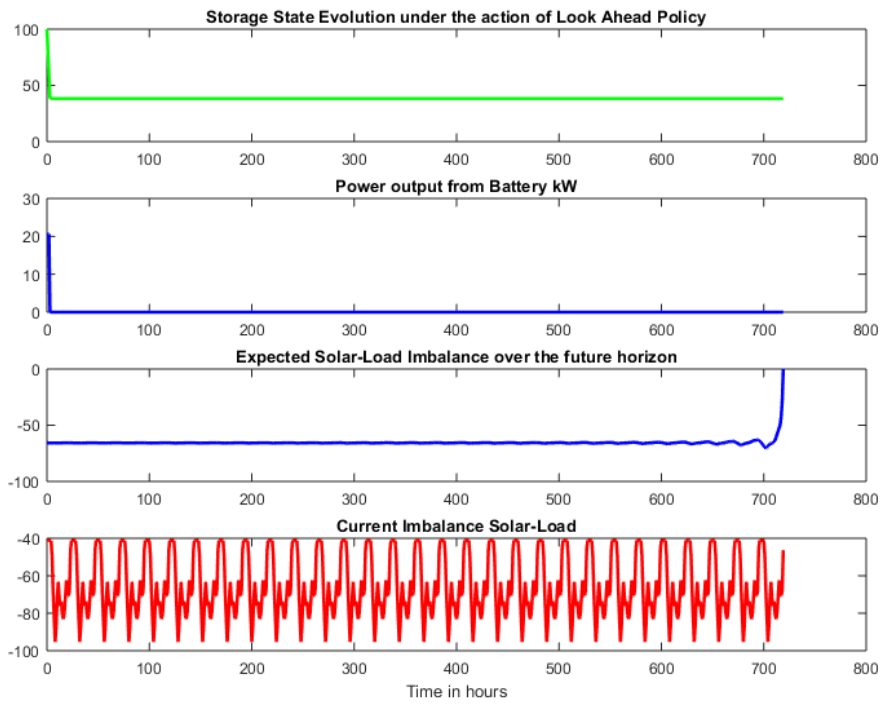

Figure 6.6: System evolution under the action of Policy 2

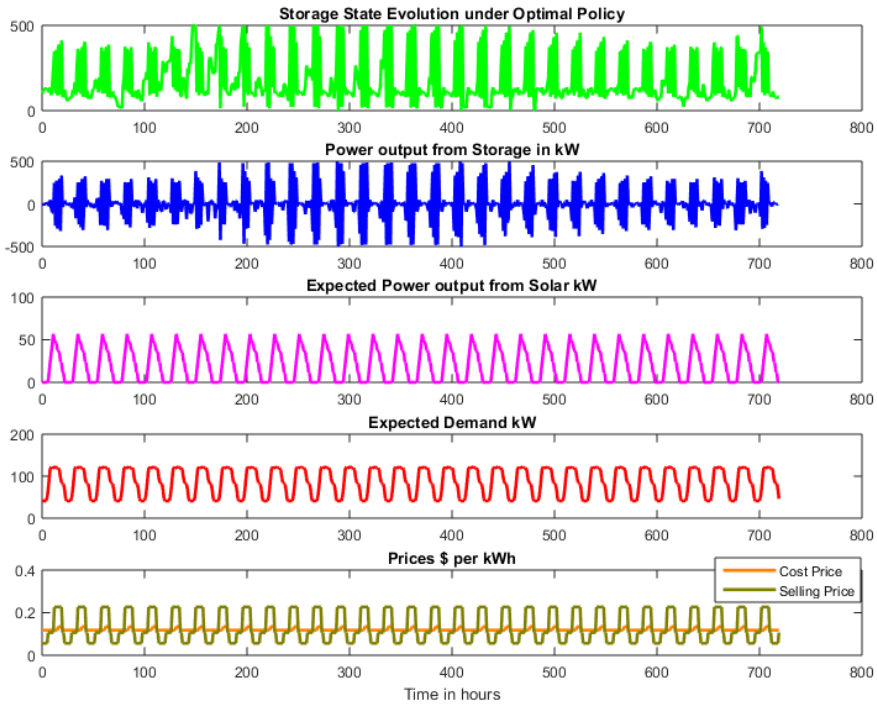

Figure 6.7: System under action of Optimal Policy over a 30 day horizon

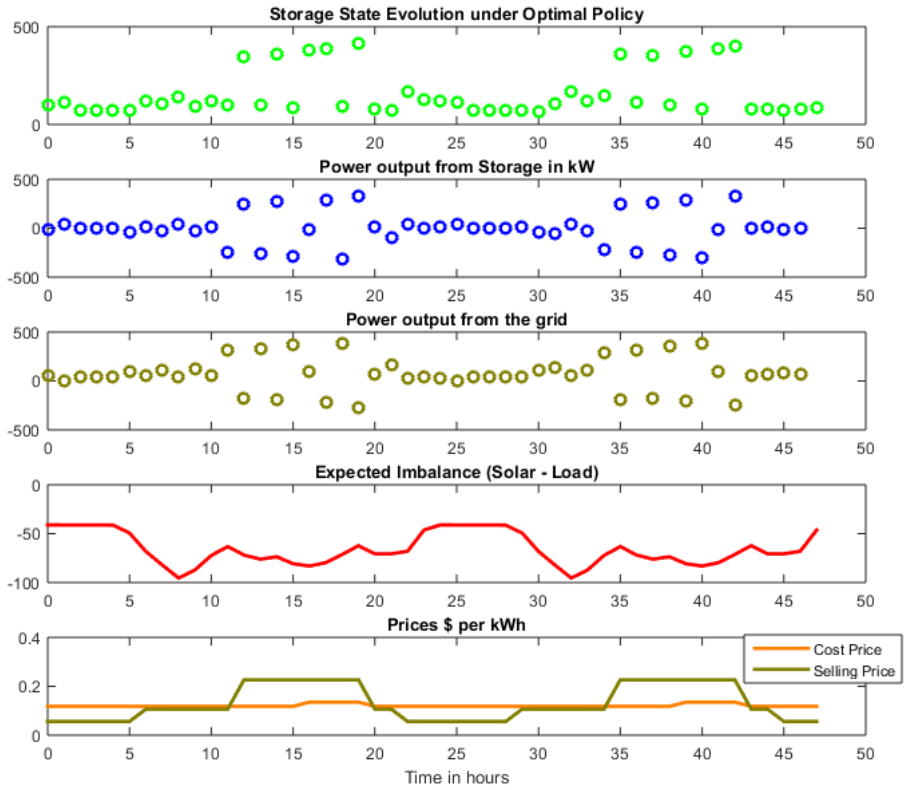

Figure 6.8: System under action of Optimal Policy over a two day horizon

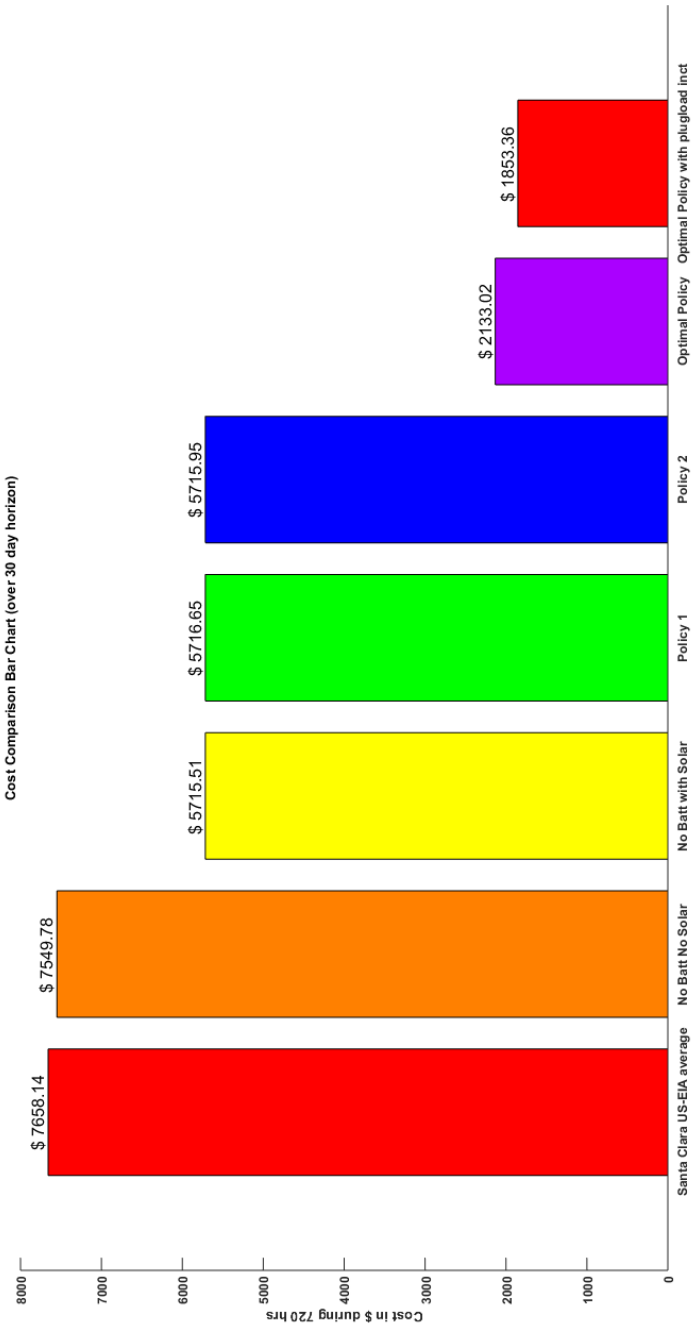

Figure 6.9: Expected savings under various policies

Chapter 7

CONCLUSIONS AND FUTURE WORK

This dissertation describes a weather-driven plugload-integrated framework for facilitating energy management in smart buildings. From a demand management perspective, the present work contributes to the advancement of existing demand response approaches by quantifying the savings due to the occupant-in-the-loop. The controlled experiments described in chapter 2 highlight important issues in both designing and implementing intervention mechanisms targeted toward promoting energy conservation practices among building occupants. The findings based on carefully controlled experimentation and analysis allows the building manager to design effective intervention mechanisms by considering the quantitative impact of the interventions using the plugload models developed in chapter 3. These results can also be used to develop more accurate building demand models as outlined in chapter 4. Furthermore, novel autoregression model with exogenous global forecast inputs is proposed in chapter 5 for augmenting the performance of local sensor data-based predictions.

The load and the solar models along with energy storage and a pricing scheme were integrated together in chapter 6 to constitute a framework for energy management in smart buildings. Two optimization problems were solved to minimize energy-related costs in the building over a finite horizon. The first problem considered the case of non-controllable demand, wherein the corresponding optimal policy was found to outperform heuristic policies by 60% in the expected case. The second optimization problem was considered within similar load profiles as the first one, but in the context of high performance buildings with plugload-integrated controllable demand. Results from the controllable demand optimization indicated a further 13% reduction in costs compared to the optimization problem with non-controllable demand. The developed framework provides new avenues for plugload-integrated strategic energy management in smart buildings. Furthermore, this framework can also be used as a tool to support design decisions such as the solar power and/or battery capacity to be installed in a building based on the expected cost reduction, or to evaluate the cost-effectiveness of utility pricing schemes.

7.1 Future work

Future work can extend our work in several directions including, 1. designing large-scale plugload studies, 2. development of game-theoretic plugload models, 3. energy management in a smart campus, 4. automated inventory management.

7.1.1 Large-scale plugload studies

The pilot study mentioned in this work can be further extended into a large-scale plugload study across several buildings to be able to strengthen the generality of the conclusions. Such studies must still adhere to the core design principles 2.2.1 but have the advantage of stricter adherence to the principles of replication and randomization compared to the pilot study. The former is due to the increase in the sample size, and allows for strengthening the generality of the resulting inferences. The latter is due to the availability of a larger scope for randomization across various nuisance factors such as job requirements and/or work schedules compared to the pilot study consisting of smaller number of samples. Furthermore, the future designs can also study the impact of the timespans for the various treatments in relation to the ability to retain the effect of the treatment on the behavior of the participants. This extension would also provide insight into the change of participant behavior under prolonged treatment, retainability, and formation of plugload energy conservation habits.

7.1.2 Game-theoretic plugload models

The results from the experiment were treated under the statistical assumptions to draw generalized conclusions. Alternatively, one could employ a game-theoretic model by assuming that the participants are playing a game to win the incentive by minimizing an unknown cost function that encompasses both comfort (consuming less than baseline plugload consumption) and the desire to win the incentive. For example, the incentive mechanisms implemented this study naturally fits the conception of a stackelberg competition. Furthermore, if the cost function is parameterized by weights corresponding to comfort and incentive components, then these parameters can be estimated based on the experiment data. Such parameters can then be assumed to represent a statistical sample of the occupant population. Using such analyses, the equilibrium behavior of a population in the presence of incentives can be studied by combining statistical and game-theoretic assumptions.

7.1.3 Energy management in a smart campus

While the optimization framework described in this dissertation is geared toward a smart building, it could be extended toward a network of smart buildings, such as a smart campus. In the context of a smart campus, individual buildings can be treated as players playing an energy conservation game with the objective of realizing both individual and collective goals. This enables the smart campus to leverage competition and cooperation to improve upon its baseline energy behavior. Furthermore, assuming interconnections between the smart buildings within the smart campus or within a network of smart campuses to allow power flows, energy trading can be investigated. In this context, the trade routes for power flows can be represented by the network topologies, which can optimized as per the designer's choice. Such designs also allow for the systematic analysis of networks such as microgrids.

7.1.4 Automated inventory management

During the plugload study, data about the devices connected to the various channels were noted. This information can be used to extract device signatures based on the power data recorded from the experiment. By storing to the device-signature maps for the set of possible device categories in a database, a signature extracted from the power signal from a channel with an unknown device can be associated with the device by referring to the database. In this manner, automated inventory management systems can be developed to identify and track the location of devices based on the knowledge about the location of the smart powerstrips.

In addition to the above, the following areas can be considered for future work: 1. Models predicting changes in energy behavior based on the screen time spent on different components of the dashboard can be developed, 2. The integration of weather forecasts into local sensor-based predictions could be explored further by the use of sophisticated modeling approaches, 3. In the context of energy management, detailed HVAC and lighting models could be employed to design and test various demand management strategies to optimize overall energy-related costs.

7.2 Summary

This dissertation provides a novel experimental design targeted toward studying occupant plugload consumption. It also addresses the challenging problem of occupant plugload modeling based on feedback and incentive interventions. It attempts to unravel the mechanisms by which these interventions influence the ob-

served changes in the occupant plugload consumption using autoregressive models. Furthermore, it proposes a novel local weather forecasting model via integration of global weather forecasts with local sensor-based data. Finally, this dissertation introduces a novel plugload-integrated energy management framework by integrating controllable plugload models and weather-driven solar generation models in the presence of energy storage and pricing models. This contribution extends energy management in buildings into a new paradigm by including occupants-in-the-loop. The practical significance of plugload control and plugload-integrated optimization resulting in cost reduction[1] is shown in Figure 7.1.

[1]Based on PG&E schedule A-10 medium demand pricing scheme, NREL rooftop potential survey (84 kW) for commercial medium office buildings [16] and commercial building energy consumption survey [23]

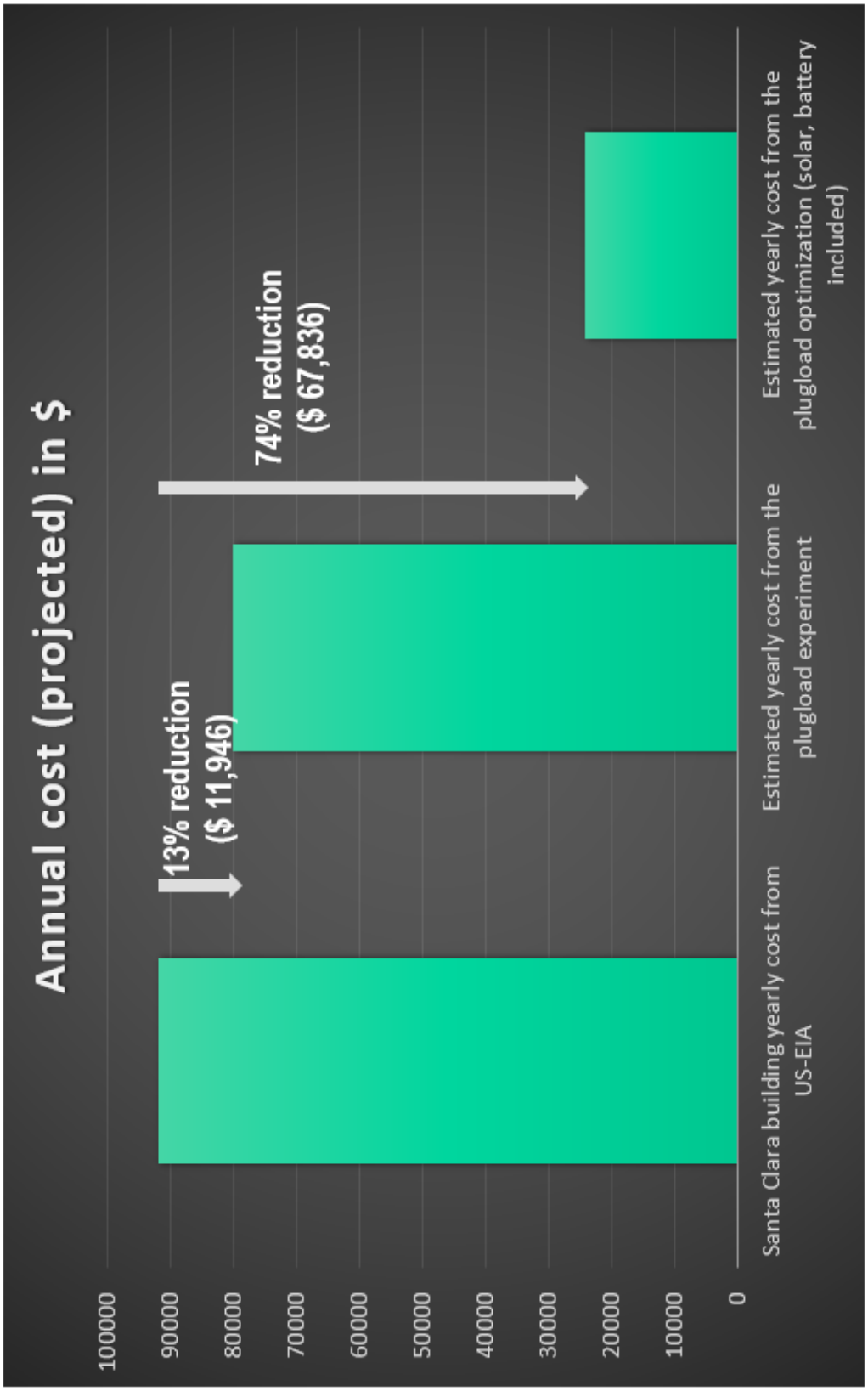

Figure 7.1: Potential savings in operating costs expected based on integration of plugloads for building energy management (does not include initial investment or maintenance costs)

BIBLIOGRAPHY

[1] Mohamed H Albadi and EF El-Saadany. "Demand response in electricity markets: An overview". In: *2007 IEEE power engineering society general meeting*. 2007.

[2] Curtis R Alexander et al. "High resolution rapid refresh (HRRR): Recent enhancements and evaluation during the 2010 convective season". In: *Preprints, 25th Conf. on Severe Local Storms, Denver, CO, Amer. Meteor. Soc*. Vol. 9. 2010.

[3] Hunt Allcott. "Social norms and energy conservation". In: *Journal of Public Economics* 95.9 (2011), pp. 1082–1095.

[4] Omid Ardakanian, Srinivasan Keshav, and Catherine Rosenberg. "Markovian Models for Home Electricity Consumption". In: *Proceedings of the 2Nd ACM SIGCOMM Workshop on Green Networking*. GreenNets '11. Toronto, Ontario, Canada: ACM, 2011, pp. 31–36. ISBN: 978-1-4503-0799-4. DOI: 10.1145/2018536.2018544. URL: http://doi.acm.org/10.1145/2018536.2018544.

[5] Ian Ayres, Sophie Raseman, and Alice Shih. "Evidence from two large field experiments that peer comparison feedback can reduce residential energy usage". In: *Journal of Law, Economics, and Organization* (2012), ews020.

[6] Peder Bacher, Henrik Madsen, and Henrik Aalborg Nielsen. "Online short-term solar power forecasting". In: *Solar Energy* 83.10 (2009), pp. 1772–1783.

[7] M. S. Bartlett. "The Effect of Non-Normality on the t Distribution". In: *Mathematical Proceedings of the Cambridge Philosophical Society* 31 (Apr. 1935), pp. 223–231. DOI: 10.1017/S0305004100013311. URL: https://www.cambridge.org/core/article/effect-of-non-normality-on-the-t-distribution/400D10D04B8C956E6F2D9783CB6BEF23.

[8] G. E. P. Box. "Non-Normality and Tests on Variances". In: *Biometrika* 40.3/4 (1953), pp. 318–335. ISSN: 00063444. URL: http://www.jstor.org/stable/2333350.

[9] Richard Brath and Michael Peters. "Dashboard design: Why design is important". In: *DM Direct* (2004).

[10] George Casella and Roger L Berger. *Statistical inference*. Vol. 2. Duxbury Pacific Grove, CA, 2002.

[11] Environmental Modeling Center. *National Centers for Environmental Prediction*. http://www.emc.ncep.noaa.gov. 1979.

[12] Changsong Chen et al. "Online 24-h solar power forecasting based on weather type classification using artificial neural network". In: *Solar Energy* 85.11 (2011), pp. 2856–2870.

[13] Dorota Chwieduk. "Towards sustainable-energy buildings". In: *Applied energy* 76.1 (2003), pp. 211–217.

[14] Caroline M Clevenger and John Haymaker. "The impact of the building occupant on energy modeling simulations". In: *Joint International Conference on Computing and Decision Making in Civil and Building Engineering, Montreal, Canada*. Citeseer. 2006, pp. 1–10.

[15] Federal Energy Regulatory Commission et al. *Energy Primer, a Handbook of Energy Market Basics*. 2012.

[16] Carolyn Davidson et al. "Nationwide Analysis of US Commercial Building Solar Photovoltaic (PV) Breakeven Conditions". In: *National Renewable Energy Laboratory, Golden, CO, USA* (2015).

[17] Richard J de Dear and Gail S Brager. "Thermal comfort in naturally ventilated buildings: revisions to ASHRAE Standard 55". In: *Energy and buildings* 34.6 (2002), pp. 549–561.

[18] Michael Deru et al. "US Department of Energy commercial reference building models of the national building stock". In: (2011).

[19] Maimouna Diagne et al. "Review of solar irradiance forecasting methods and a proposition for small-scale insular grids". In: *Renewable and Sustainable Energy Reviews* 27 (2013), pp. 65–76.

[20] Inc. Enmetric Systems. *Enmetric Plug Load Management System*. `https://www.enmetric.com/platform`. Accessed: 2016-10-29.

[21] Energy Environmental. *Executive Order 13693*. `https://www.whitehouse.gov/the-press-office/2015/03/19/executive-order-planning-federal-sustainability-next-decade`. 2015.

[22] O Erdinc, B Vural, and M Uzunoglu. "A dynamic lithium-ion battery model considering the effects of temperature and capacity fading". In: *Clean Electrical Power, 2009 International Conference on*. IEEE. 2009, pp. 383–386.

[23] Public Use Microdata File. "Commercial buildings energy consumption survey (CBECS)". In: (2016).

[24] Kwong Fai Fong, Victor Ian Hanby, and Tin-Tai Chow. "HVAC system optimization for energy management by evolutionary programming". In: *Energy and Buildings* 38.3 (2006), pp. 220–231.

[25] Pacific Gas and Electric. *Electric Schedule A-10*. URL: `http://www.pge.com/tariffs/tm2/pdf/ELEC_SCHEDS_A-10.pdf`.

[26] Pacific Gas and Electric. *Small Renewable Generator Power Purchase Agreement*. URL: http://www.pge.com/includes/docs/pdfs/b2b/energysupply/wholesaleelectricsuppliersolicitation/standardcontractsforpurch ELEC_FORMS_79-1103_Nov2012.pdf.

[27] Hugh G Gauch. *Scientific method in practice*. Cambridge University Press, 2003.

[28] US General Services Administration (GSA). *Plugload Introduction*. URL: http://www.gsa.gov/portal/content/178463.

[29] Rimas Gulbinas and John E Taylor. "Effects of real-time eco-feedback and organizational network dynamics on energy efficient behavior in commercial buildings". In: *Energy and buildings* 84 (2014), pp. 493–500.

[30] Rimas Gulbinas et al. "Network ecoinformatics: Development of a social ecofeedback system to drive energy efficiency in residential buildings". In: *Journal of Computing in Civil Engineering* 28.1 (2013), pp. 89–98.

[31] Hongwen He, Rui Xiong, and Jinxin Fan. "Evaluation of lithium-ion battery equivalent circuit models for state of charge estimation by an experimental approach". In: *Energies* 4.4 (2011), pp. 582–598.

[32] T. Hiyama and K. Kitabayashi. "Neural network based estimation of maximum power generation from PV module using environmental information". In: *IEEE Trans. Energy Convers.* 12 (1997), pp. 241–247.

[33] Rishee K Jain, John E Taylor, and Gabriel Peschiera. "Assessing eco-feedback interface usage and design to drive energy efficiency in buildings". In: *Energy and buildings* 48 (2012), pp. 8–17.

[34] Hristiyan Kanchev et al. "Energy management and operational planning of a microgrid with a PV-based active generator for smart grid applications". In: *IEEE Transactions on Industrial Electronics* 58.10 (2011), pp. 4583–4592.

[35] David Kaneda et al. "Plug load reduction: The next big hurdle for net zero energy building design". In: *ACEEE Summer Study on Energy Efficiency in Buildings*. 2010, pp. 120–130.

[36] A.J. Marszal et al. "Zero Energy Building – A review of definitions and calculation methodologies". In: *Energy and Buildings* 43.4 (2011), pp. 971–979. ISSN: 0378-7788. DOI: http://dx.doi.org/10.1016/j.enbuild.2010.12.022. URL: http://www.sciencedirect.com/science/article/pii/S0378778810004639.

[37] Douglas C Montgomery. *Design and analysis of experiments*. John Wiley & Sons, 2008.

[38] B Morvaj, L Lugaric, and S Krajcar. "Demonstrating smart buildings and smart grid features in a smart energy city". In: *Energetics (IYCE), Proceedings of the 2011 3rd International Youth Conference on*. IEEE. 2011, pp. 1–8.

[39] M. Muselli et al. "First order Markov chain model for generating synthetic "typical days" series of global irradiation in order to design photovoltaic stand alone systems". In: *Energy Conversion and Management* 42.6 (2001), pp. 675–687. ISSN: 0196-8904. DOI: http://dx.doi.org/10.1016/S0196-8904(00)00090-X. URL: http://www.sciencedirect.com/science/article/pii/S019689040000090X.

[40] NASA. *NASA Sustainability base*. http://www.nasa.gov/ames/facilities/sustainabilitybase. Accessed: 2016-10-22.

[41] National Renewable Energy Laboratory (NREL). "Assessing and Reducing Plug and Process Loads in Office Buildings". In: *US Department of Energy* (2010).

[42] National Oceanic and Atmospheric Administration. *NOAA's National Centers for Environmental Prediction*. URL: http://www.nco.ncep.noaa.gov/.

[43] Masahiro Ono et al. "Energy-efficient control of a smart grid with sustainable homes based on distributing risk". PhD thesis. Massachusetts Institute of Technology, 2012.

[44] OpenEI. *Commercial and Residential Hourly Load Profiles for all TMY3 locations in the United States*. 2013. URL: http://en.openei.org/datasets/dataset/commercial-and-residential-hourly-load-profiles-for-all-tmy3-locations-in-the-united-states.

[45] Jyoti P Painuly. "Barriers to renewable energy penetration; a framework for analysis". In: *Renewable energy* 24.1 (2001), pp. 73–89.

[46] Hugo TC Pedro and Carlos FM Coimbra. "Assessment of forecasting techniques for solar power production with no exogenous inputs". In: *Solar Energy* 86.7 (2012), pp. 2017–2028.

[47] Luis Pérez-Lombard, José Ortiz, and Christine Pout. "A review on buildings energy consumption information". In: *Energy and buildings* 40.3 (2008), pp. 394–398.

[48] John E Petersen et al. "Dormitory residents reduce electricity consumption when exposed to real-time visual feedback and incentives". In: *International Journal of Sustainability in Higher Education* 8.1 (2007), pp. 16–33.

[49] Petromil Petkov et al. "Motivating domestic energy conservation through comparative, community-based feedback in mobile and social media". In: *Proceedings of the 5th International Conference on Communities and Technologies*. ACM. 2011, pp. 21–30.

[50] Chaitanya Poolla et al. "Neural network forecasting of solar power for NASA Ames sustainability base". In: *Computational Intelligence Applications in Smart Grid (CIASG), 2014 IEEE Symposium on*. IEEE. 2014, pp. 1–8.

[51] A.C. Bhaktivedanta Swami Prabhupada. *Bhagavad Gita as it is, v 15:15*. 1983. URL: http://www.vedabase.com/bg/15/15.

[52] E.M.G. Rodrigues et al. "Energy storage systems supporting increased penetration of renewables in islanded systems". In: *Energy* 75 (2014), pp. 265–280. ISSN: 0360-5442. DOI: http://dx.doi.org/10.1016/j.energy.2014.07.072. URL: http://www.sciencedirect.com/science/article/pii/S0360544214008949.

[53] Z. M. Salameh, M. A. Casacca, and W. A. Lynch. "A mathematical model for lead-acid batteries". In: *IEEE Transactions on Energy Conversion* 7.1 (1992), pp. 93–98. ISSN: 0885-8969. DOI: 10.1109/60.124547.

[54] Timothy I Salsbury. "A survey of control technologies in the building automation industry". In: *IFAC Proceedings Volumes* 38.1 (2005), pp. 90–100.

[55] Eleonora Riva Sanseverino et al. "An execution, monitoring and replanning approach for optimal energy management in microgrids". In: *Energy* 36.5 (2011), pp. 3429–3436.

[56] Daniel Schwartz et al. "The Hawthorne effect and energy awareness". In: *Proceedings of the National Academy of Sciences* 110.38 (2013), pp. 15242–15246.

[57] Manuela Sechilariu, Baochao Wang, and Fabrice Locment. "Building integrated photovoltaic system with energy storage and smart grid communication". In: *IEEE Transactions on Industrial Electronics* 60.4 (2013), pp. 1607–1618.

[58] Dezso Sera, Remus Teodorescu, and Pedro Rodriguez. "PV panel model based on datasheet values". In: *Industrial Electronics, 2007. ISIE 2007. IEEE International Symposium on*. IEEE. 2007, pp. 2392–2396.

[59] Pervez Hameed Shaikh et al. "A review on optimized control systems for building energy and comfort management of smart sustainable buildings". In: *Renewable and Sustainable Energy Reviews* 34 (2014), pp. 409–429.

[60] Navin Sharma et al. "Predicting solar generation from weather forecasts using machine learning." In: IEEE, 2011, pp. 528–533. ISBN: 978-1-4577-1704-8. URL: http://dblp.uni-trier.de/db/conf/smartgridcomm/smartgridcomm2011.html#SharmaSIS11.

[61] Trudie Wang, Daniel O'Neill, and Haresh Kamath. "Dynamic control and optimization of distributed energy resources in a microgrid". In: *IEEE Transactions on Smart Grid* 6.6 (2015), pp. 2884–2894.

[62] Yao-Jung Wen and Alice M Agogino. "Personalized dynamic design of networked lighting for energy-efficiency in open-plan offices". In: *Energy and Buildings* 43.8 (2011), pp. 1919–1924.

[63] Yao-Jung Wen and Alice M Agogino. "Wireless networked lighting systems for optimizing energy savings and user satisfaction". In: *Wireless Hive Networks Conference, 2008. WHNC 2008. IEEE*. IEEE. 2008, pp. 1–7.

[64] Liu Yang, Haiyan Yan, and Joseph C Lam. “Thermal comfort and building energy consumption implications–a review”. In: *Applied Energy* 115 (2014), pp. 164–173.

[65] Atsushi Yona et al. “Application of neural network to one-day-ahead 24 hours generating power forecasting for photovoltaic system”. In: *Intelligent Systems Applications to Power Systems, 2007. ISAP 2007. International Conference on*. IEEE. 2007, pp. 1–6.

[66] Ray Yun et al. “Sustainability in the workplace: nine intervention techniques for behavior change”. In: *Persuasive Technology*. Springer, 2013, pp. 253–265.

[67] Ray Yun et al. “Toward the design of a dashboard to promote environmentally sustainable behavior among office workers”. In: *Persuasive Technology*. Springer, 2013, pp. 246–252.

Appendix A

IRB APPROVALS

The approvals for conducting the experiment was obtained from both NASA and CMU. They were also renewed by both the institutional review boards. The original approvals are enclosed herewith for supporting the claim.

NASA IRB Approval

The following message is sent on behalf of Ralph Pelligra, M.D., Chair, Human Research Institutional Review Board (HRIRB):

Dear Dr. Rosenberg:

Protocol **HRII-15-11**, "Impact of Dashboard Feedback on Plug Load Energy Consumption at NASA Ames Sustainability Base," received approval by expedited review from the Chair, HRIRB on June 04, 2015. You are authorized to conduct research studies subject to Ames Procedural Requirements (APR) 7170.1, Human Research Planning and Approval. The approval period for HRII-15-11 is valid from**June 04, 2015** through **June 03, 2016**. Please note the expiration date on your calendar. Any modifications to an approved protocol require the approval of the Chair, HRIRB and/or a designated HRIRB member.

HRII-15-11 will be presented to the HRIRB for ratification at the next scheduled board meeting. You may be contacted for clarification and/or additional information, should any concerns or questions arise.

Please retain a copy of this confirmation message for your files. Begin a renewal request six weeks prior to **June 03, 2016**, the protocol's expiration date. Allow two to three weeks for processing in the OPRP office, prior to an HRIRB meeting. If you do not renew the protocol, submit the end of study report within 30 days of the protocol's expiration. Both forms are available on the HRIRB web site, http://hrirb.arc.nasa.gov.

If you have questions, contact me at 650.604.5163, or by e-mail, Ralph.Pelligra-1@nasa.gov. Immediately notify me of any injury to a human participant, whether or not it was considered a risk inherent to the research. Injury includes, but is not limited to, bodily harm, psychological trauma or release of potentially damaging personal information.

Good luck in your research efforts.

Ralph Pelligra, M.D.
Chair, HRIRB
By
Elaine Timm
Recorder, Human Research Institutional Review Board
Assistant to Dr. Ernle Young
Office for the Protection of Research Participants, M/S 243-2
Bldg. 243, Room 120
voice: 650.604.0119
fax: 650.604.6233
E-mail: Elaine.M.Timm@nasa.gov

CMU IRB Approval

Certification of IRB Approval

IRB Protocol Number: HS14-767

Title: Impact of Dashboard Feedback on Plug Load Energy Consumption at NASA Ames

Sustainability Base

Investigator(s): Steven Rosenberg, Chaitanya Poolla, and Sreejita Ray

Department(s): CMU – Silicon Valley

Date: June 10, 2015

Carnegie Mellon University Institutional Review Board (IRB) reviewed the above referenced research protocol in accordance with 45 CFR 46 and CMU's Federal wide Assurance. The research protocol has been given APPROVAL by Expedited Review on June 9, 2015, as authorized by 45 CFR 46.110 (7) and 21 CFR 56.110. This APPROVAL expires on June 8, 2016, unless suspended or terminated earlier by action of the IRB.

All untoward or adverse events occurring in the course of the protocol must be reported to the IRB within three (3) working days. Any additional modifications to this research protocol or advertising materials pertaining to the study must be submitted for review and granted IRB approval prior to implementation. Please refer to the above-referenced protocol number in all correspondence.

Federal regulations require that all records relating to this research protocol be maintained for at least three (3) years after completion of the research, and be accessible for inspection and copying by authorized representatives at reasonable times and in a reasonable manner.

The Investigator(s) listed above in conducting this protocol agree(s) to follow the recommendations of the IRB and the Office of the Provost of any conditions to or changes in procedure subsequent to this review. In undertaking the execution of the protocol, the investigator(s) further agree(s) to abide by all CMU research policies including, but not limited to the policies on responsible conduct research and conflict of interest.

The IRB maintains ongoing review of all projects involving humans or human materials, and at continuing intervals, projects will require update until completion. At the end of the current approval, a continuing review form, current application/protocol and current consent form(s) must be submitted by the PI to the IRB summarizing progress on the protocol during that period. Please be advised that the continuing review form requests information pertaining to women and minorities; therefore, this information should be tracked with your participants' data. Note that submitting for continuing review in a timely manner is the responsibility of the PI.

Please call the Office of Research Integrity and Compliance at 412-268-7166 if you have any questions regarding this certification.

Thank you.

John Zimmerman, IRB Chair

Appendix B

HANDLING CONSTRAINTS IN THE OPTIMIZATION PROBLEM

The constraints in the decision-making problem include the following: (i) the power limits during the storage charge-discharge process, (ii) storage state/charge limits, and the (iii) power balance constraint (equation 6.3).

The decisions that do not violate the above constraints are referred to here as the feasible decisions. Similarly, the policies that result in such feasible decisions shall be known as the feasible policies. We now attempt to determine the feasible decision space, as it is required to solve the Bellman equation 6.11. In what follows, $e_k^{(r_e)} \in \{e^{min}, \cdots, e^{max}\}$ and $l_k^{(r_l)} \in \{l^{min}, \cdots, l^{max}\}$ represent a realization of the stochastic processes e_k and l_k respectively at the time instant t_k and s_k represents the storage state at t_k.

B.0.1 Handling State Constraints

Given the dynamics of the battery 6.1 and the state constraints $s_k \in [0, \mathcal{S}]$ kWh, the following can be stated by taking advantage of the discrete time formulation. If the state constraint needs to be satisfied at any time step t_{k+1} assuming it holds at t_k, then the following holds true:

$$\begin{aligned} s_{k+1} \in [0, \mathcal{S}] \text{ given } s_k \in [0, \mathcal{S}], \\ \iff \eta_s s_k - \xi_p v_k \Delta t \in [0, \mathcal{S}] \; s_k \in [0, \mathcal{S}] \\ (i.e.) - \frac{\eta_s s_k}{\xi_p \Delta t} \leq \; l_k + u_k + e_k \leq \frac{\mathcal{S} - \eta_s s_k}{\xi_p \Delta t} \\ (or) - \frac{\eta_s s_k}{\xi_p \Delta t} - l_k^{(r_l)} - e_k^{(r_e)} \leq \; u_k \leq \frac{\mathcal{S} - \eta_s s_k}{\xi_p \Delta t} - l_k^{(r_l)} - e_k^{(r_e)} \end{aligned} \tag{B.1}$$

Let the decision constraint in equation B.1 be written as $u_k \in \Theta(s_k, l_k^{(r_l)}, e_k^{(r_e)})$. It is easy to observe that, if $u_k \in \Theta(s_k, l_k^{(r_l)}, e_k^{(r_e)})$ and $s_k \in [0, \mathcal{S}]$, then the above proves that the state constraint at t_{k+1} is not violated.

B.0.2 Handling Power Constraints

Since the storage power flow v_k must be within the limits $[P_{min}, P_{max}]$ kW, we can use equation 6.3 to claim the following:

$$\begin{aligned} v_k &\in [P_{min}, P_{max}] \\ \iff l_k^{(r_l)} + u_k + e_k^{(r_e)} &\in [P_{min}, P_{max}] \\ (i.e.)\ P_{min} - l_k^{(r_l)} - e_k^{(r_e)} \leq u_k &\leq P_{max} - l_k^{(r_l)} - e_k^{(r_e)} \end{aligned} \tag{B.2}$$

Let the decision constraint in equation B.2 be written as $u_k \in \Gamma(s_k, l_k^{(r_l)}, e_k^{(r_e)})$. It is easy to observe that, if $u_k \in \Gamma(s_k, l_k^{(r_l)}, e_k^{(r_e)})$, then the battery power constraints hold as proved above.

Since the equations B.1 and B.2 constrain the same decision variable u_k, the feasible decision space can be obtained by the intersection of these constrained spaces. Let the intersection be represented by $\mathcal{U}_{s_k}^{(r)} := \Theta(s_k, l_k^{(r_l)}, e_k^{(r_e)}) \cap \Gamma(s_k, l_k^{(r_l)}, e_k^{(r_e)})$. Thus $\mathcal{U}_{s_k}^{(r)}$ can be written as,

$$\begin{aligned} max(P_{min}, -\frac{\eta_s s_k}{\xi_p \Delta t}) - l_k^{(r_l)} - e_k^{(r_e)} &\leq u_k \\ \leq min(P_{max}, \frac{\mathcal{S} - \eta_s s_k}{\xi_p \Delta t}) - l_k^{(r_l)} - e_k^{(r_e)} \end{aligned} \tag{B.3}$$

From equation B.3, we note the following observations:

1. The decision space $\mathcal{U}_{s_k}^{(r)}$ is guaranteed to have a positive Lebesgue measure, since $max(P_{min}, -\frac{\eta_s s_k}{\xi_p \Delta t}) \leq 0$ and $min(P_{max}, \frac{\mathcal{S} - \eta_s s_k}{\xi_p \Delta t}) \geq 0$ but both cannot be simultaneously 0. Thus the existence of a non-empty feasible decision space is guaranteed by definition.

2. The bounds of the decision space $\mathcal{U}_{s_k}^{(r)}$ depend on the realizations $e_k^{(r_e)}$ and $l_k^{(r_l)}$ of the stochastic processes e_k and l_k respectively. However, during the optimal policy design phase, the realizations of the stochastic processes $e_k^{(r_e)}$ and $l_k^{(r_l)}$ are unknown until the time instant t_k occurs in the real world.

3. Despite the guaranteed existence of a feasible decision space, it is unknown on the account of uncertainty in the generation and load processes.

In order to eliminate the dependence of the feasible decision space on the unknown solar and load in the real world at t_k, we use the information about the bounds of the stochastic processes e_k and l_k. Let the range space of these random variables

at time instant t_k be represented by: (i) $[e_k^{min}, e_k^{max}]$ for the solar generation, and (ii) $[l_k^{min}, l_k^{max}]$ for the load demand. Since the solar generation and load are bounded in the real world, the bounds $\{e_k^{min}, e_k^{max}, l_k^{min}, l_k^{max}\}$ are physically well-defined. Using these bounds, we construct a subset of the feasible space $\mathcal{U}_{s_k}^{(r)}$ and call it the computable feasible decision space ($\mathcal{U}_{s_k}$) as follows:

$$\begin{aligned} max(P_{min}, -\frac{\eta_s s_k}{\xi_p \Delta t}) - l_k^{min} - e_k^{min} \leq u_k \\ \leq min(P_{max}, \frac{\mathcal{S} - \eta_s s_k}{\xi_p \Delta t}) - l_k^{max} - e_k^{max} \end{aligned} \tag{B.4}$$

It is easy to verify that $\mathcal{U}_{s_k}$ is constructed by the intersection of the feasible decision spaces across all sample paths with non-zero probability. In other words, $\mathcal{U}_{s_k} := \bigcap_{r=\{0,\cdots,N_r\}} \mathcal{U}_{s_k}^{(r)}$, where $\left[P^l(k, l_k = l^{(r_l)}) \times P^e(k, e_k = e^{(r_l)})\right] \neq 0$.

Though the computable feasible decision space $\mathcal{U}_{s_k}$ possibly introduces sub-optimality, it is nevertheless a sufficient condition to ensure that the system constraints are upheld under all possible realizations of the stochastic processes. However, its existence is contingent on the measure of $\mathcal{U}_{s_k}$ being well-defined. Therefore, the necessary conditions for the existence of a computable feasible decision space

of non-zero measure are:

$$
\begin{aligned}
&(l_k^{max} + e_k^{max}) - (e_k^{min} + l_k^{min}) \\
&\leq min(P_{max}, \frac{\mathcal{S} - \eta_s s_k}{\xi_p \Delta t}) - max(P_{min}, -\frac{\eta_s s_k}{\xi_p \Delta t}) \\
&= min(P_{max}, \frac{\mathcal{S} - \eta_s s_k}{\xi_p \Delta t}) + min(-P_{min}, \frac{\eta_s s_k}{\xi_p \Delta t}) \\
&= min(P_{max}, \frac{\mathcal{S} - \eta_s s_k}{\xi_p \Delta t}) + min(P_{max}, \frac{\eta_s s_k}{\xi_p \Delta t}) \\
&\qquad \big[\text{Assuming } P_{min} = -P_{max}\big] \\
&= \begin{cases} 2 \times P_{max}, & \text{if } P_{max} < min(\frac{\mathcal{S}-\eta_s s_k}{\xi_p \Delta t}, \frac{\eta_s s_k}{\xi_p \Delta t}) \\ \frac{\mathcal{S}-\eta_s s_k}{\xi_p \Delta t} + P_{max}, & \text{if } \frac{\mathcal{S}-\eta_s s_k}{\xi_p \Delta t} \leq P_{max} < \frac{\eta_s s_k}{\xi_p \Delta t} \\ P_{max} + \frac{\eta_s s_k}{\xi_p \Delta t}, & \text{if } \frac{\eta_s s_k}{\xi_p \Delta t} \leq P_{max} < \frac{\mathcal{S}-\eta_s s_k}{\xi_p \Delta t} \\ \frac{\mathcal{S}}{\xi_p \Delta t}, & \text{if } P_{max} > max(\frac{\mathcal{S}-\eta_s s_k}{\xi_p \Delta t}, \frac{\eta_s s_k}{\xi_p \Delta t}) \end{cases} \\
&= min\Big(2P_{max}, \frac{\mathcal{S} - \eta_s s_k}{\xi_p \Delta t} + P_{max}, P_{max} + \frac{\eta_s s_k}{\xi_p \Delta t}, \frac{\mathcal{S}}{\xi_p \Delta t}\Big) \\
&\geq min\Big(P_{max}, \frac{\mathcal{S}}{\xi_p \Delta t}\Big) \qquad \text{(B.5)} \\
&\Big[\text{equality iff } s_k = 0 \; or \; \eta_s s_k = \mathcal{S} \; or \; \frac{\mathcal{S}}{\xi_p \Delta t} \leq P_{max}\Big]
\end{aligned}
$$

It is easy to verify that, if $(l_k^{max} + e_k^{max}) - (e_k^{min} + l_k^{min}) \leq min(P_{max}, \frac{\mathcal{S}}{\xi_p \Delta t})$, then the inequation B.4 holds true. Hence, the inequation $(l_k^{max} + e_k^{max}) - (e_k^{min} + l_k^{min}) \leq min(P_{max}, \frac{\mathcal{S}}{\xi_p \Delta t})$ provides a stricter condition for the existence of a non-empty feasibel decision space $\mathcal{U}_{s_k}$. Progressively stronger sufficiency conditions can be derived as

follows:

$$(l_k^{max} + e_k^{max}) - (e_k^{min} + l_k^{min}) \leq min\Big(P_{max}, \frac{\mathcal{S}}{\xi_p \Delta t}\Big), \ or \tag{B.6}$$

$$e_k^{max} - l_k^{min} \leq min\Big(P_{max}, \frac{\mathcal{S}}{\xi_p \Delta t}\Big) \tag{B.7}$$

$$\big[\text{since } -e_k^{min} \leq 0, l_k^{max} \leq 0 \text{ by definition}\big]$$

$$(i.e.) \max_{k \in \{0,\cdots,N\}} (e_k^{max} - l_k^{min}) \leq min\Big(P_{max}, \frac{\mathcal{S}}{\xi_p \Delta t}\Big)$$

$$\big[\text{Let } \bar{l}_k = -l_k, \text{ and let } \bar{l}_k \in \{\bar{l}^{min}, \cdots, \bar{l}^{max}\}\big]$$

$$\max_{k \in \{0,\cdots,N\}} (e_k^{max} + \bar{l}_k^{max}) \leq min\Big(P_{max}, \frac{\mathcal{S}}{\xi_p \Delta t}\Big)$$

$$\big[\text{Since } \max_{k \in \{0,\cdots,N\}} \bar{l}_k^{max} = -l^{max}\big]$$

$$(e^{max} - l^{min}) \leq min\Big(P_{max}, \frac{\mathcal{S}}{\xi_p \Delta t}\Big) \tag{B.8}$$

Note that the left-hand side (LHS) of equation B.6 represents the maximum possible supply-demand offset gap at the instant $t_k \in \mathcal{T}$, the LHS of equation B.7 represents the maximum supply-demand sum at the instant t_k, and the LHS of B.8 maximum possible supply-demand over the horizon $\{0, \cdots, N\}$. In each of these sufficiency conditions, the right-hand side represents a time-independent expression dependent on a subset λ_k of the storage parameters z_k.

Equations B.4-B.8 represent the worst case sufficiency conditions that ensure that the existence of a corresponding computable feasible decision space $\mathcal{U}_{s_k}$ despite the unknown realizations of the solar and load processes. Furthermore, given any grid transaction decision $u_k \in \mathcal{U}_{s_k}$, it is ensured that the corresponding feasible battery decision space is the same as the space defined by the battery constraint since $\mathcal{V}_{s_k} = [P_{min}, P_{max}]$ is equivalent to equation B.2 by definition.

Let the parameters λ_k satisfying the sufficiency condition[1] in equation B.4 belong to the space $\Lambda_k \subseteq \mathbb{R}^{dim(\lambda_k)}$, where $dim(\lambda_k)$ refers to the dimension of λ_k. We call Λ_k as the computable feasible configuration space of the system for which a computable feasible decision space exists. Therefore, satisfying the sufficiency condition $\lambda_k \in \Lambda_k$ guarantees the existence of such computable feasible decision spaces which are required to design the near-optimal policy. Only decisions belonging to the computable feasible decision space are considered admissible

[1]Since the conditions represented by equations B.4-B.8 are in the increasing order of strictness requirements, satisfying any of these equations ensures that equation B.4 is satisfied.

for computing the near-optimal policy, hence we also refer to this decision space $(\mathcal{U}_{s_k}, \mathcal{V}_{s_k})$ as the admissible decision space for the optimal decision-making problem.

As aforementioned, a feasible decision space is guaranteed to exist for every realization of the stochastic processes (equation B.3), but is unknown at the time of determining the optimal policy. However, the optimal policy design as per equation 6.11 involves computing the expected state at the next instant of time $E(\hat{s}_{k+1})$, and thus requires that all possible realizations of $\hat{s}_{k+1}$ be pre-computed, accounting for every possible realization of the load and solar stochastic processes. In the pre-computation process, the realization of $\hat{s}_{k+1}$ can be represented as a function of the decision u_k. Thus the state constraints on $\hat{s}_{k+1}$ translate into corresponding control constraints u_k for every possible realization of the load and solar stochastic processes. In other words, respecting the state and control constraints while making optimal decisions amidst uncertainties based on dynamic programming not only restricts the admissible decision space $(\mathcal{U}_{s_k}, \mathcal{V}_{s_k})$ but also artificially imposes constraints on the system parameters as shown in equations B.5-B.8.

Appendix C

QUESTIONNAIRE

Questionnaires were designed to obtain responses of the participants regarding their energy awareness, their thermal comfort, and for their feedback on the dashboard design. Two questionnaires were provided to the participants in each experiments, one prior to the experiment and the other at the end of the experiment. These questionnaires are enclosed below for reference.

Begin-of-study survey: 232

Please answer the following questions to the best of your knowledge.

* Required

1. **Enter the first two letters of your first name followed by the last two letters of your last name** *

2. **How would you rate your awareness level about your energy consumption?** *

   Mark only one oval.

	1	2	3	4	5	6	7	8	9	10	
Completely unaware	◯	◯	◯	◯	◯	◯	◯	◯	◯	◯	Extremely aware

3. **In general, when do you use electrical devices at the workplace? Please select all options that apply.** *

   Check all that apply.

   - [ ] Weekdays, Mon-Fri (9 AM - 6 PM)
   - [ ] Weekdays, Mon-Fri (6 PM - 12 AM OR 12 AM - 9 AM)
   - [ ] Weekends, Sat-Sun

4. **Please indicate the dates between sep 12, 2016 and nov 15, 2016 when you will not use any electric power at your cubicle? Exclude weekends and federal holidays. Write 'NA' if you do not anticipate any such day.** *

Begin-of-study survey: CMU

Please answer the following questions to the best of your knowledge.

* Required

1. **Enter the first two letters of your first name followed by the last two letters of your last name** *

2. **How would you rate your awareness level about your energy consumption?** *

   Mark only one oval.

	1	2	3	4	5	6	7	8	9	10	
Completely unaware	◯	◯	◯	◯	◯	◯	◯	◯	◯	◯	Extremely aware

3. **In general, when do you use electrical devices at the workplace? Please select all options that apply.** *

   Check all that apply.

   - [ ] Weekdays, Mon-Fri (9 AM - 6 PM)
   - [ ] Weekdays, Mon-Fri (6 PM - 12 AM OR 12 AM - 9 AM)
   - [ ] Weekends, Sat-Sun

4. **Please indicate the dates between sep 12, 2016 and nov 15, 2016 when you will not use any electric power at the workplace? Exclude weekends and federal holidays. Write 'NA' if you do not anticipate any such day.** *

End of study survey: 232

Thank you very much for participating in the plugload study. Your participation helped us to systematically study about the plugload consumption among building occupants. Please take a minute or two to answer the following questions.

* Required

1. **Please enter the first two letters of your first name followed by the last two letters of your last name.** *

   _____

2. **How would you rate your awareness level about your energy consumption?** *

   Mark only one oval.

	1	2	3	4	5	6	7	8	9	10	
Completely unaware	◯	◯	◯	◯	◯	◯	◯	◯	◯	◯	Extremely aware

3. **Please check one or more options below that best describe your work responsibilities.** *

   Check all that apply.

   - [ ] Engineering
   - [ ] FInance
   - [ ] Human resources
   - [ ] Operations
   - [ ] Research
   - [ ] Other: _____

4. **Which of the following elements on the dashboard (more than one may apply) do you consider useful in motivating occupants to reduce their energy consumption?** *

   Check all that apply.

   - [ ] Comfort report
   - [ ] Central dial
   - [ ] Scoreboard/Leaderboard
   - [ ] Line charts
   - [ ] Bar charts
   - [ ] None of the above

5. **Which range of temperatures would you consider as being thermally hot?**
Mark only one oval.

- 65 F and higher
- 70 F and higher
- 75 F and higher
- 80 F and higher
- 85 F and higher
- 90 F and higher
- 95 F and higher

6. **Which range of temperatures would you consider as being thermally cold?**
Mark only one oval.

- 90 F and lower
- 85 F and lower
- 80 F and lower
- 75 F and lower
- 70 F and lower
- 65 F and lower
- 60 F and lower

7. **What is be your feedback about the study? Please list the positive and/or negative aspects. Please be assured that all the survey data is analyzed anonymously to protect your privacy.** *

End of study survey: CMU

Thank you very much for participating in the plugload study. Your participation helped us to systematically study about the plugload consumption among building occupants. Please take a minute or two to answer the following questions.

* Required

1. **Please enter the first two letters of your first name followed by the last two letters of your last name.** *

   _____

2. **How would you rate your awareness level about your energy consumption?** *

   Mark only one oval.

	1	2	3	4	5	6	7	8	9	10	
Completely unaware	◯	◯	◯	◯	◯	◯	◯	◯	◯	◯	Extremely aware

3. **Please check one or more options below that best describe your work responsibilities.** *

   Check all that apply.

   - [ ] Engineering
   - [ ] FInance
   - [ ] Human resources
   - [ ] Operations
   - [ ] Research
   - [ ] Other: _____

4. **Which of the following elements on the dashboard (more than one may apply) do you consider useful in motivating occupants to reduce their energy consumption?** *

   Check all that apply.

   - [ ] Comfort report
   - [ ] Central dial
   - [ ] Scoreboard/Leaderboard
   - [ ] Line charts
   - [ ] Bar charts
   - [ ] None of the above

5. **Which range of temperatures would you consider as being thermally hot?**
Mark only one oval.

- 65 F and higher
- 70 F and higher
- 75 F and higher
- 80 F and higher
- 85 F and higher
- 90 F and higher
- 95 F and higher

6. **Which range of temperatures would you consider as being thermally cold?**
Mark only one oval.

- 90 F and lower
- 85 F and lower
- 80 F and lower
- 75 F and lower
- 70 F and lower
- 65 F and lower
- 60 F and lower

7. **What is be your feedback about the study? Please list the positive and/or negative aspects. Please be assured that all the survey data is analyzed anonymously to protect your privacy.** *

Appendix D

CONSENT FORM

The participants at sustainability base were recruited based on the NASA ARC 475 consent form, which was filled and signed by each participant at NASA after being briefed about the experiment protocol. The consent form used is enclosed below for reference. It can also be found at https://hrirb.arc.nasa.gov/content/arc-475-category-ii.

Ames
Research
Center

CATEGORY II – HUMAN RESEARCH MINIMAL RISK CONSENT

To the Research Participant: Please read this consent form and the attached protocol and/or subject instructions carefully. Make sure all your questions have been answered to your satisfaction before signing.

A. I agree to participate in the _____ research experiment as described in the attached protocol or subject instructions. I understand that I am employed by_____ who can be contacted at _____.

B. I understand that my participation could cause me minimal risk*, inconvenience, or discomfort. The purpose and procedures have been explained to me and I understand the risks and discomforts as described in the attached research protocol.

C. To my knowledge, I have no medical conditions, including pregnancy, that will prevent my participation in this study. I understand that if my medical status should change while I am a participant in the research experiment there may be unforeseeable risks to me (or the embryo or fetus if applicable). I agree to notify the Principal Investigator (PI) or medical monitor of any known changes in my condition for safety purposes.

D. My consent to participate has been freely given. I may withdraw my consent, and thereby withdraw from the study at any time without penalty or loss of benefits to which I am entitled. I understand that the PI may request my withdrawal or the study may be terminated for any reason. I agree to follow procedures for orderly and safe termination.

E. I am not releasing NASA or any other organization or person from liability for any injury arising as a result of my participation in this study. I will be contacted by the PI if an unusual or abnormal (anomalous) finding is detected during this study.

F. In the event of injury or illness resulting from this study and calling for immediate action or attention, NASA will provide, or cause to be provided, the necessary emergency treatment. If I am eligible for and receive workers' compensation benefits while participating in this study, I cannot sue my employer because the law makes workers' compensation my only remedy against my employer. I may have other remedies against other persons or organizations, depending on the circumstances of the injury. The United States Government will pay for any claims of injury or loss of life to the extent required by the Federal Employees Compensation Act or the Federal Tort Claims Act.

G. I hereby agree that all records collected by NASA in the course of this study are available to the research study investigators, support staff, and any duly authorized research review committee. I grant NASA permission to reproduce and publish all records, notes, or data collected from my participation, provided there will be no association of my name with the collected data and that confidentiality is maintained, unless specifically waived by me. All stated precautions will be taken to protect anonymity, but there is a small risk that some or all of the participants' data could become identifiable.

H. I have had an opportunity to ask questions and have received satisfactory answers to all my questions. I understand that the Pl for the study is the person responsible for this activity and that any questions regarding the research will be addressed to him/her during the course of the study. I have read the above agreement, the attached protocol and/or subject instructions prior to signing this form and I understand the contents.

* *Minimal Risk* means that the probability and magnitude of harm or discomfort anticipated in the research are not greater, in and of themselves, than those ordinarily encountered in daily life or during the performance of routine physical or psychological examinations or tests.

Signature of Research Participant	Date	Signature of Principal Investigator	Date
Printed/Typed Name of Research Participant		Printed/Typed Name of Principal Investigator	
Telephone Number of Research Participant		Telephone Number of Principal Investigator	
Address		Subject Signature: Authorization for Videotaping	
City, Sate, Zip Code			